Università di Bologna

Facoltà di Scienze Matematiche, Fisiche e Naturali

Dottorato di Ricerca in Geofisica

Ciclo XX

Elastic Propagation in random media: applications to the imaging of volcano structures

Dott. Anna Tramelli

matr. n. 237808

Settore scientifico disciplinare: FIS/06

Esame finale anno 2008

Relatore:
Prof. Edoardo Del Pezzo

Referente:
Prof. Aldo Zollo

Coordinatore:
Prof. Michele Dragoni

Dedicated to
my parents

Abstract

High-frequency seismograms contain features that reflect the random inhomogeneities of the earth. In this work I use an imaging method to locate the high contrast small-scale heterogeneity respect to the background earth medium. This method was first introduced by Nishigami (1991) and than applied to different volcanic and tectonically active areas (Nishigami, 1997, Nishigami, 2000, Nishigami, 2006).

The scattering imaging method is applied to two volcanic areas: Campi Flegrei and Mt. Vesuvius. Volcanic and seismological active areas are often characterized by complex velocity structures, due to the presence of rocks with different elastic properties. I introduce some modifications to the original method in order to make it suitable for small and highly complex media. In particular, for very complex media the single scattering approximation assumed by Nishigami (1991) is not applicable as the mean free path becomes short. The multiple scattering or diffusive approximation become closer to the reality. In this thesis, differently from the ordinary Nishigami's method (Nishigami, 1991), I use the mean of the recorded coda envelope as reference curve and calculate the variations from this average envelope. In this way I implicitly do not assume any particular scattering regime for the "average" scattered radiation, whereas I consider the variations as due to waves that are singularly scattered from the strongest heterogeneities. The imaging method is applied to a relatively small area (20 x 20 km), this choice being justified by the small length of the analyzed codas of the low magnitude earthquakes.

I apply the unmodified Nishigami's method to the volcanic area of Campi Flegrei and compare the results with the other tomographies done in the same area. The scattering images, obtained with frequency waves around 18 Hz, show the presence of high scatterers in correspondence with the submerged caldera rim in the southern part of the Pozzuoli bay. Strong scattering is also found below the Solfatara crater, characterized by the presence of densely fractured, fluid-filled rocks and by a strong thermal anomaly.

The modified Nishigami's technique is applied to the Mt. Vesuvius area. Results show a low scattering area just below the central cone and a high scattering area around it. The high scattering zone seems to be due to the contrast between the high

rigidity body located beneath the crater and the low rigidity materials located around it. The central low scattering area overlaps the hydrothermal reservoirs located below the central cone.

An interpretation of the results in terms of geological properties of the medium is also supplied, aiming to find a correspondence of the scattering properties and the geological nature of the material.

A complementary result reported in this thesis is that the strong heterogeneity of the volcanic medium create a phenomenon called "coda localization". It has been verified that the shape of the seismograms recorded from the stations located at the top of the volcanic edifice of Mt. Vesuvius is different from the shape of the seismograms recorded at the bottom. This behavior is justified by the consideration that the coda energy is not uniformly distributed within a region surrounding the source for great lapse time.

Contents

Chapter 1

Seismic coda waves: review

When an earthquake occurs, seismic waves propagate away from the source. After the P, S and various surface waves passage, the area around the seismic source is still vibrating. The amplitude of vibrations is uniform in space, except for the local site effect. These residual vibrations are called seismic coda waves and they decay slowly with time. The rate of decay is roughly the same, independent of the locations of seismic source and recording station, as long as they are located in a given region.

We can imagine if someone shoots a gun in a room, the sound energy would remain for a long time because of incoherent multiple reflections. This residual sound has a very stable, robust nature similar to seismic coda waves, independent of the locations where the gun was shot or where the sound in the room was recorded. The residual sound remains in the room because of multiple reflections at the rigid wall, ceiling, and floor of the room. In the case of lithosphere we attribute seismic coda waves to backscattering from numerous heterogeneities in the earth. Seismic coda may be considered as waves trapped in a random medium (Aki, 1996).

1.1 First studies on the seismic coda waves

The first observation about coda waves in seismology was the evidence of similarity in their spectral content for local events for different epicenter - station path (Aki, 1956). A new method for the determination of the magnitude of earthquakes using coda waves was introduced by the Hungarian scientist Bisztricsany (1958). Solov'ev, in 1965, observed that total time duration of seismic waves is independent of epicentral distance, for epicentral distance shorter than about 100 km. In particular he demonstrated the proportionality between the logarithm of the duration of a local seismogram and the magnitude calculated from amplitudes. The duration of the seismogram is intended to be the time length measured from P-wave arrival to the time when the S-coda amplitude decreases to the level of noise. In this way he introduced the concept

of duration magnitude (Md). He established a relationship between the magnitudes of teleseismic events at epicentral distances between 4° to 160° recorded in eastern Europe (Budapest, Prague and Warsaw) and the logarithm of the duration of their surface wave train. He observed that seismic wave's amplitudes were attenuated with distance, but surface waves duration were relatively constant.

All these results received new attention when the need to analyze seismic waves in a laterally heterogeneous medium led to search for statistical methods. The attention moved also to backscattering waves, formed by the superposition of waves generated by the interaction between scatterers and primary waves. Since in this case the scatterers can be considered as new sources, the backscattering waves can be represented as the superposition of many independent events suitable for a statistical approach. If these waves exist, they must be located in time principally after the passage of all the primary waves, that is, in the coda waves. The above observations were supported and confirmed by Aki (1969). He analyzed the aftershocks of the Parkfield, California, earthquake of 1966 and described the evidence that the power spectrum of coda waves of a local earthquakes has a common decay curve that is only a function of lapse time, measured from the origin time of the source, and is independent of the location of source and recording site. The path independence suggested the coda power spectra separation into source and path effect, after a correction for the surface geology of the station site. Based on this assumption Aki (1969) proposed a new method of determining the seismic moment of local earthquakes from coda waves. The cornerstone equation in coda wave analysis was written by Aki in this paper:

$$P(\omega \mid t) = S(\omega)C(\omega \mid t) \tag{1.1}$$

where $P(\omega \mid t)$ is the power spectrum of the coda for the angular frequency ω at lapse time t, the time calculated from the origin time of the earthquake. $S(\omega)$ is the source effect and $C(\omega \mid t)$ represent the effect that a large geographical area surrounding the source has on the propagation of the waves and is independent of distance and details of path connecting source and station.

The condition that 1.1 holds for t grater than about twice the travel time of S waves was introduced by the extensive study of coda waves in central Asia by Rautian and Khaltuin (1978). They manually measured the decay of the envelopes in many frequency bands. Their study was conducted on a complete data set composed of earthquakes with different magnitudes and different hypocentral depths, recorded at different stations in different regions. They found that early portions of coda are different from station to station; however, the coda of band-pass filtered seismograms have a common shape at all stations after about two times the S wave travel-time from the source to the receiver. Only the amplitude of the coda was different for different locations of the stations.
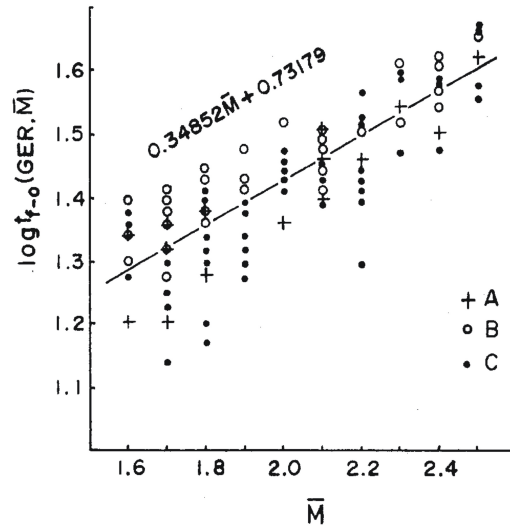
Figure 1.1: Logarithm of coda duration (in seconds) vs. local magnitude before(A) and after (C) the Western Nagano earthquake, Japan, of Ms=6.8. The solid line is the regression line for all the data. (From Sato, 1987)

Aki and Chouet (1975) made the first pioneer attempt to predict the explicit form of $P(\omega \mid t)$ for a mathematical model of earthquake source and earth medium. For this analysis they neglected the multiple scattering and assumed that scatterers are distributed randomly and uniformly. In their model both primary and scattered waves were S waves. This assumption was supported by various observations, such as the common site amplification (Tsujiura, 1978) and the common attenuation (Aki, 1966) between S waves and coda waves. It is also supported theoretically because the S to P conversion scattering due to a localized heterogeneity is an order of magnitude smaller than the P to S scattering as shown by Aki (1992) with the reciprocal theorem. Zeng (1993) showed that the above difference in conversion scattering between P to S and S to P leads to the dominance of S waves in the coda. It was already known, from array observations (Aki et al., 1958, Aki and Tsujiura, 1959), that the coda is not composed of regular plane waves coming from the epicenter, but of wavelets with randomly varying directions.

An other innovation introduced by Aki and Chouet (1975) was the diffusion model for the coda waves. They used both the diffusion and the single scattering model as two extreme model to describe mathematically the coda shape. The diffusion model describes a high scattering medium and it was found to be the proper model to describe the lunar seismograms.

1.2   Moonquakes

On July 20, 1969, the lunar module of Apollo 11 landed on the moon surface and together with footsteps and the flag Amstrong and colleagues left also a seismometer. When the first moonquakes registration arrived on the Earth it was immediately clear that there was a big difference with the earthquakes. Lunar seismograms are characterized by a very long duration, exceeding 1 hour, and a very slow growth from the first arrival to the maximum amplitude. The coda is very large and occupies almost the whole seismogram (Nakamura et al., 1970). These features suggested that there is more intense scattering and much lower absorption on the Moon than on the Earth demanding a method based upon diffusion models.
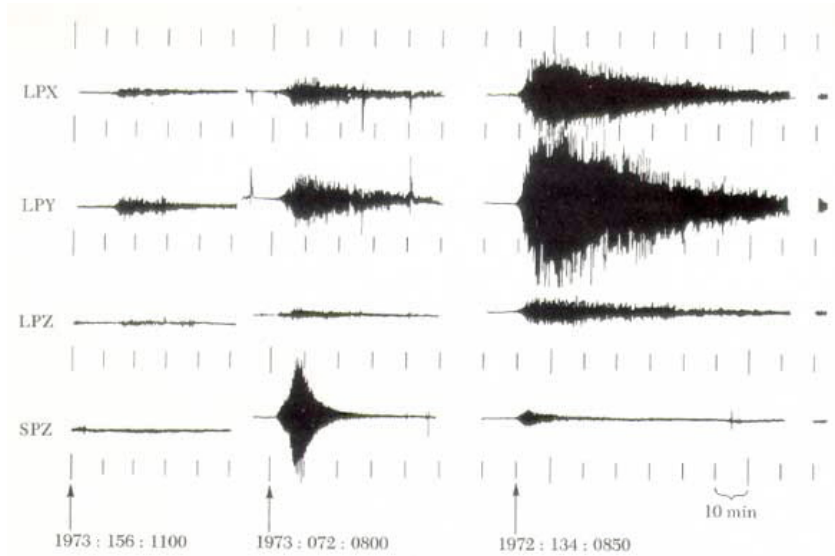
Figure 1.2: Seismograms from three types of moonquakes recorded at the Apollo 16 station. LPX, LPY, and LPZ are the three long-period components and SPZ is the short-period vertical component. The first column shows a deep-focus moonquake; the center column, a shallow moonquake; the third column shows records of the impact of meteoroid on the lunar surface. [Courtesy of NASA]

After the moonquakes discovered, some researcher got the beliefs that diffusion theory was inapplicable to terrestrial coda although it can be used for lunar data (e.g. Dainty and Toksoz, 1981; Kopnichev, 1977).

1.3   Introduction of coda Q

To characterize the smooth decay of coda amplitude coda Q^{-1}, Q_c^{-1}, was introduced as attenuation factor that characterize the spectral decay of the coda waves with lapse

time (as shown in equation (3.8)). Sato (1977) introduced the scattering coefficient η_s, which characterizes coda excitation strength as a geophysical parameter, to model scattering in time and space (see section 3.1). This two parameters were studied in many tectonically interesting areas through the world (see Sato and Fehler, 1998, for a review).

These parameters were used to monitor the temporal change in the coda characteristics. The first to observe the change was Chouet, in 1979. He reported a temporal change in Q_c^{-1} from observations made in Stone Canyon, California but he didn't related it to any seismic activity. On the contrary, Jin and Aki (1986) reported a temporal change associated with the occurrence of the Tangshan earthquake in China. In fact the variation of Q_c^{-1} is correlated with the fracturation and the attenuation that characterize the medium and a variation in its value can be a precursor for the occurrence of an earthquake or the eruption of a volcano.

1.4 Coda waves simulations

To explain the shape of coda waves at long lapse time, the multiple scattering model was introduced (Gao et al., 1983). This model was described by Hoshiba, in 1995, using the Monte Carlo method to simulate the multiple non-isotropic scattering.

Zeng, in 1991, extended the stationary energy transport theory to the time dependent case and obtained the scattered wave energy equation applicable to a random isotropic scattering medium. He obtained a general solution of temporal variation of scattered energy density as Neumann series expansion characterized by power of the scattering coefficient. The first term is the same found by Sato (1977) to describe the single scattering and the calculated scattering terms up to the third order find confirmation in the Monte Carlo simulation of Hoshiba (1991). He also evidenced as multiple scattering becomes very important as the scattering coefficient increases especially at later travel-time. Instead, for the weak scattering case, both single scattering and energy flux models are in good agreement with the multiple scattering result.

1.5 Localization of the heterogeneities

Up to this moment, it was only possible to define the mean Q_c^{-1} and η_s in the medium covered by the ray-path. In 1991, Nishigami developed a new inversion method of coda waveforms from local earthquake to localize the inhomogeneous spatial distribution of scattering coefficient in the crust and upper mantle. In this work, and in his later works of 1997, 2000 and 2006, he analyzed tectonically active zones and demonstrated that strong scatterers are related with the major active faults. He also verified that horizontal variation of scattering coefficient is smaller in the uppermost mantle than

in the crust.

Successively, Taira et al. (2003) estimated the spatial distribution of small-scale heterogeneities as anomalous amplification of coda level in the Hidaka region, Japan. They estimated the coda wave amplitude for each source - station pair, after the correction for the site effect, finding anomalies in the amplitude values due to the non-uniform distribution of heterogeneities.

The work developed in this thesis grow up in this context as it aims to localize the heterogeneity below two of the campanian volcanoes: Campi Flegrei and Mt. Vesuvius.

Chapter 2

Experimental properties of coda waves

The most prominent evidence for the short-wavelength random heterogeneity of the earth is the presence of coda waves in seismograms. Typically on high frequency seismograms of local earthquakes the direct S wave is followed by wave trains whose amplitude decreases smoothly with time. These wave trains are called "S coda waves". Initially the word "coda" was used to refer to the oscillations of the ground persisting after the surface waves passage. Successively, this word has been used to refer to all wave trains except the direct waves: "P coda" for waves between P and S wave and "S coda" for waves following the direct S-wave (see figure 2.1). The term "Coda waves" is commonly used to indicate the "S coda wave".
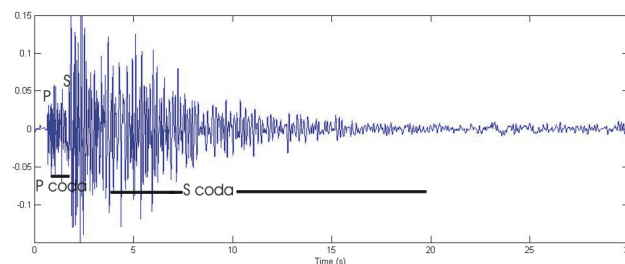
Figure 2.1: Seismogram of a local earthquake recorded on 16 January 1984 by the E-W component of the station W04 located at Campi Flegrei. The P and S arrival and P and S coda are indicated. The amplitude is in cm/s.

Rautian and Khalturin (1978) studied coda amplitude for a wide range of lapse time and frequency bands and found that early portions of the coda are different from station to station; however, the coda of bandpass-filtered seismograms have a common

shape at all stations after about two times the S wave travel time from the source to the receiver. This shape is the same independently of the epicentral distance and of the location of sources and receivers (see figure 2.2).
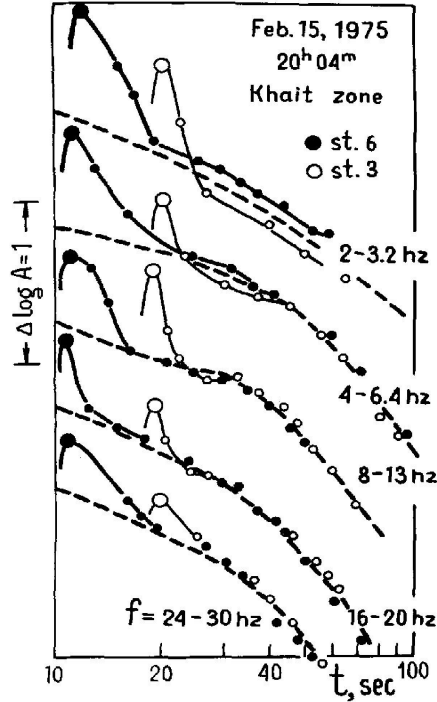
Figure 2.2: Coda envelopes versus time for a local earthquakes of the Khait region, Central Asia, recorded at two different stations (Rautian and Khaltuin, 1978).

As said in section 1.1, the magnitude of local earthquakes calculated from the average of the direct wave amplitudes measured at many stations after a distance correction has been found to be proportional to the logarithm of the duration of a local seismogram (Solov'ev, 1965). This correlation between magnitude and duration time is consistent with the similarity in shape of the later portion of seismograms observed at regional seismic stations and with the conclusion that coda portions of seismograms are composed of scattered waves.

The nature of coda waves has been studied using array observations. Aki and Tsujiura (1959) analyzed correlations of seismograms among six vertical-component seismographs deployed on granitic rock at the foot of Mt. Tsukuba in Kanto, Japan, and they showed that the direct waves are dominated by energy arriving from the direction of the event. On the other hand, the S coda shows no consistent arrival directions. Successive analysis (Spudich and Bostwick, 1987, Scherbaum et al., 1991) on the arriving direction of coda waves showed that the early coda, starting immediately

after the direct S wave and ending at twice the S wave travel-time, was dominated by waves that are multiply scattered near the station since the propagation direction is upward and almost the same as the direct S wave. However, latter S coda waves are composed of wavelets leaving the source region in a variety of directions (the preferential arriving direction of the seismic waves to the array is shown in figure 2.3). The transition between the two types often takes place 1.5 - 2 times the S wave travel-time from source to receiver. The pulse broadening around the direct S wave was explained by Abubakirov and Gusev (1990) using the forward scattering approximation (large angle between incident and scattered wave direction).
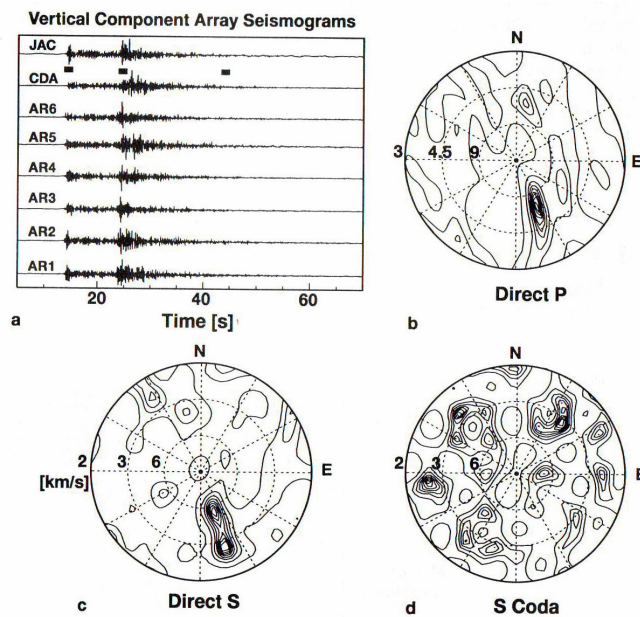
Figure 2.3: (a) Vertical component seismograms recorded by an array located in the Valles Caldera, New Mexico, USA. The earthquake recorded is located approximately 80 km SSE of the array. (b) Results of the frequncy-wavenumber analysis calculated for the filtered (between 2 and 5 Hz) vertical component in a time window around the direct P-arrival. (c) Results of the frequncy-wavenumber analysis of the EW component data, filtered between 1.3 and 3 Hz, surrounding the direct S-arrival. (d) Results of the frequncy-wavenumber analysis of the EW component S coda data, filtered between 1.3 and 3 Hz, beginning 20 s after the direct S-arrival (Sato and Fehler, 1998).

The above observation strongly suggested an incoherent nature for high-frequency coda waves. We cannot expect phases other than direct P and S waves if the propagation medium is transparent.

The composition of coda waves has been extensively studied and it become evident that scattered waves are principally S waves. This assumption has been supported by various observations, such as common site amplification (Tsujiura, 1978) and common

attenuation (Aki, 1980b, Sarker and Abers, 1998) between S waves and coda waves. The theoretical observation that the S to P conversion scattering due to a localized heterogeneity is an order of magnitude smaller than the P to S scattering supports this assumption (Aki, 1992, Zeng, 1993).

The evidence that the seismograms recorded in boreholes shows different coda shapes from the seismograms recorded uphole leaded to conclude that the contribution of surface waves cannot be neglected. Models for coda envelopes which include scattered surface waves are fitted to data recorded in Parkfield, USA, by Blakeslee and Malin (1990) and on the Etna Volcano, Italy, by Del Pezzo et al. (2007). The theoretical formulation for the coda wave envelope that take into account the S to S and S to surface waves conversion is described by Zeng (1996).

The coda waves of local earthquakes can be described by the time dependent power spectrum $P(\omega \mid t)$ where ω is the angular frequency and t is the lapse time. As stated from the Parceval theorem, $P(\omega \mid t)$ can be calculated as the square of the bandpass (centred on ω) filtered velocity seismogram or as the squared Fourier amplitude obtained from a time window centered in t. The peculiar property of the coda power spectrum is the simple separability of the effect of seismic source, propagation path and recording site response expressed by the following equation:

$$P_{ij}(\omega \mid t) = S_j(\omega)R_i(\omega)C(\omega \mid t) \tag{2.1}$$

for t grater than about twice the travel time of S waves from the j-th earthquake to the i-th station. Crucial is the meaning of this equation as $P_{ij}(\omega \mid t)$ can be written as a product of a term that depends only on the earthquake source, $S_j(\omega)$, a term that depends only on the recording site, $R_i(\omega)$, and a term common to all the earthquakes and recording sites in a given area, $C(\omega \mid t)$ (Aki, 1969). Numerous studies demonstrated the validity of equation (2.1) for earthquakes around the world, as summarized in a review article by Herraiz and Espinosa (1987) and in the book of Sato and Fehler (1998). For this peculiarity coda waves are used for a variety of practical applications, including mapping of the frequency-dependent site amplification factor (Phillips and Aki, 1986, Su and Aki, 1995), discriminating the quarry blasts from earthquakes (Su et al., 1991) and for determining frequency-dependent attenuation coefficients with the single station method (Mayeda et al., 1992). In the following chapters I will describe the properties of the function $C(\omega \mid t)$.

Chapter 3

Models of coda waves excitation

As already discussed, the excitation of S coda waves is one of the most compelling pieces of evidence supporting the existence of random heterogeneity in the lithosphere. By treating the earth's lithosphere as a random and uniform distribution of point-like scatterers in a homogenous background medium having a constant propagation velocity, Aki (1969), Aki and Chouet (1975) and Sato (1977) studied the coda waves as single backscattered waves. Since then, the single backscattering model has been widely used to interpret the observations. However this model neglects all the other multiple scattered waves. In order to clarify which is the approximation introduced by the use of the single scattering models many theories have been proposed and a number of numerical simulations have been conducted to investigate the multiple scattering process. Kopnichev (1977) and Gao et al. (1983) studied the two- and three-dimensional multiple isotropic scattering problem by adding higher order scattered wave contributions to the single scattering model; however, their models do not conserve total energy. Using a different approach, Wu (1985) introduced stationary energy transport theory for the multiple scattering problem. He was the first to apply this method to the study of the high-frequency seismogram envelopes of local earthquakes. The multiple scattering method was first used in the field of astrophysics to describe multiple scattering of light (Chandrasekhar, 1960). At that time it was derived phenomenologically on the basis of conservation of energy. Later, the equation of radiative transfer was derived directly from the wave equation in the case of acoustic waves (Rytov et al., 1987) as well as in the case of elastic waves (Weaver, 1990). Wu and Aki (1988) used the energy transport theory to separate the effects of scattering and intrinsic attenuation for the Hindu Kush region.

Using a 2-D and 3-D finite difference simulation of wave propagation in inhomoge-

neous media, Frankel and Wennerberg (1987) developed an alternative phenomenological model called the energy-flux model. In their model the waves scattered from the direct wave rapidly spread over the spherical volume behind the direct wavefront. The spatiotemporal distribution of energy for the energy-flux model is consistent with observations that seismograms envelopes recorded at different distances asymptotically approach a common decay curve and with the similarity of coda amplitude in the region behind the S wavefront for large lapse time.

Hoshiba (1991) used a Monte Carlo simulation to study the multiple isotropic scattering problem incorporating the energy conservation low. His results provided a numerical proof of the energy conservation for the multiple scattering model. For large lapse time, direct energy is small and the multiple scattering will dominate compared with the single scattering.

In the case of strong multiple scattering the equation of radiative transfer reduces to the diffusion equation. Weaver (1990) showed that this is also true for the case of elastic waves. The diffusion equation is much simpler, compared with the multiple scattering equation, and analytical solutions can be obtained. The diffusion model, because of its simplicity and its good fit with the late coda envelope, has been in use before realizing that is the approximation of the multiple scattering model for late lapse time and high scattering (Zeng et al., 1991). The diffusive solution was used to explain the seismograms recorded on the Moon (Nakamura, 1970), the late coda of local earthquakes (Margerin et al., 1998b) and seismograms recorded on volcanoes (Wegler, 2004).

Zeng et al. (1991) formulated the scattered wave energy equation by extending the stationary energy transport theory described by Wu (1985) to the time dependent case. Zeng provided a complete analysis of scattered wave energy propagation in a random isotropic scattering medium.

In this chapter I will present first the complete multiple scattering model formulated by Zeng (1991) and successively I will introduce the two extreme approximations to this model: single scattering and diffusion model.

3.1   Multiple scattering model

Modelling the lithosphere as homogeneous background medium filled with a randomly homogenous and isotropic distribution of point-like scatterers with number density n_0, the scattering coefficient g is given by the product of the number density of the scatterers and the differential scattering cross section, $\frac{d\sigma}{d\Omega}$ (Aki and Chouet, 1975, Sato and Fehler, 1998):

$$g = 4\pi n_0 \frac{d\sigma}{d\Omega} \tag{3.1}$$

g has the dimension of reciprocal length and is used to characterize the scattering power. In this formulation, is not possible to distinguish between a small number distribution of strong scatterers and a large number of weak scatterers. The total scattering coefficient, η_s, is defined as the average over all directions:

$$\eta_s = n_0\sigma = l^{-1} \tag{3.2}$$

where σ is the integral of the differential scattering cross section over a solid angle and l^{-1} is the reciprocal of the mean free path. The values found for η_s are shown in figure 3.1.
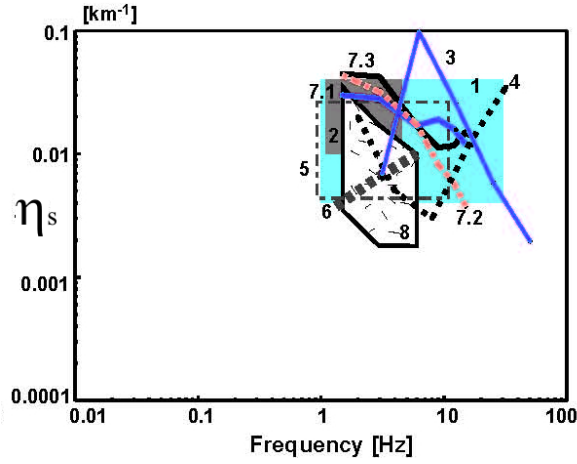

Figure 3.1: Total scattering coefficient η_s for S to S scattering vs. frequency from regional measurements made throughout the world: results obtained using the single scattering model are labeled 1-5 (plots include backscattering coefficient): 1-2, Kanto, Japan; 3, New Brunswick, Canada ; 4, western Nagano, Japan; 5, central Greece. Results based on the multiple lapse-time window analysis (Isotropic scattering is assumed) are labeled 6-8: Kanto-Tokai, Japan; 7.1, central California; 7.2, Hawaii; 7.3, Long Valley, California; 8, 16 measurements in Japan. Detailed references are given by Sato and Fehler (1998) (reprinted from Sato and Fehler, 1998).

Assuming an impulsive spherical source, the scattered wave energies in a 3-D elastic medium with unperturbed velocity v and randomly distributed scatterers are directly additive and the energy equation in this medium at time t can be written as:

$$E(r,t) = E_{in}(\mathbf{r}_0, \mathbf{r}, t - \frac{|\mathbf{r} - \mathbf{r}_0|}{v}) + \sum_{\mathbf{r}_1 \neq \mathbf{r}} E_s(\mathbf{r}_1, \mathbf{r}, t - \frac{|\mathbf{r}_1 - \mathbf{r}|}{v}) \tag{3.3}$$

The first term on the right-hand side of equation (3.3) indicates the incident wave energy, emitted from the source located in $\mathbf{r}_0$, at the receiver point $\mathbf{r}$. The second term is the sum of all the incoherent wave energies generated by an incident wave

arriving at all possible scatterer points $\mathbf{r}_1$ and reaching the receiver $\mathbf{r}$. Assuming the medium defined above, characterized by uniformly distributed isotropic scatterers, the scattered wave energy can be expressed as the product of:

- the scattering cross section σ,

- the energy density at the scattering point $E(\mathbf{r}_1, t - \frac{|\mathbf{r}_1 - \mathbf{r}|}{v})$,

- the geometrical spreading factor for the spherical body waves $\frac{1}{4\pi|\mathbf{r}_1 - \mathbf{r}|^2}$,

- the scattering and intrinsic attenuation occurring over the path from the scattering point to the receiver $e^{-\eta|\mathbf{r}_1 - \mathbf{r}|}$; where $\eta = \eta_i + \eta_s$, η_i is the intrinsic absorption coefficient.

Likewise the incident wave energy expression, first term on the right-hand side of equation (3.3), can be expressed using the same parameter for geometrical spreading and attenuation. Equation (3.3) becomes (Zeng et al. 1991):

$$
\begin{aligned}
E(r,t) &= E_{in}(\mathbf{r}_0, \mathbf{r}, t - \frac{|\mathbf{r} - \mathbf{r}_0|}{v}) \frac{e^{-\eta|\mathbf{r} - \mathbf{r}_0|}}{4\pi \, |\mathbf{r} - \mathbf{r}_0|^2} \\
&\quad + \int_V \eta_s E(\mathbf{r}_1, t - \frac{|\mathbf{r}_1 - \mathbf{r}|}{v}) \frac{e^{-\eta|\mathbf{r}_1 - \mathbf{r}|}}{4\pi \, |\mathbf{r}_1 - \mathbf{r}|^2} dV_1
\end{aligned}
\tag{3.4}
$$

In equation (3.4) any scatterer is assumed to be a new source and the energy is summed up to find the total energy that reaches the receiver. As well shown in Zeng's paper, by an iterative manipulation, the integral part of equation (3.4) can be decomposed into a sum of Neumann series with each term characterized by a power of scattering coefficient η_s. The first-order term gives the wave energy scattered once from all possible scatterer points $\mathbf{r}_1$ to the receiver point $\mathbf{r}$. That is the equation used in the single scattering model.

The solution of equation (3.4) in one dimension has been solved a long time ago by Hemmer (1961) for particle physics. In two and four dimensions an explicit solution can be found, as shown by Zeng et al. (1991) and Paasschens (1997). In three dimensions the solution is obtained numerically. Paasschens (1997) and Zeng (1991) found different analytical approximations. Using numerical examples Zeng et al. (1991) showed that multiple scattering becomes very important as the scattering coefficient increases. As shown in figure 3.2, for the weak scattering case (figure 3.2.a), the single scattering and the energy flux model agrees well with the multiple scattering solution. For the strong scattering case (figure 3.2.b), the diffusion model approximate quite well the multiple scattering model, whereas the single scattering and the energy flux model underestimate the energy values. In case of no intrinsic attenuation, figure 3.3 shows that the contribution of multiple scattering dominates over the single scattering for lapse times larger than the mean free time, $\bar{t} >> 1$, where $\bar{t}$ is a non-dimensional quantity equals to $v\eta_s t$.

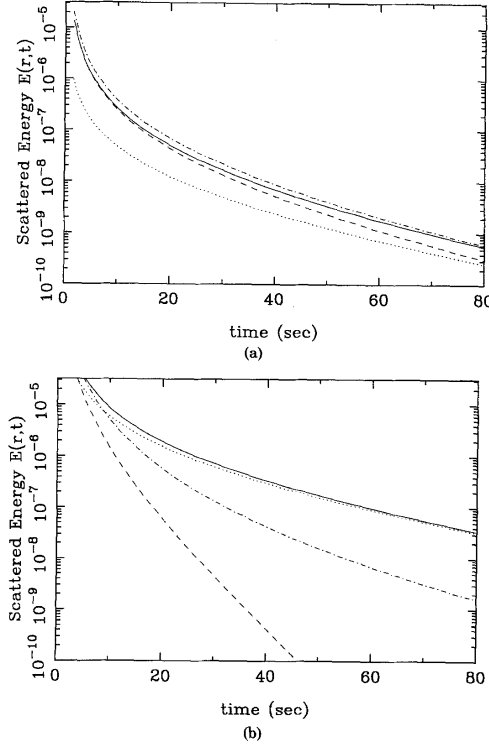Zeng's assumption is to keep the direct and the single scattered wave energy ex-

Figure 3.2: (a) Scattered wave energy decay curves for the source receiver co-located case with $E_0 = 1$, $v = 3$ km/s, $\eta_i = 0.01$ km^{-1}, $\eta_s = 0.002$ km^{-1}. Solid curve represents the multiple scattered wave equation solution of Zeng that is compared with the results of single scattering (dashed), energy flux (dot dashed) and diffusion model (dot lines). (b) Same as (a) but for the scattering coefficient $\eta_s = 0.05$ km^{-1} (Zeng, 1991).

pression and let the rest of the multiple scattered wave energy distributed in space and time as if it were a causal diffusion energy field. In this way Zeng obtained an approximate solution for the multiple scattered wave energy that is usually referred to as hybrid single-scattering-diffusion solution:

$$
\begin{aligned}
E(r,t) \quad \simeq \quad & E_0 e^{-\eta v t} \left[\frac{\delta(t - r/v)}{4\pi v r^2} + \frac{\eta_s H(t - r/v)}{4\pi v r t} \ln\left(\frac{1 + r/(vt)}{1 - r/(vt)} \right) \right] \\
& + cH\left(t - r/v\right) \left(\frac{3\eta_s}{4\pi vt} \right)^{3/2} e^{-\frac{3\eta_s r^2}{4vt} - \eta_i vt}
\end{aligned}
\tag{3.5}
$$

where c is obtained from the energy conservation condition that let the total causal diffusion energy equal the rest of multiple scattered energy for the scattering order
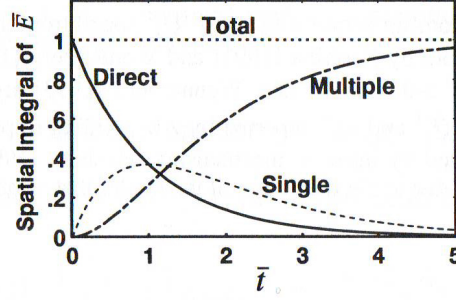
Figure 3.3: Temporal variation in the spatial integral of the normalized energy density for direct, single scattering and multiple scattering for the case of no intrinsic attenuation (Sato and Fehler, 1998)

higher than two:

$$c = \frac{E_0 \left[1 - (1 + \eta_s vt)\, e^{-\eta_s vt}\right]}{\left(\frac{4}{\sqrt{\pi}} \int_0^{\sqrt{3\eta_s vt}/2} e^{-\alpha^2} \alpha^2 d\alpha\right)} \tag{3.6}$$

3.2   Single scattering model

The first-order term of the multiple scattering energy equation gives the wave energy scattered once from all possible scatterers, which coincides with the formulation of the single scattering model. This model was described first by Aki and Chouet (1975) for the case of common source and receiver location. The authors assumed the scattering as a weak process and used the Born approximation i.e. the loss of energy from the primary waves as well as the multiple scattering is neglected. The model was successively generalized for the case of general source and receiver location getting to the form (Sato, 1977):

$$E_{ss}(r,t) = \frac{\eta_s E_0 H(t - r/v) e^{-2\pi f Q_c^{-1} t}}{4\pi v r t} \ln\left(\frac{1 + r/(vt)}{1 - r/(vt)}\right) \tag{3.7}$$

When $vt \gg r$ the equation can be reduced to:

$$E_{ss}(r,t) \simeq \frac{\eta_s E_0}{2\pi v^2 t^2} e^{-2\pi f Q_c^{-1} t} \tag{3.8}$$

that is the expression found by Aki and Chouet. The exponential term $e^{-2\pi f Q_c^{-1} t}$ takes into account the energy lost for intrinsic and scattering attenuation. Q_c^{-1} is the so called coda attenuation factor. It can be estimated from experimental data best fitting the filtered coda envelopes to the single scattering model. The Q_c values result to be dependent on frequency. Its physical meaning is argument of manifold

discussions. I will face this problem in the next chapter.

3.3 Diffusion model

As lapse time increases, the multiple scattering will dominate compared to the single one. In the case of strong multiple scattering the equation of radiative transfer reduces to the diffusion equation. Weaver (1990) showed that this is also true for the case of elastic waves. The diffusion equation can be analytically solved. It was used to explain the seismograms recorded on the Moon (Nakamura, 1970), the late coda of local earthquakes (Margerin et al. 1998b) and seismograms recorded on volcanoes (Wegler, 2004). Consider a medium having a randomly homogenous and isotropic distribution of isotropic scatterers in which energy E_0 is spherically radiated from a source located at the origin and the source time function is a delta function in time. The analytical solution of the diffusion equation, at the frequency f, can be written:

$$E_D(r,t) = \frac{E_0}{(4\pi Dt)^{3/2}} e^{-\frac{r^2}{4Dt} - \eta_i vt} H(t) \tag{3.9}$$

where $D = \frac{v}{3\eta_s} = \frac{vl}{3}$ is the diffusivity for isotropic scattering.

The diffusion equation has been widely used for the coda wave modelization as it gives analytical solution also in the case of depth dependent scattering coefficient. In particular Margerin et al. (1998 and 1999), presented an analytical solution for the problem of a scattering layer over an homogeneous half space. In comparison to the diffusion equation in a full space an additional exponential decay arises, which describes the continuos loss of energy from the scattering layer into the underlying homogeneous half space. This solution was applied to the Vesuvius volcano by Wegler (2004).

3.4 The frequency dependence of the models

In the above models we always consider the scatterers as point-like heterogeneities, but as it is shown in figure 3.4 the scale length of heterogeneities, linear dimension of the heterogeneities, in the crust spans eight order of magnitude. The largest inhomogeneity scale length is of the order of the Earth circumference, as oceans and continents, while the smallest may be the dimension of the grain size of crystals or the length of microcracks in rock. These heterogeneities with different scales have different effects to the seismic waves (Wu and Aki, 1988a).

In order to get an overall view on the seismological scattering problems, it is possible to classify the different regions using the two non-dimensional parameter controlling the scattering phenomena, $k\alpha$ and kL. $k\alpha$ is 2π times the ratio of inhomogeneity scale
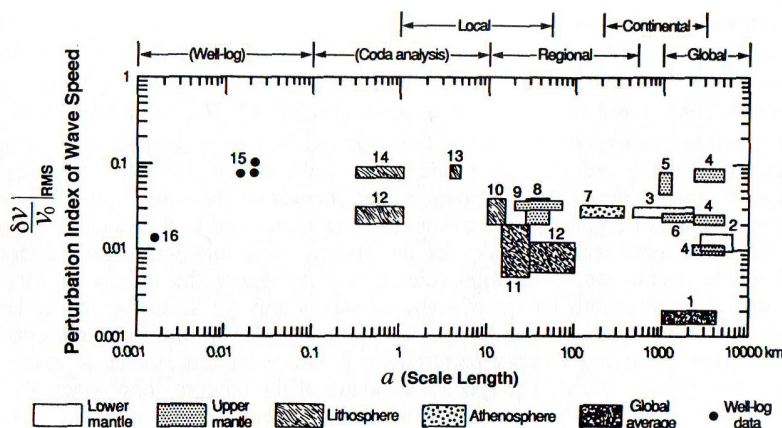
Figure 3.4: Strength-scale distribution of heterogenities in the earth estimated by various methods: 1, global average, free oscillation splitting mode; 2-3, lower mantle, velocity tomography; 4-9, upper mantle, surface wave inversion and velocity tomography; 10-12, lithosphere, transmission fluctuation; 13-14, lithosphere, coda wave excitation; 15-16 upper crust, acoustic well log (Wu and Aki, 1988)

length α to the wavelength λ, and measures the smoothness or roughness of inhomogeneity within a wavelength. kL is 2π times the number of wavelength traveled by the primary waves through an inhomogeneous region. Figure 3.5 shows the different scattering phenomena in terms of the different propagation regimes. The wave parameter D that appears in figure 3.5 is the ratio of the size of the first Fresnel zone to the scale length of inhomogeneities:

$$D = \frac{4L}{k\alpha^2} \tag{3.10}$$

When D is small, and in particular, when $\alpha > L$ the inhomogeneity is so smooth that can be considered a piecewise homogeneous region; the earth medium is than equivalently homogenous, characterized by averaged properties, till to the value of $k\alpha < 0.01$. The scattering may become negligible when the inhomogeneity scale is much smaller than the wavelength. The problem becomes more complex when $1 < k\alpha < 10$. In this interval the Born approximation is valid. In particular, when $k\alpha < 1$, the propagation regime is of the Rayleigh type and the scattered power is proportional to k^2. When $k\alpha \simeq 1$, the sizes of heterogeneities are comparable to the wavelength and the scattering effects are most significant. This is called large-angle scattering or Mie scattering regime. When $k\alpha >> 1$, most of the scattered power is concentrated near the forward direction and the scattering regime is called small-angle scattering or forescattering regime (Wu and Aki, 1988a, Aki and Richards, 1980). Our analysis are concentrated in the Mie scattering regime. In the interpretation of the scattering analysis it is important to take into consideration the frequency band used
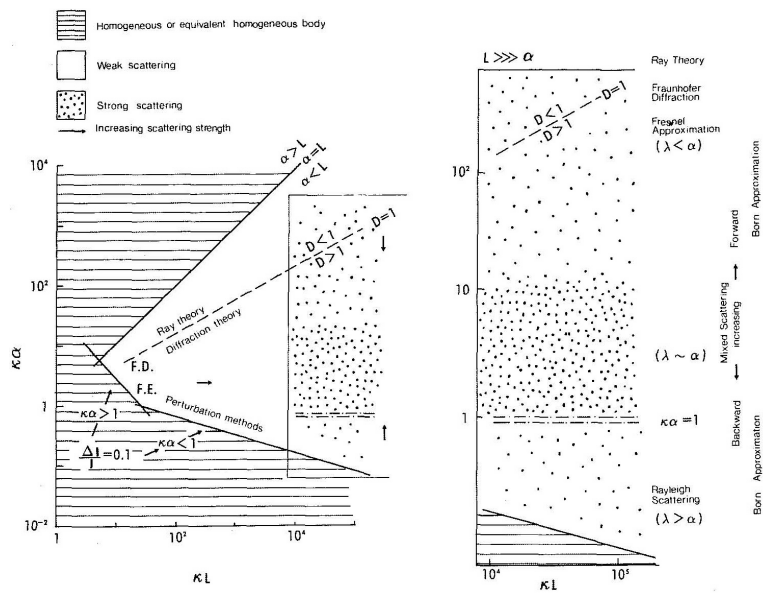
Figure 3.5: Classification of scattering problems and applicable methodes in the $k\alpha - kL$ diagram. Left: general overview. Right: region of interest for the scattering phenomena (Herraiz and Espiosa, 1987).

for the analysis as it is in a biunivocal correlation with the heterogeneity size.

Chapter 4

Seismic parameters derived by coda waves analysis

Since the initial studies of coda waves it has been clearly stated that coda waves are an effective resource in estimating source and site parameters and in extracting informations about the characteristics of wave paths. The power of coda waves resides in its stability. We are especially interested in the parameters that characterize the medium spanned by the seismic waves. Coda waves can be used to estimate the attenuation quality factors and the scattering coefficient.

4.1 Attenuation of high-frequency seismic waves

Seismic wave amplitude decreases with increasing travel distance through the earth. This change in amplitude is usually exponentially related to travel distance and decay rates are proportional to Q^{-1} which characterizes the spatial total attenuation for P or S waves, Q_P^{-1} and Q_S^{-1} respectively. The parameter Q is called the quality factor of the medium and is defined as:

$$Q = -2\pi \frac{E}{\Delta E} \tag{4.1}$$

where E is the peak strain energy stored in the volume and $-\Delta E$ is the energy lost in each cycle because of imperfections in the elasticity of the material and because of the loss for scattering (Aki and Richards, 1980). Seismic attenuation is principally due to intrinsic and scattering attenuation, so that the total attenuation is the sum of the two:

$$Q^{-1} = Q_{sc}^{-1} + Q_i^{-1} \tag{4.2}$$

The attenuation is expressed by the inverse of the quality factor. The relation between the scattering or intrinsic attenuation and the scattering or intrinsic coefficient is:

$$\eta_{s|i} = \frac{2\pi f Q_{sc|i}^{-1}}{v} \tag{4.3}$$

Except when wave interference occurs, for spherically outgoing body waves in a uniform velocity structure, the spectral amplitude of the seismic S wave can be expressed as:

$$u_S(r; f) \propto \frac{e^{-\pi r f Q_S^{-1}/v}}{r} \tag{4.4}$$

where r^{-1} is the geometrical spreading factor for the body waves.

In figure 4.1 the result of Q_S^{-1} measurements from various region of the world are shown (see Sato and Fehler, 1998, for more details). Despite of regional variations, it is clear that Q_S^{-1} is of the order of 10^{-2} at 1 Hz and decreases with increasing frequency to 10^{-3} at 20 Hz. The frequency dependence at $0.1 \sim 1$ Hz remains poorly understood as seismic measurements are difficult to make in this band.
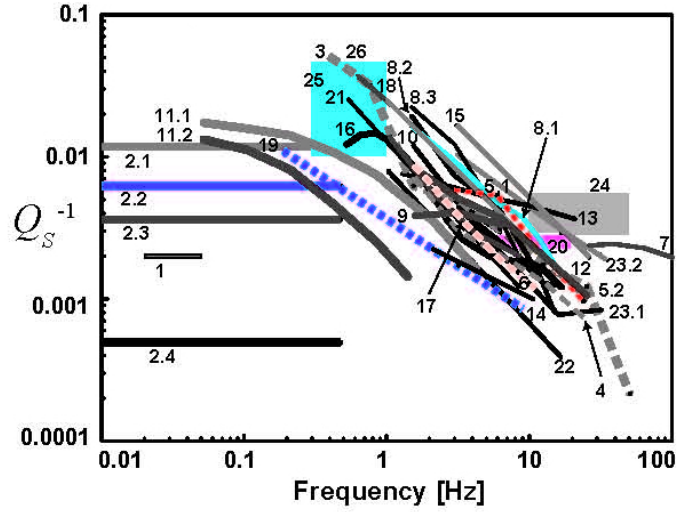

Figure 4.1: Reported values of Q_S^{-1} for the lithosphere: surface wave analysis, 1-7; multiple lapse-time window analysis, 8-12; spectral decay analysis, 11-26 (**?**).

4.1.1   Intrinsic attenuation

Intrinsic attenuation refers to various mechanisms that convert vibration energy into heat through friction, viscosity and thermal relaxation processes. Models of intrinsic

absorption were initially proposed to explain an apparently frequency-independence Q^{-1} at low frequencies (Dziewonski, 1979, Jackson and Anderson, 1970). For seismic waves to remain causal in the presence of attenuation there must be frequency-dependent amplitude and phase changes (Aki and Richards, 1980).

Many proposed methods are based on the observation that crustal rocks have microscopic cracks and pores which may contains fluids and which dimensions are much smaller than wavelength of regional seismic waves. The friction of the cracks or the viscous dissipation in the fluid or the thermal movement of the fluids in the rock structure can predict the experimental values of Q_S^{-1}.

Aki (1980a) discussed a relation between physical dimensions and the observed and partially conjectured frequency-dependence of Q_S^{-1} having a peak on the order of 0.01 around 0.5 Hz. He preferred thermoelasticity as the most viable model to explain intrinsic attenuation at lithospheric temperatures since the required scales for rock grains and cracks along with the amount of attenuation caused by thermoelasticity are in closest agreement with observations.

4.1.2   Scattering attenuation

Scattering due to heterogeneities distributed in the earth also causes a decrease in amplitude with travel distance (Aki, 1980a). The characteristic frequency is determined by a characteristic spatial scale, such as the correlation length of random media or the crack length. The interaction between these heterogeneities and the direct seismic waves generates the coda waves in seismograms. The attenuation per travel distance is approximately constant for 1 to 20 Hz as shown by Yoshimoto et al. (1993) in Kanto, Japan. Its value results of the order of 10^{-1} km^{-1}, which is nearly the same order as the total scattering coefficient η_s of S waves as shown in figure 3.1. The coincidence between η_s and lQ_S^{-1} (where l is the mean free path) leads to the idea that scattering attenuation may be the dominant mechanism for amplitude attenuation of seismic waves in the lithosphere (Aki, 1980a, Aki, 1982). This position is completely revised by Yoshimoto and Jin (2008). Analyzing the frequency dependence of the ratio of scattering attenuation to the total attenuation calculated by different authors in various seismic regions, Yoshimoto and Jin (2008) show that this ratio gets to 1/2 at about 5 Hz, indicating that scattering and intrinsic attenuation give the same contribution to the total attenuation at this frequency. This ratio decreases with increasing frequency showing that intrinsic attenuation dominates over the scattering one for frequencies above 5 Hz. This trend is due to the different frequency dependence of Q_i^{-1} and Q_{sc}^{-1}, as both decrease with frequency but the decreasing rate is weaker for Q_i^{-1}. Anyway this ratio shows quite different trends from one area to an other as the scattering attenuation is strongly dependent on the size of heterogeneities that characterize the area.

A crucial point is to understand whether the scattering attenuation is controlled by some characteristic scale in time or space. We know that scattering attenuates direct wave amplitude while excites coda waves as scattering redistributes wave energy within the medium but does not remove energy from the overall wavefield. Considering impulsive waves they propagate without large attenuation when the wavelength is shorter than the correlation distance, however the Q_{sc}^{-1} value predicted from the usual mean wave formalism (Born approximation) monotonously increases with frequency even in the high frequency limit. Such a frequency dependence would imply that the high frequency waves, also the ones with wavelength shorter than the correlation distance, would be attenuates more than the low frequency waves. Sato (1982) proposed a statistical method in which the mean wave is defined after the correction of travel-time (phase) fluctuations caused by velocity fluctuation. An other attempt to explain the discrepancy between observations and predictions of Q_S^{-1} trend was made by Wu (1982). He neglects scattering in the forward direction during calculation of the attenuation. A demonstration for scalar wave of the two methods can be found in Sato and Fehler (1998).

The study of the influence on the elastic properties of rocks due to the presence of microscopic cracks and inclusions having length much smaller than the seismic wavelength demonstrated that they have an important influence on the attenuation of seismic waves (Walsh, 1965). In particular it has been shown that the seismograms obtained for waves that travel through a medium containing a suite of solid inclusions are dominated by the direct-arriving energy and have little codas. On the contrary the seismograms for the medium with empty pores contain significant coda energy whose amplitude are similar to those of the direct arrivals (Huang and Mora, 1996). In both cases the inclusions were randomly distributed and have sizes ranging between 0.0625 and 0.15 times the wavelength of the incident wave.

The most important evidence of the scattering effects on the seismic waves is the generation of the seismic coda. However there are other effects of heterogeneity on the propagation of the seismic waves. An important consequence of scattering is that the observed P waves particle motion is elliptical, while, in a simple medium, it should be linearly polarized along the direction of travel in case of absence of any scattering phenomena. The strength of scattering can be calculated using square root of the ratio of the middle to the maximum eigen value of the covariance matrix composed of three-component data for a short interval of time around the P wave (Sato, 1989). In addition, scattering causes a broadening of the pulse width with increasing travel distance while preserve the high-frequency content of waveform. Such a modulation effect has been studied as a tool for characterizing random media (Lerche and Menke, 1986).

4.2   Coda Q

The parameter Q_c, called coda Q, is introduced to express the attenuation in the single-scattering model expressed by equation (3.8) (Aki and Chouet, 1975). Larger Q_c^{-1} means rapid decay of coda amplitude. According to this equation, coda Q^{-1} is the slope of the straight line fitting the measured $\ln(t^2 E_{ss}(\omega|t))$ versus ωt. Since it experimentally results that the slope depends on the time window for which the fit is made, it is necessary to specify the time window for each measured coda Q^{-1} or, that is the same, to specify the time elapsed from the origin time to the coda end, called lapse time. It has been observed that Q_c^{-1} decreases with increasing lapse time and takes almost a constant value after a certain lapse time (Su et al. 1991, Kosuga, 1992). According to Wennerberg (1993), Akinci et al. (1994) and Del Pezzo et al. (1990), a plausible cause of Q_c^{-1} decreasing with lapse time is the decrease of the intrinsic attenuation with depth in the lithosphere. The characteristic lapse time for Q_c^{-1} to become a constant value is frequency and location dependent. It seems to be the tendency that the higher frequencies require earlier lapse time for Q_c^{-1} to reach a stable value. Since the measurement of coda Q^{-1} according to equation 3.8 is very simple, it has been measured worldwide as a local attenuation parameter characterizing the spatial average of the lithospheric seismic attenuation (Singh and Herrmann, 1983, Jin and Aki, 1986). Regional measurements of Q_c^{-1} made through the world have been compared with seismotectonic activity; generally active regions are characterized by low values of Q_c^{-1} and strong frequency dependence (see the review papers of Herraiz and Espinosa, 1987, and Matsumoto, 1995). Figure 4.2 shows a compilation of reported Q_c^{-1} in several area characterized by different tectonic settings. However, the physical meaning of coda Q is still subject of debate. Within the context of the single scattering theory, Q_c^{-1} appears to represent an effective attenuation including both absorption and scattering loss. This idea prevailed after Aki (1980) found a close agreement between coda Q^{-1} and Q^{-1} of S waves measured in Kanto region, Japan. On the other hand, numerical experiments (Frankel and Clayton, 1986), laboratory experiments (Matsunami, 1991) and theoretical studies including multiple scattering effects (e.g. Shang and Gao, 1988) concluded that the Q_c^{-1} measured from the time window later than the mean free time (mean free path divided by wave velocity) should correspond only to the intrinsic absorption and should not include the effect of scattering loss. From several studies in lots of different regions (Hoshiba, 1993, Jin et al., 1994, Mayeda et al. 1992) it appears clearly that coda Q^{-1} is bounded rather narrowly between intrinsic Q^{-1} and total Q^{-1}, although models with nonuniform scattering and absorption coefficients are necessary for a more complete understanding of its physical meaning. With this understanding of coda Q^{-1}, we shall now proceed to the spatial and temporal correlation observed between coda Q^{-1} and seismicity.
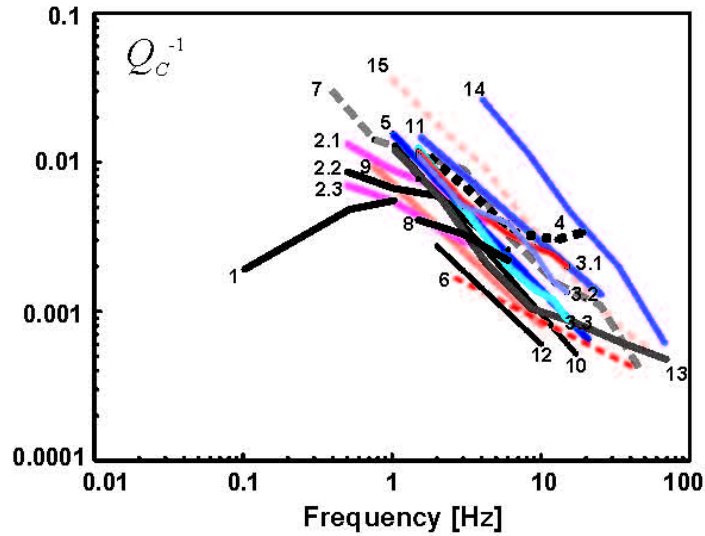
Figure 4.2: Coda attenuation Q_c^{-1} against frequency for various regions: 1, central and south central Alaska; 2.1, Iceland, 2.2, Galapagos, 2.3, Guam, oceanic lithosphete; 3.1, central Califonia; 3.2, Hawaii; 3.3, Long Valley in California; 4, Campi Flegrei volcano, southern Italy; 5, Dead sea; 6, Garm, central Asia; 7, Hindu-Kusu; 8, Kanto-Tokai, Japan; 9, New England, USA; 10, southern Norway; 11, Petatlan, Gurrero, Mexico; 12, South Carolina, USA; 13, western Nagano, Japan; 14, shallow crust at Ashio, Kanto, Japan; 15, shallow crust at western Nagano, Japan (from Sato and Fehler, 1997)

4.2.1   Geographic variation in coda Q^{-1}

Numerous studies show that coda Q^{-1} varies systematically with the tectonic activity (Singh and Herrmann, 1983, Jin and Aki, 1988, Hoshiba, 1993). As evinced from figure 4.2, these variations can be larger than one order of magnitude. For example, large coda Q^{-1}, at high frequencies, has been observed around active volcanoes, implying strong intrinsic absorption due to high temperature volcanic medium (Matsumoto and Hasegawa, 1989, Wu et al., 1988).

Singh and Herrmann (1983) were the first to construct a map of coda Q^{-1} all over the USA. The spatial resolution was quite poor, since the stations and earthquakes coverage in several areas was sparse. Subsequently Baqer and Mitchell (1998) estimated the Lg coda Q^{-1} regional variation of the entire United States. From their results it appears clearly that the United States can be divided into two large Q^{-1} provinces. One spans the east part and is characterized by low coda Q^{-1}; the other spans the weaves part and is characterized by high coda Q^{-1} values. This two provinces are divided by the Rocky Mountains. Clearly California has the highest coda Q^{-1} and the northeast has the lowest indicating that coda Q^{-1} reflects the current seismicity better than other geophysical parameters such as P and S velocity. Similar results
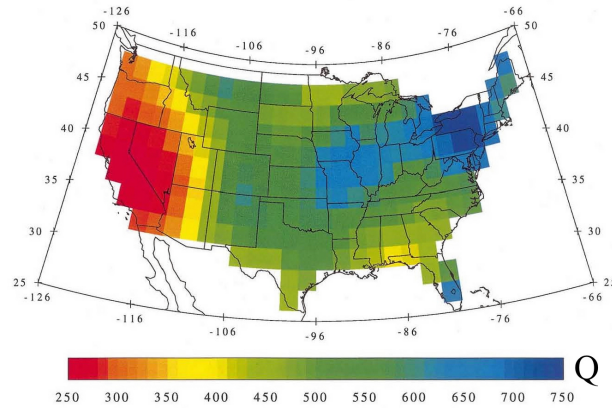
Figure 4.3: Tomographic map of Lg coda Q at 1 Hz for the continental United States (Baqer and Mitchell, 1998)

were found by Jin and Aki (2005) for Japan. They performed an high resolution coda Q analysis finding that there is an high frequency dependence of Q^{-1}. In general, high coda Q^{-1} regions in the lower frequencies are correlated with seismically active areas, while high coda Q^{-1} areas for higher frequencies are correlated with the areas of quaternary volcanoes.

The spatial coincidence found by these studies shows the importance of the coda Q^{-1} parameter that may help in modeling the earthquakes loading process.

4.2.2 Temporal change in coda Q^{-1}

The observed correlation of coda Q^{-1} with the level of tectonic activity leaded to analyze wether it shows any variation in correspondence to earthquakes or volcanic eruptions.

Chouet (1979) was the first to report a significant temporal change in Q_c^{-1} at Stone Canyon, California, during an observational period of about one year. This increase in Q_c^{-1} showed a weak negative correlation with the temporal change in the Gutenberg-Richter b parameter (Aki, 1985). The b parameter is a measure of the ratio between the number of small to large earthquakes and is defined by the formula $\log N = a - bM$, where N is the number of the events with magnitude greater than M.

As is going to be shown, several study revealed that the temporal correlation between coda Q^{-1} and seismicity is not as simple as the spatial one described above. In 1986, Jin and Aki observed a temporal increase in Q_c^{-1} before the occurrence of the Tanghshan earthquake ($M_S = 7.9$, July 27, 1976), China; they also described a temporal change of Q_c^{-1} before and after the Haicheng earthquake ($M_S = 7.3$, February

4, 1975), China. Gusev and Lemzikov (1985**?**) reported a precursor-like decrease in coda decay parameter, corresponding to an increase in Q_c^{-1}, a half year before the Ust-Kamchatsk earthquake ($M_S = 7.8$, December 15, 1971) in Kamchatka. An increase in scattering among individual measurements of Q_c^{-1} was reported before an earthquake with $M_L = 5.2$ (February 26, 1983) in central Asia (Sato et al., 1988); while a change in the relationship between coda duration and local magnitude determined from the network average of maximum amplitudes was reported by Sato (1987) for the western Nagano earthquake ($M_S = 6.8$, September 14, 1984) in Japan. Yan and Mo (1984) reported a decrease of the ratio of coda duration on the horizontal component to that on the vertical one few days before the Jianchuan earthquake ($M_L = 5.3$, July 27, 1976) in China. The temporal change in Q_c^{-1} has been studied also as a precursor for volcanic eruptions. Fehler et al. (1988) reported a change in Q_c^{-1} before and after an eruption of Mt. St. Helens volcano as is shown in figure 4.4. Jin and Aki (1989)
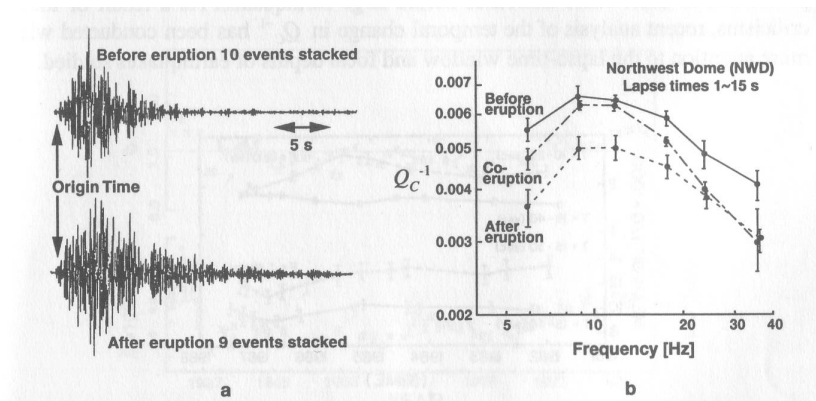
Figure 4.4: a) Stacked seismograms before and after an eruption of Mt. St. Helens showing the different coda characteristics for the two periods. b) Coda attenuation before, during and after the eruption (Fehler et al. 1988)

reported a systematic temporal change in coda Q^{-1} for southern California for the 55 year between 1933 and 1987. They also found a strong positive correlation between coda Q^{-1} and b parameter. In a review paper of 1993, Jin and Aki had to conclude that the coda Q^{-1} precursor is not reliable, because a similar pattern sometimes was not followed by a major earthquake, and some major earthquakes were not preceded by the pattern. In addition there are many criticisms of these studies. The most serious ones concern the fact that many investigators who have studied temporal variation have not reported the lapse times used, and their results may be influenced by variation in the lapse times. An other criticism concerns the different focal mechanisms of the analyzed earthquakes that can significantly influence the early coda. And finally the signs of Q changes are not systematic among the studies reported; sometimes increases

before the earthquakes, sometimes decreases.

Several convincing cases of temporal correlation between coda Q^{-1} and b value are also reported. Also in this case the results showed a negative correlation in some cases (Aki, 1985, Jin and Aki, 1986) and a positive correlation in other cases (Jin and Aki, 1989). Jin and Aki (1989) proposed the creep model, in which creep fractures near the brittle-ductile transition zone of the lithosphere are assumed to have a characteristic size in a given seismic region. The increased creep activity in the ductile part would then increase the seismic attenuation and, at the same time, produce stress concentration in the upper brittle part favoring the occurrence of earthquakes with magnitude M_c corresponding to the characteristic size of the creep fracture. Then, if M_c is in the lower end of the magnitude range from which the b value is evaluated, the b value would show a positive correlation with coda Q^{-1}, and if M_c is in the upper end the correlation would be negative (Aki, 1996).

4.3   Coda normalization Method

The coda normalization method provides a reliable way to separate source, site and propagation effects from the seismic signal. The quantification of these effects is useful in the seismic risk assessment and most of the applied seismology is focused on these studies. The estimate of source and site amplification factors at regional distance relay on the use of direct P or S arrivals on the seismic trace. Since regional networks are usually designed to reliably record mainly the time of the first arrival, the first arrival waveforms are often clipped. The coda waves are generally not clipped and can be used to estimate source and site parameters.

The coda normalization method is based on the empirical observation that the coda energy is uniformly distributed within a region surrounding the source for great lapse times. Support to the method comes from the observation that for local earthquakes at lapse time grater than roughly twice the S wave travel time from the source to the receiver, the envelope of a bandpass-filtered seismogram has a common shape that is independent of the source-receiver distance as shown in figure 2.2. The amplitude of the envelope varies with source size and recording site amplification but the shape remains constant.

Important is to note that the coda normalization method is not founded on any theoretical model of wave propagation in the earth. In particular, it does not relay on the validity of the single scattering model; the original foundation of the approach is empirical (Sato and Fehler, 1998).

The coda normalization method for measuring the direct S wave attenuation with travel distance was first proposed by Aki (1980) and was extended by Yoshimoto et al. (1993) to measure the attenuation of the direct P waves with travel distance. The Aki's method was designed to normalize the source spectral amplitude using coda spectra

at some fixed lapse time to measure the S wave quality factor, Q_S, using single station data. The spectral amplitude of the S wave for the i-th event may be written as:

$$A_i(\omega) = S_i(\omega, \theta) R(\omega, \theta) \frac{\exp(-\pi f D Q_S^{-1}/v)}{D} \tag{4.5}$$

where $S_i(\omega, \theta)$ is the source spectrum radiated in the source - receiver direction θ and $R(\omega, \theta)$ is the site effect at the receiver which may depend on θ. D is the source - receiver distance and it expresses the correction for the geometrical spreading of the body waves. This is the form in which this equation is always found, but the explicit form would contain the ratio $\frac{D}{D_0}$, where D is the radius of the spherical wave and D_0 the radius at the source where the radiation first began, i.e. the critical distance for the far field condition (Shearer, 1999).

On the other hand, when lapse time t is greater than twice the S wave travel time, the coda waves can be written as:

$$A_i^C(\omega, t) = S_i^C(\omega) R^C(\omega) P(\omega, t) \tag{4.6}$$

where $P(\omega, t)$ is independent of both the source - receiver distance and direction. This empirical conclusion can be explained by assuming in the model that coda waves are waves back-scattered from randomly distributed inhomogeneities in the earth (Aki, 1969).

In order to combine equations (4.5) and (4.6) the following assumption has to be made: $\ln(\frac{S_i(\omega, \theta)}{S_i^C(\omega)})$ and $\ln(\frac{R(\omega, \theta)}{R^C(\omega)})$ become independent of θ when averaged over many events in a wide range of directions from the station and that these value have not systematic geographical variation. Taking the natural logarithm of the ratio of hypocentral distance and the direct S wave amplitude to the averaged coda amplitude, the site amplification and source terms cancel out, and we get:

$$\left\langle \ln(\frac{A_i(\omega) D}{A_i^C(\omega, t_0)}) \right\rangle_{D \pm \Delta D} = a - \frac{\pi f Q_S^{-1}}{v} D \tag{4.7}$$

where the logarithm is averaged over events located within a distance range $D - \Delta D$ to $D + \Delta D$. Thus we would expect a linear relation between the left-hand side of equation (4.7) and D. The slope of the linear relation will give the value of Q_S^{-1}. Aki (1980) applied this method to high frequency seismograms of 900 earthquakes recorded in Kanto, Japan and the plot of the results for the left-hand side of equation (4.7) is showed in figure 4.5.
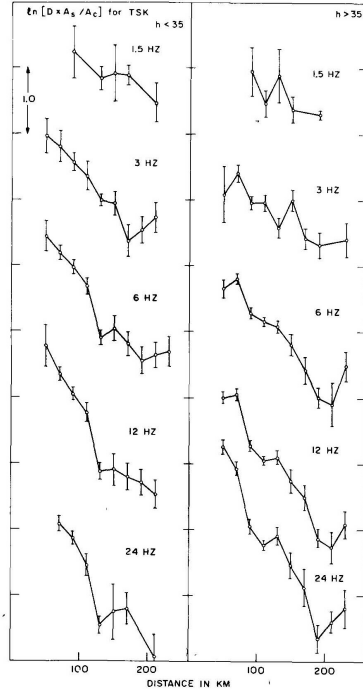
Figure 4.5: The average of the natural logarithm of S to coda ampliude ratio multiplied by soure-receiver distance D plotted against D for station Tsukuba (Aki, 1980a).

4.3.1 Site effects

At lapse time t_c large enough that energy is uniformly distributed in a volume surrounding the seismic source that contains two recording site, the relative amplitude of the seismograms recorded at the two sites should be the same except for the influence of the near-recording site amplification (Sato and Fehler, 1998). Using equation (4.6) the relative amplitude can be expressed as:

$$\frac{A_{i,j}^C(\omega, t_c)}{A_{i,k}^C(\omega, t_c)} = \frac{R_j^C(\omega)}{R_k^C(\omega)} \tag{4.8}$$

where $A_{i,j}^C(\omega, t)$ is the coda amplitude of the i-th event registered at the j-th station and the site, k, is chosen as the reference site. The coda amplitude is usually substituted with the bandpass filtered coda envelope, calculated using the Hilbert transform, to obtain a more robust measure. A more stable result can be obtained by taking the average of the ratio determined for many time windows.

Tsujiura (1987) was the first to demonstrate that the relative site amplification calculated with this method equals the one calculated using the S waves. This demonstration was also used to support the hypothesis that S coda is composed mostly of S waves.

Phillips and Aki (1986) assumed that the shape of the coda decay curves is the same at all sites for all the sources and they assumed that only the amplitude of the curves differs, depending on the site and source factor. They developed an expression relating source factor, site amplification factor and the shape of the common decay curve.

4.3.2   Source effects

The coda normalization method provides an easy method for characterizing the spectral differences in source radiation among seismic sources without requiring knowledge of source radiation pattern or propagation effects. Thus, the relative seismic moment, or magnitude, can be reliably determined using the coda normalization method.

From equation (4.6), the relative source radiation can be expressed as a function of frequency as:

$$\frac{A_{i,j}^{C}(\omega, t_c)}{A_{k,j}^{C}(\omega, t_c)} = \frac{S_i^{C}(\omega)}{S_k^{C}(\omega)} \tag{4.9}$$

where $A_{i,j}^{C}(\omega, t)$ is the amplitude at lapse time t_c of the seismogram recorded at the site j for the i-th event. The source k is chosen as the reference source. In this case we use two different events recorded at the same site.

Since coda waves are scattered, waves leaving the source region in all directions arrive at a given receiver and, at the first order, coda waves average over the radiation pattern of the source.

Mayeda and Walter (1996) compared the source radiation obtained with the direct waves with that obtained using coda waves at two stations. They showed that there is a more consistent relationship between the measurement made on coda waves even though there is a large station separation of 500 km.

Chapter 5

Study of inhomogeneity from fluctuations in coda waves

As explained in the previous chapters, coda waves can be used to analyze the mean attenuation properties of the medium. The time variations in the shape of the coda envelopes are associated with the time variations of the elastic properties and hence with the changes in the stress field acting on the area (Snieder, 2006). On the other hand, the coda waves can also be used for the analysis of the source and site transfer function. In addition, coda waves are used to study the scattering coefficient distribution in the space, when they are recorded by a small aperture array of seismometers and/or by a network of seismic stations. This thesis work is developed in this section and aims to analyze the spatial variations of the scattering properties.

The analysis developed for the back-scattering imaging can be considered as an extension of the techniques used in reflection seismology. Reflection seismology considers wavelets reflected by discontinuities; scattering imaging, instead, assumes isotropic scattering and locate the position of the scatterers emitting more energy.

The models for S coda envelopes described in chapter 3 are based on the assumption of a homogenous distribution of isotropic scatterers and predict results consistent with the observed characteristics of coda. However, detailed observations show that there may be departures from the observed characteristics of S coda waves. In this case a coordinate-dependent total scattering coefficient may be introduced in the theory.

Nishigami (1991) developed a technique to estimate the spatial inhomogeneity of the total scattering coefficient using the temporal differences between the coda envelope registered and the one predicted from the single scattering theory. Also Nishimura et al. (1997) used the single scattering approach to generate synthetic data and fit the observed envelopes with them. They used the explosions of an active experiment conducted across the Jemez volcanic field, New Mexico, USA, as sources.

As shown by Taira (2004) the use of local seismic array gives an alternative possibility of estimating the spatial distribution of heterogeneities beneath the array in a deterministic way. The application of array techniques (e.g. semblance analysis and frequency-wavenumber, $f - k$, spectral analysis) allows the quantitative estimate of the distribution of small scale heterogeneities from coherent arrivals in coda. Gupta et al. (1990) analyzed the seismic signal generated by US and USSR nuclear explosions on a seismic array using the $f - k$ analysis and located several distinct scatterers. The 1995 Hyogo-ken Nanbu earthquake was analyzed by Matsumoto et al. (1998) using the slant stack method and the presence of strong scatterers just below the hypocenter was shown. In Italy, La Rocca et al. (2001) analyzed the seismograms from explosive sources recorded from an array located on Mt. Vesuvius. They found a high concentration of scatterers in and around the volcanic edifice, suggesting that topographical irregularities play an important role in the generation of the scattering phenomena.

An inversion method to estimate the 3-D spatial variation of scattering coefficient that takes into account a realistic velocity model, source radiation and scattering attenuation was developed by Asano and Hasegawa (2004). They analyzed the 2000 M 7.3 Tottori earthquake locating the strong scatterers along and around the main shock fault.

In the next paragraph I will describe the Nishigami's technique that is the one that I use (with some modifications) in this thesis work.

5.1   Nishigami's technique

The Nishigami's technique is an inversion method of coda waveform of local earthquakes to estimate the inhomogeneous spatial distribution of scattering coefficient in the crust. It allows to construct an image of the distribution of the scattering coefficient that is commonly called scattering tomography. It is introduced by Nishigami (1991) for the analysis of the scattering properties of the seismically active Hokuriku district, central Japan. He analyses the S coda waves from local earthquakes on the base of the single isotropic scattering model. He assumes spherical radiation from a seismic source in three dimensional half space with constant S wave velocity, v, and only S to S waves conversion. According to Sato (1977) the energy density $E(t)$ of single scattered waves at lapse time t can be expressed as:

$$E(t) = \iiint \frac{E_0}{4\pi v r_a^2} \eta_s(\overrightarrow{x}) \frac{1}{4\pi r_b^2} e^{-2\pi f Q_c^{-1} t} \delta\left(t - \frac{r_a + r_b}{v}\right) d\overrightarrow{x} \qquad (5.1)$$

where E_0 is the energy radiated from the source, $\eta_s(\overrightarrow{x})$ the scattering coefficient at the position $\overrightarrow{x}$, r_a and r_b the distances hypocenter - scatterer and scatterer - station respectively and v is S wave velocity. The exponential term is the same as in equation (3.7). Equation (5.1) says that the coda energy can be seen as the sum of all the

contributions of the energy that is single scattered by the heterogeneity. The volume integral is taken over the "scattering shell" where the travel times of single scattered waves equal the coda lapse times. When the spatial distribution of scatterers is random and uniform with the averaged value $\overline{\eta_s}$ and for lapse times grater than about twice the S wave travel times, equation (5.1) become equation (3.8) where $\eta_s = \overline{\eta_s}$. However the actual observation of coda envelopes show fluctuations due to non-uniform distribution of scatterers.

In equation (5.1), the exponential term can be moved out of the integral as Q_c is assumed constant over all the studied area, that is a realistic assumption as already discussed in the sections 4.2 and 4.3.

The studied area is now discretized into small blocks of volume δV; equation (5.1) is changed into a summation form by integrating the left side about a lapse time t and the right side about the radial direction r of the scattering shell. In this integration he assumes $dt \approx \frac{2}{v}dr$, where the scattering shell is approximated by a sphere. Consequently, when the scattering coefficient take a constant value $\overline{\eta_s}$, equation (5.1) becomes:

$$\overline{E(t)}dt = \frac{E_0\overline{\eta_s}}{(4\pi)^2 v}e^{-2\pi f Q_c^{-1}t}\sum_{i=1}^{N}\frac{1}{r_{a,i}^2 r_{b,i}^2}dV \tag{5.2}$$

where $r_{a,i}$ and $r_{b,i}$ are the distance from the center of the i-th block to the hypocenter and to the station, respectively. The summation is made over N blocks that verify the relation $|t - t_i| \leq \delta t/2$, where t_i is the travel time of the wave single scattered at the center of the i-th block. This condition implicitly says that we are considering all the blocks that lay on the surface described as the geometrical space of the points for which the sum of the distance from the hypocenter and from the receiver is constant and equal to $t_i * v$; that is the surface of a prolate ellipsoid which has the hypocenter and the receiver as foci.

On the other hand, when the scattering coefficient has a spatial perturbation, we can write $\eta_s = \overline{\eta_s} * \alpha_i$ and equation (5.2) become:

$$E(t)dt = \frac{E_0\overline{\eta_s}}{(4\pi)^2 v}e^{-2\pi f Q_c^{-1}t}\sum_{i=1}^{N}\frac{\alpha_i}{r_{a,i}^2 r_{b,i}^2}dV \tag{5.3}$$

Nishigami defines the coda energy residuals as:

$$res(t) = \frac{u(t)}{\overline{u(t)}} \tag{5.4}$$

where $\overline{u(t)}$ is the exponential best fit of the filtered energy coda envelope $u(t)$, according to equation (3.8). An example of the process to estimate the coda energy residual is given in figure 5.1. The coda energy residuals are considered to reflect mostly the non-uniform distribution of scattering coefficient.
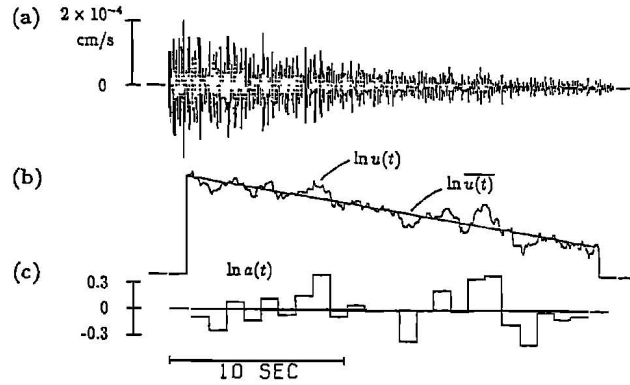
Figure 5.1: An example of the process to estimate coda energy residuals. (a) Band-pass filtered coda waves. (b) Logarithmic coda trace $ln(u(t))$ after running mean-squared and corrected for geometrical spreading effect. The straight line shows the linear function $ln(\overline{u(t)})$ best fitted to the logarithmic trace. (c) Logarithm of coda energy residuals, $ln(a(t))$ avereged in the time window of 1.0 s (redrown from Nishigami 1991).

At this point, dividing equation (5.3) for equation (5.2) we get the ratio of the observed coda energy density to the averaged one, which corresponds to the observed coda wave energy residual $res(t_j)$ at lapse time t_j:

$$res(t_j) = \frac{1}{\sum \frac{1}{r_{a,i}^2 r_{b,i}^2}} \sum_i \frac{\alpha_i}{r_{a,i}^2 r_{b,i}^2} \qquad (5.5)$$

This is the equation of observation for a given hypocenter - station pair, at a given lapse time, t_j. For a large number of source - station pairs and lapse times the system of the equation in the unknowns α_i is largely overdetermined (number of equations $\gg$ number of α_i) and can be solved with an optimization procedure. Nishigami (1991) uses an approximated technique based on the simple "average", called the prolate ellipsoid technique, to solve this system of equation. This technique utilizes the overlaps of the prolate ellipsoids given by the geometrical space of all the points where the sum of the distance from the hypocenter and station is constant and equal to $t_j * v$. Each energy residual is associated with all the points of the ellipsoidal surface. Using a large number of different hypocenter - station couples and lapse time, t_j, lot of different ellipsoids that overlap in different points will be obtained. For each overlapping point the scattering strength can be calculated as the geometrical average of the coda energy residuals associated to that point. Nishigami (1997) solved equation 5.5 by the recursive stochastic method applying the technique to several region of Japan and to the San Andreas fault system, California. He found the presence of high scattering coefficient in correspondence to active faults (Nishigami, 2000, Nishigami, 1991, Nishigami, 2006) or active volcanos (Nishigami, 1997). These results show that

the scattering tomography may be useful to estimate inhomogeneous structures in the crust. In contrast to approaches that are based on array measurements of coherency in the coda (Nikolaev and Troitskiy, 1987, Del Pezzo et al., 1997, La Rocca et al., 2001) the advantage of this method is that it can be easily applied to data recorded by an ordinary seismological network, like the one that is in operation in Campi Flegrei and Vesuvius.

5.2 Limitations of the single scattering assumption: discussion and perspectives

As it is well known, the single scattering is the first order approximation of the multiple scattering model. Zeng et al. (1991) provided a complete formulation of the scattered wave energy in a random medium. In a successive paper Zeng (1991) presented the compact equation (equation 3.5 of the present thesis, reported here for clarity):

$$
\begin{aligned}
E(r,t) \quad \simeq \quad & E_0 e^{-\eta vt} \left[\frac{\delta(t - r/v)}{4\pi v r^2} + \frac{\eta_s H(t - r/v)}{4\pi v r t} \ln \left(\frac{1 + r/(vt)}{1 - r/(vt)} \right) \right] \\
& + c H\left(t - r/v\right) \left(\frac{3\eta_s}{4\pi vt} \right)^{3/2} e^{-\frac{3\eta_s r^2}{4vt} - \eta_i vt}
\end{aligned}
\tag{5.6}
$$

This equation can be divided into:

1. the part representing the direct energy,

$$
E_{dire}(r,t) = E_0 e^{-\eta vt} \frac{\delta(t - r/v)}{4\pi v r^2}
\tag{5.7}
$$

2. the part describing the single scattering energy

$$
E_{ss}(r,t) = E_0 e^{-\eta vt} \frac{\eta_s H(t - r/v)}{4\pi v r t} \ln \left(\frac{1 + r/(vt)}{1 - r/(vt)} \right)
\tag{5.8}
$$

3. the part describing the energy envelope generated by higher order scattering processes

$$
E_{dif}(r,t) = c H\left(t - r/v\right) \left(\frac{3\eta_s}{4\pi vt} \right)^{3/2} e^{-\frac{3\eta_s r^2}{4vt} - \eta_i vt}
\tag{5.9}
$$

$E(r,t)$ can be equivalently expressed as the sum of all the contributions due to each scattering order E_n:

$$
E_n(r,t) = E_0 (\eta_s vt)^{n-3} \frac{\eta_s^3 B_n\left(\frac{r}{vt}\right)}{2\pi} e^{-\eta vt}
\tag{5.10}
$$

but the expression for $B_n(\frac{r}{vt})$ need to be numerically calculated. Hoshiba (1992) calculated B_n up to the order eight, just for the case of coincident hypocenter and station.

To show in a diagram the contribution of the single and multiple scattering terms, I plot the envelope shape in the approximate formulation of Zeng (1991), formula 5.6, in two extreme cases. The first case describes a medium for which intrinsic dissipation prevails $(\eta_s < \eta_i)$, whereas the second describes a medium with scattering phenomena prevailing over dissipation $(\eta_s > \eta_i)$. In figure 5.2 (dissipation predominates) it is clear how the single scattering term predominates in the early part (till 15 s) of the total energy envelope, whereas the diffusion model contributes to the later part. Figure 5.3

Figure 5.2: Plot of the energy model proposed by Zeng (1991). The curves are calculated for $\eta_i = 0.3$ km^{-1} and $\eta_s = 0.02$ km^{-1} at a hypocenter - station distance of 5 km. Abscissa reports the lapse time in seconds.
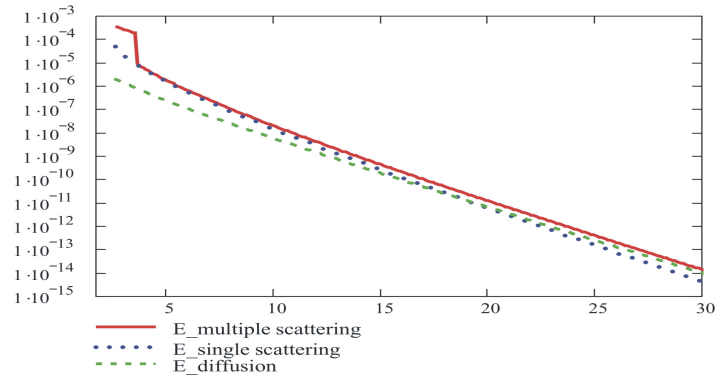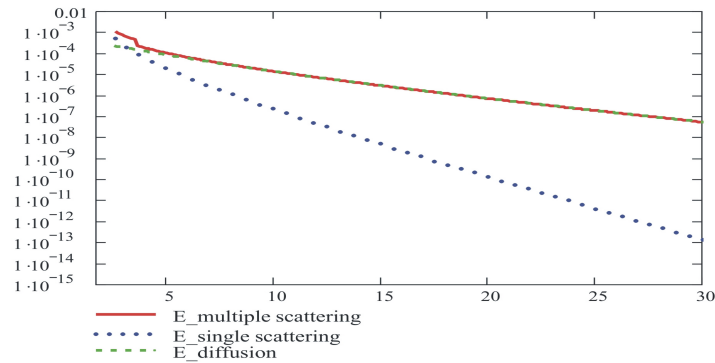

Figure 5.3: Plot of the energy model proposed by Zeng (1991). The curves are calculated for $\eta_i = 0.1$ km^{-1} and $\eta_s = 0.2$ km^{-1} at a hypocenter - station distance of 5 km. Abscissa reports the lapse time in seconds.

shows, on the contrary, the case in which scattering predominates. Is evident how the single scattering term has a negligible influence on the total energy also at short lapse times. This may produce a problem in the interpretation of the results obtained with the Nishigami's method, that, as already said, is based on the assumption of single scattering.

In reality, Nishigami calculates the ratio between the experimental energy envelope and the "average" envelope obtained fitting the experimental envelope with the single scattering model, whose analytical expression is a function of the kind

$$f(t) = \frac{Const}{t^2} \exp(-kt) \tag{5.11}$$

where k is obtained by the fit with the envelope of the seismogram. In the single scattering model k represents $\eta_s + \eta_i$ multiplied by the wave speed.

On the other hand, it can be demonstrated that a sufficient approximation of the multiple scattering energy envelope is (Wennerberg, 1993)

$$E(r,t) \simeq \frac{\eta_s}{4\pi r^2} K(vt/r)\Phi(t - r/v) \exp(-\eta_i t) \tag{5.12}$$

for a large range of η_i and η_s values. This equation can be written in an approximate summation form as

$$E(r,t) \simeq \frac{\eta_s}{(4\pi)^2} \frac{1}{v} \sum_S \frac{1}{r_a^2 r_b^2}$$

where S is the prolate ellipsoidal shell (Sato and Fehler, 1998) containing all the scattering points contributing to the energy envelope. As already discussed in section 4.2, fitting the envelope to find k of formula (5.11), in reality, we estimate a quantity that is close to η_i. Thus, the Nishigami's method can be applied in earth media under assumptions more general than those of single scattering. The only strong assumption of Nishigami's method results to be that the energy residuals are produced by the single scattering by scatterers located on the prolate ellipsoid. To quantify how much this assumption affects the interpretation, I write the equation of the single scattering introducing the term due to fluctuations of the scattering coefficient as:

$$E_{ssf}(r,t) = E_0 e^{-\eta vt} \frac{(\eta_s + \delta\eta_s(r))H(t - r/v)}{4\pi vrt} \ln\left(\frac{1 + r/(vt)}{1 - r/(vt)}\right) \tag{5.13}$$

and calculate the value of $\delta\eta_s$ that produces a measurable variation in the total envelope. In figure 5.4 I plot in blue the envelope generated using the standard Zeng's equation (5.6) and in red color the envelope generated modifying this equation introducing, in the single scattering term, the part due to the fluctuations of the scattering coefficient (equation 5.13). The fluctuations $\delta\eta_s(r)$ are introduced adding to the envelope a white noise with zero mean and standard deviation equals to 5. In figure
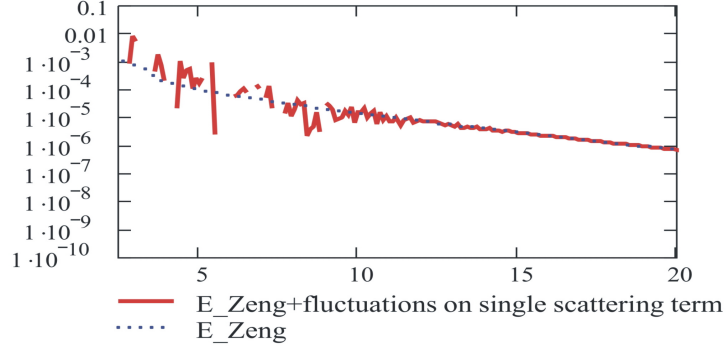
Figure 5.4: Plot of the energy model as proposed by Zeng (1991) (blue) and the one modified in case of fluctuations of the scattering coefficient. The curves are calculated for $\eta_i = 0.1$ km^{-1} and $\eta_s = 0.2$ km^{-1} at a hypocenter - station distance of 5 km. Abscissa reports the lapse time in seconds.

5.5, the ratio between equations (5.13) and (5.6) is plotted. As before, I show two opposite extreme examples the first associated with a strongly scattering and the second associated with a strongly dissipative earth medium. In figure 5.5 I show the first case ($\eta_s > \eta_i$) and in figure 5.6 the second one. The results are different. In the first case the residuals decrease with lapse time whereas in the second one they maintain an almost constant value. The different behavior is clearly due to the fact that, when $\eta_s > \eta_i$ the single scattering contribution is negligible respect to the contribution of the diffusive part.

These considerations indicate that for the area of Mt. Vesuvius, where a strong predominance of η_s is present, the Nishigami's method underestimates the η_s variations associated with large lapse times, producing darkened images at the borders of the investigated area.

A possible suggestion to correct this bias may be given by the following considerations, that I did not apply to the present data but may give a possible improvement for the next future.

I find an empirical formula that allows to correct this bias, once the average values of η_i and η_s are measured in the area under study. The formula is

$$F(r, t, \eta_i, \eta_s) = \exp(\eta_s(vt - r) + C(\eta_i, \eta_s)(1 - \frac{r}{vt})) \tag{5.14}$$

As evinced by figure 5.7 the corrected single scattering energy becomes a good approximation to the multiple scattering coda energy also at early lapse time. The

Figure 5.5: Ratio of the energy calcolated in case of fluctuation of the scattering coefficient over the energy calcolated with the equation (5.13). The ratio is calculated for $\eta_i = 0.1$ and $\eta_s = 0.2$ at a hypocenter - station distance of 5 km. Abscissa reports the lapse time in seconds.

coda energy residuals can be expressed by

$$res(r,t) = \frac{E_{ssf}(r,t) * F(r,t,\eta_i,\eta_s)}{E_{dire}(r,t) + E_{ss}(r,t) + E_{dif}(r,t)} \tag{5.15}$$

where $E_{ssf}(r,t) * F(r,t,\eta_i,\eta_s)$ is the single scattering contribution, with the fluctuations in the scattering coefficient, multiplied for the empirical correction term and the denominator is the total energy as formulated by Zeng (equation 5.6).
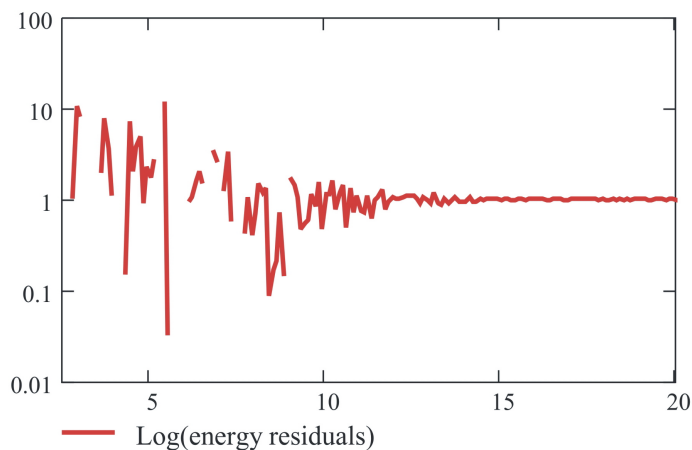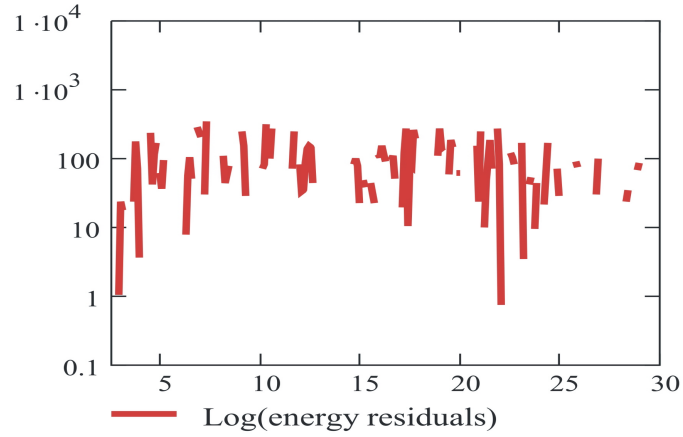
Figure 5.6: Ratio of the energy calcolated in case of fluctuation of the scattering coefficient over the energy calcolated with the equation (5.13). The ratio is calculated for $\eta_s = 0.02$ km^{-1} and $\eta_i = 0.3$ km^{-1} at a hypocenter - station distance of 5 km. Abscissa reports the lapse time in seconds.
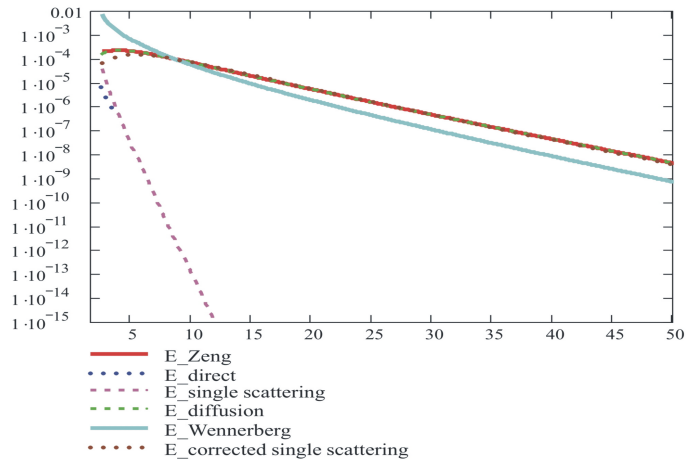
Figure 5.7: Coda energy envelope as described by equation (5.6) (red) divided into the part due to the direct enegry (dotted blue), the single scattering (dashed magenta) and the diffusive one (dashed green). Equation (5.12) is rapresented by the ciano color curve. The single scattering energy corrected by F is rapresented by the dotted brown curve, c is taken equal to 7. The curves are calculated for $\eta_i = 0.1$ km^{-1} and $\eta_s = 1$ km^{-1} at a hypocenter - station distance of 5 km. Abscissa reports the lapse time in seconds.

Chapter 6

Scattering image of Campi Flegrei

6.1 Geological and structural set up of Campi Flegrei

Campi Flegrei is a resurgent caldera that is located 15 km west of Naples, Southern Italy (figure 6.1). The caldera formation is believed to be related to two main explosive eruptions that occurred 37-39 kyears ago and about 12 kyears ago (Orsi et al., 1996). In the past ten thousand years, the volcanic activity has been characterized by the occurrence of explosive eruptions with a return period of thousands of years. The most recent eruption occurred in 1538, with the formation of a spatter cone that reached an altitude of about 200 meters a.s.l. and that was preceded by a ground uplift in the eruption zone to a maximum of several meters. After this event, the caldera floor sank continuously at an average rate of about 1 cm per year, from 1538 until 1950. After 1950, this general tendency was three times interrupted by three resurgence episodes that occurred in 1950, 1970-72 and 1982-84. The last two resurgence episodes were accompanied by a nearly symmetrical deformation pattern, with maxima in the center of the caldera (in the town of Pozzuoli). After both ground uplift episodes, the ground slowly subsided and at present it remains approximately 1.6 m above the pre-1970 levels. The uplift episodes were accompanied by small magnitude earthquake swarms (up to m=4.0 in 1982-84), which were characterized by foci that were very close to Pozzuoli (distance from hypocenter, less than 2 km) and that therefore caused a lot of damage. In addition, a new anomalous ground uplift that was comparable to that which occurred in 1982-84 could be the precursor of a new eruption similar to that which occurred in 1538. After the 1982-84 crisis, the only other significant seismic episodes occurred in July-August 2000 (Saccorotti et al., 2002), which were
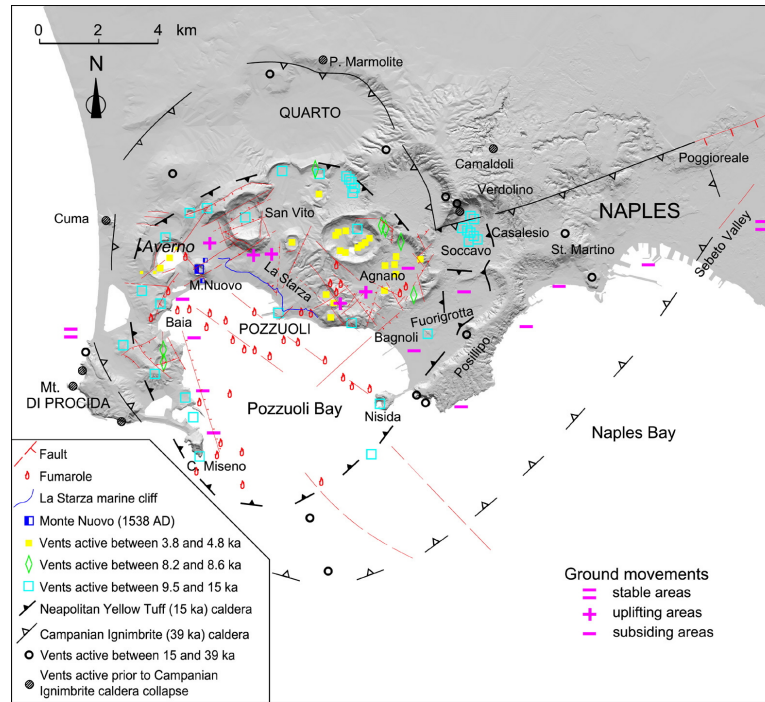
Figure 6.1: Map of Campi Flegrei with the geologichal structures (modified from Orsi et al., 2004)

characterized by the presence of low-period events.

Many studies have been carried out in this area that have been aimed at imaging the first 5 km below the surface. They are well summarized and discussed in De Lorenzo et al. (2001a), De Lorenzo et al. (2001b), Zollo et al. (2003) and in De Lorenzo et al. (2007). De Lorenzo et al. (2001a) compared a 3-D image of total seismic attenuation in the upper 3 km below the surface at Campi Flegrei with previously obtained P and S velocity tomography. The results were jointly interpreted in terms of the thermal state of this volcano (see also De Lorenzo et al., 2001b), where the high attenuation (low Q) zones are coincident with the high temperature zones. Zollo et al. (2003) obtained a new tomographic image using P-arrival times from shots that were fired in the bay of Pozzuoli and recorded at 62 sea-bottom and 72 on-shore receivers. This image focused on the buried inner rim of the caldera, which was clearly detected as a ring shape at a depth between 0.8 and 2 km. The shape of a positive gravity anomaly (Capuano et al., 2003) closely matched this image. These studies confirmed that the limestone basement is less than 4 km deep, with no evidence of a shallower magma body. This is in contrast to a previous study by Ferrucci et al. (1992), who detected the top of a magmatic body at a depth of about 3-4 km through the interpretation of a converted P-Sv phase on transmission and the extrapolation to greater depths of

the strong temperature gradients measured at rather shallow depths (450 °C at 3 km in depth).

The caldera now appears to be filled with a layer of volcanic deposits that is a few km thick, and which forms an inner basin that is characterized by a low Vp, a high Vp/Vs ratio and a high P wave attenuation (Aster and Meyer, 1988). This has been confirmed by Vanorio et al. (2005) in the light of an improved data set.

Although much has already been learned about the structure of the Campi Flegrei caldera, there still remain many problems. One of the most important of these is whether the magma body really exists, and if so, where it is actually located and how much it is laterally extended. Debate also remains as to where the southern borders of the outermost old caldera rim are located beneath the sea in Pozzuoli Bay, again, if it exists (Judenherc and Zollo, 2005). The total attenuation and the body-wave velocity tomographic imaging only partially answer these questions at present. Indeed, an interpretation problem arises in the attenuation structure obtained from inverting the total attenuation, which, as is well known, is produced by the sum of the intrinsic and scattering effects. For this reason, the total attenuation images cannot be interpreted unequivocally. If, for example, a low-velocity zone is found in correspondence with a high-attenuation zone, this can be interpreted as being due either to the presence of a magma body in that zone (which would produce an increase in the shear-wave intrinsic attenuation and a decrease in the body-wave velocity, due to the increase in temperature), or to an increasing heterogeneity and/or a high density of fractures (which would mainly produce an increase in the scattering attenuation).

The present thesis aims to give a further contribution towards this interpretation problem through the application of a relative scattering imaging method to the Campi Flegrei area. For this, I have used the Nishigami's method described in section 5.1.

The main result of this analysis is the evidence of a high-scattering-strength zone that matches the inner border of the caldera rim, which is well delineated beneath sea level, where geological observations are lacking. There is also evidence of a heterogeneity (which is imaged using longer wavelength radiation) that is close to the zone of residual volcanic activity. A uniform distribution of the scattering coefficient is found at depths greater than 4 km.

6.2   Inversion method

I apply the standard Nishigami's technique in a constant velocity model as it is described in section 5.1. I create the system of equations (5.5). As the number of equations, N, is large (the system is highly overdetermined), the system appears difficult to solve using a PC or a workstation with a limited amount of RAM. In contrast to Nishigami (1991), to perform the inversion on my computers, I use a hybrid jackknife-SVD (Singular Value Decomposition) method in which the original set of N equations

is divided into N_{su} subsets, omitting N_{wr} equations from each subset without replacement, in such a way that $N_{eq} - N_{wr}$ is anyway much larger than the number of unknowns. I thus obtain each subset through the following procedure: first, I generate a vector of integer random numbers that are uniformly distributed and sorted between 1 and the number of equations in the original set (system of equations 5.5); the integer random numbers of this set correspond to the order of the extraction. A pseudo inversion for each subset is then carried out with an SVD approach that is based on standard MATLAB routines that are designed for sparse matrices, giving partial information about the model. Finally, the averages of the partial models obtained give the model estimate, together with a robust estimation of its variance. Even though very slow, this method can be run on a modern PC; the method also allows for a qualitative test of the robustness of the final solution simply by comparing the solutions obtained from each subset with the overall solution.

The validity of this procedure is tested by also performing the inversion for the complete set of data available at 6 Hz. For this frequency band, the number of equations is sufficiently low to allow for the direct application of the ordinary SVD approach in one step. The results for this test are in complete agreement with those obtained using the hybrid technique.

6.2.1   Uncertainties and limitations of the method used

The single scattering assumption is strictly valid for only short lapse times. In reality, I fit each band-pass filtered seismogram to a negative exponential (obtaining for each trace a different Q_c^{-1}), and calculate the energy residual (as explained in section 5.1). Consequently, as I use a different Q_c^{-1} value for each seismogram, this method takes into account the smooth spatial fluctuation of the attenuation properties of the medium. The assumption of single scattering is, in practice, maintained only for the "strong" scatterers, which produce the deviation from the negative-exponential law. In other words, I assume that the coda residuals are produced by strong scatterers that are encountered only once from the energy of the primary waves. On the other hand, there is a lack of information about the true absolute values of the scattering coefficients retrieved, as this estimation does depend on the scattering model. For this reason, the resulting distribution of relative scattering coefficients does not contain enough information to quantitatively separate the contributions of the scattering attenuation from the intrinsic absorption, once a separate estimate of total attenuation is available.

As described in section 5.1, in the uniform model assumption, the scattering shells are ellipsoids that tend to a spherical shape with increasing lapse time. I test numerically that for a velocity increasing with depth, the spherical shape of the scattering shells becomes distorted, and this distortion is more effective with increasing lapse

time. I test the effects of a velocity-depth model described by a linear function that interpolates the values of the velocity that are obtained by the velocity tomography of Aster and Meyer (1988). Using this model, I trace all the rays connecting a source located close to Solfatara crater at a depth of 2.5 km, where most of the real sources are effectively located, with a suite of uniformly distributed scatterers in the earth volume under investigation, and from the scatterers to the receiver (coincident with the epicenter). Then I trace the scattering shells in the range of the lapse times used in the present application of the Nishigami's technique, and I compare them with the shells obtained in the case of a uniform velocity. I find that the distortion of the spherical shells produces an overestimation of the depth at which the strong scatterers are located and a maximum lateral shift of less than one cell length. Due to the shortness of the maximum lapse time at which I measure the coda residuals in the present study (of the order of 15-20 seconds, at least), this distortion of the scattering images produced by the uniform velocity assumption is effective only at the external borders of the earth volume under investigation.

6.3 Application to the data set

The data used in the present study consist of a subset of more than 10,000 events that were recorded by a portable, high dynamic range, three-component, digital seismic network that was operated during the intense bradyseismic uplift episode of 1984. The network (the UW net) was set up and operated by the INGV - Osservatorio Vesuviano (Naples, Italy), in cooperation with University of Wisconsin (Madison, USA). The network recorded high-quality signals in the magnitude range from -1 to 4.2 from several hundred microearthquakes. This data set has been widely studied by many groups, as described previously (see De Lorenzo et al., 2001a, and references therein). Recently, part of the data that were not used in these studies has been recovered from the old field tapes at the University of Wisconsin, thus adding new waveforms to the old data set (P. Capuano, personal communication). In figure 6.2, I show the station positions and the earthquake epicenters of the complete data set. The events are located with ordinary procedures (Hypo) using a velocity model derived from the tomography study of Aster and Meyer (1988). The station coordinates are reported in the table 6.1. The stations were costitued of 3-component digital recording seismographs with wide dynamic range (106 db); the sensors were HS101 type seismometers with a natural frequency of 1 Hz. Earthquake signals were detected by an automatic triggering system (Del Pezzo et al., 1987).

I select the data for the present analysis using the following criteria: first, I discard the seismograms showing spikes and/or other types of electronic noise. As most of the data from NS components are unfortunately very noisy and do not pass this selection criterion, I decide to consider only the vertical and EW components for my data

Name	Location	UTM Latitude (m)	UTM Longitude (m)	Elevation (m)
W 02	Solfatara	4519912	427553	100
W 03	Astroni	4522214	428657	35
W 04	Mt. Nuovo	4521052	422828	70
W 05	Camaldoli	4523385	432054	457
W 06	Cappella	4518260	420830	45
W 07	Mt. Ruscello	4523761	423854	170
W 10	Capo Miseno	4514719	423240	50
W 11	Darsena	4519447	425932	82
W 12	Solfatara B	4520056	427920	180
W 13	Castello Baia	4518222	422700	20
W 14	Nisida	4516672	429630	40
W 15	Mt. Spina	4519874	429576	150
W 16	Pirelli	4520146	424505	80
W 18	Madonna	4519508	427268	90
W 19	Anfiteatro	4519961	426344	37
W 20	Mt. S. Angelo	4522945	424056	306
W 21	Fondi di Cigliano	4521680	426544	175

Table 6.1: Name, location and coordinate of the utilized stations

analysis. This can lead to minor problems in the interpretation of the results, as the coda wave energy is, at a first approximation, equally partitioned among the components of the ground motion (Sato and Fehler, 1998).

As a first step, I band-pass filter all of the seismograms in the frequency bands centered at $fc = 6, 12$ and 18 Hz. The values of the center frequency for the band-pass filter are set equal to those used in a first determination of the average coda Q in the Campi Flegrei area (using part of the same data set as described in Aster et al., 1989). The traces filtered at $fc = 1.5$ and 3 Hz show unstable results for the coda Q determination, and for this reason they are not used in the present study. For each frequency band and component, I estimate the coda energy density by calculating the squared envelope of the filtered trace as:

$$E_{obs}(t_j) = H(S)^2 + S(t_j)^2 \tag{6.1}$$

where $S(t_j)$ is the seismic coda trace band-pass filtered at fc and sampled at times t_j, starting from twice the travel time of the direct S waves, up to the coda end (I have assumed that the coda ends at the time point where the signal-to-noise ratio falls to 2), and where $H(S)$ is its Hilbert transform. Then, I fit $E_{obs}(t_j)$ with equation (3.8), to obtain Qc and the product $E_0\overline{\eta_s}$ that best fits the data. Thus, I obtain an estimate of $\overline{E(t_j)}$ (equation 5.2) for each station - source couple. An example of the data analysis is given in figure 6.3, where the energy envelope estimations for the seismograms relative to an earthquake filtered at 12 Hz at different stations is given, together with the best-fit models.
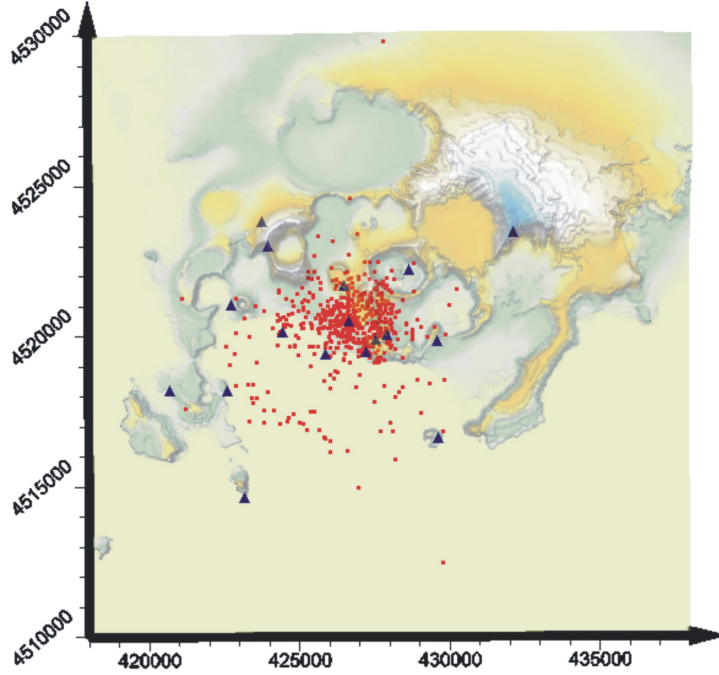
Figure 6.2: Map of the Campi Flegrei with the seismic stations points (blue triangles) end the epicenters (red squares). Coordinates are in UTM (meters).

A further selection of the data set is then carried out through eliminating all of the seismograms for which the correlation coefficient of the fit is lower than 0.65. After this selection, the data set is composed of 735 earthquakes that were recorded at an average of five stations, with two components. We then calculated the ratio between $E_{obs}(t_j)$ and the theoretical values, which gives an evaluation of the parameters $res(t_j)_{ik}$, where i and k indicate the station and the receiver respectively.

For the present study, I select a region covering an extension of 20 x 20 km and spanning down to 6 km in depth. As a first step, I divide this volume into cubic blocks with 2 km sides, obtaining 300 blocks (Grid 1 in figure 6.4). For the inversion of the scattering coefficient distribution in each of these blocks, I segment the coda envelopes into steps of 1 s duration that fulfill the inequality $\delta t \leq 2\frac{\delta D}{v}$, where δD is the side of the cubic box. Than I log-average all of the residuals $res(t_j)_{ik}$ of each of these time segments. For a more detailed inversion, I select an inner region (Grid 2 in figure 6.4) of 10 x 10 km spanning down to 3 km in depth. I divide this sub-volume into blocks with 1 km sides, obtaining 300 blocks again. In this case, the coda is segmented at intervals of 0.5 s, in which I log-average the residuals $res(t_j)_{ik}$.

The inversion is carried out separately for each of the two grids and for each frequency and component.
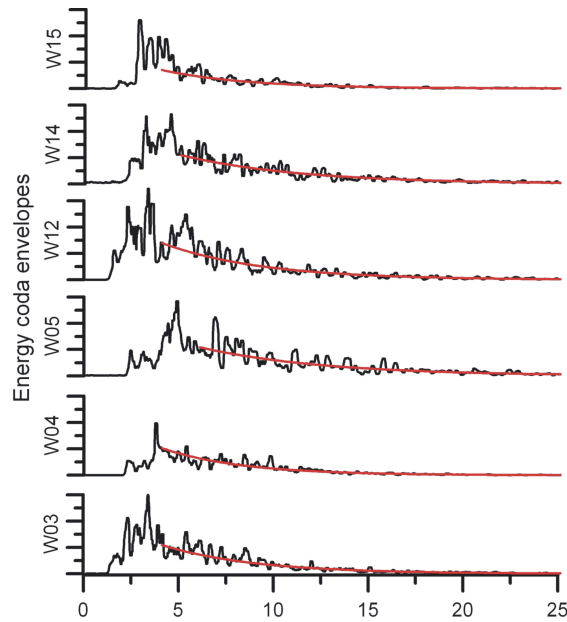
Figure 6.3: An example of the data analysis. The plots represent the energy envelopes (in arbitrary logarithmic scales) as a function of the lapse time for the same seismogram that was filtered at 12 Hz and recorded at different stations. The fit with the theoretical curve (in red), which starts from twice the S wave travel time, is superimposed on each dataset.

6.3.1 Resolution test

To check the validity and resolution of the method and algorithm, I carry out several tests using synthetic data. Here, I report only two characteristic tests:

a) I considered a single strong scattering cubic body with a dimension of 3 km in a uniform random medium located NW of the Caldera. For this case, I test both the configuration with the upper face coincident with the zero level of topography, and the configuration with the upper face at the depth of 3 km.

b) A "checkerboard" structure of cubes with 3 km sides with alternating scattering contrast.

I create synthetic envelopes with a positive 100% contrast in the anomalous zones, and then analyze them with the same procedures as used for the actual data. All of the solutions show a sufficient separation of the anomalous patches at all depths investigated. Figure 6.5 gives the results for both of these tests.
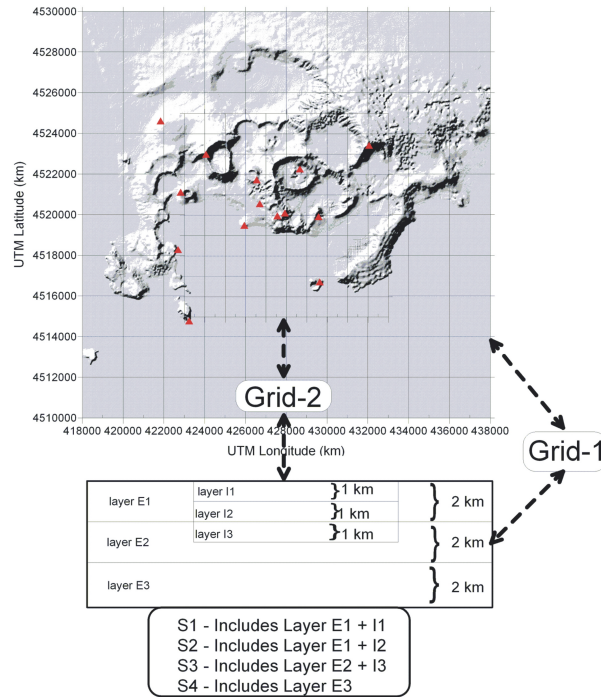
Figure 6.4: The earth volume under investigation and its division into two sub-volumes. The inner volume is divided into blocks of 1 x 1 x 1 km (Grid 2), while the external volume is divided into blocks of 2 x 2 x 2 km. In the bottom panel of the figure, the scheme of the subdivisions with depth are shown.

6.4 Results

I first check that the results obtained for Grid 1 and Grid 2 are consistent, where each of the blocks of Grid 1 contains 8 blocks of Grid 2 (figure 6.4). This demonstrate that the average of the α parameters obtained from the inversion for each block of Grid 2 almost coincide with the value of α obtained for Grid 1. I also check that the pattern of the space distribution of the scattering coefficient changes is similar for the two components of ground motion that we use in the present study. Figure 6.6 thus shows the plots of the stacks (over the components) of the values obtained from the inversions for Grid 2 for the inner zone and Grid 1 for the external volume. The results are plotted separately for each frequency band. The stack is weighted for the variance obtained for each single estimate. In each block, a symbol representing the value of $\log(\alpha)$ is plotted. The crosses and circles represent the scattering coefficients higher and lower than the mean, respectively. Each plot represents a "layer". In total, three layers are shown, which reach a depth of 4 km. The bottom panel of figure 6.4 explains how the inner and outer grids (Grid 1 and Grid 2) are included in each of these layers.
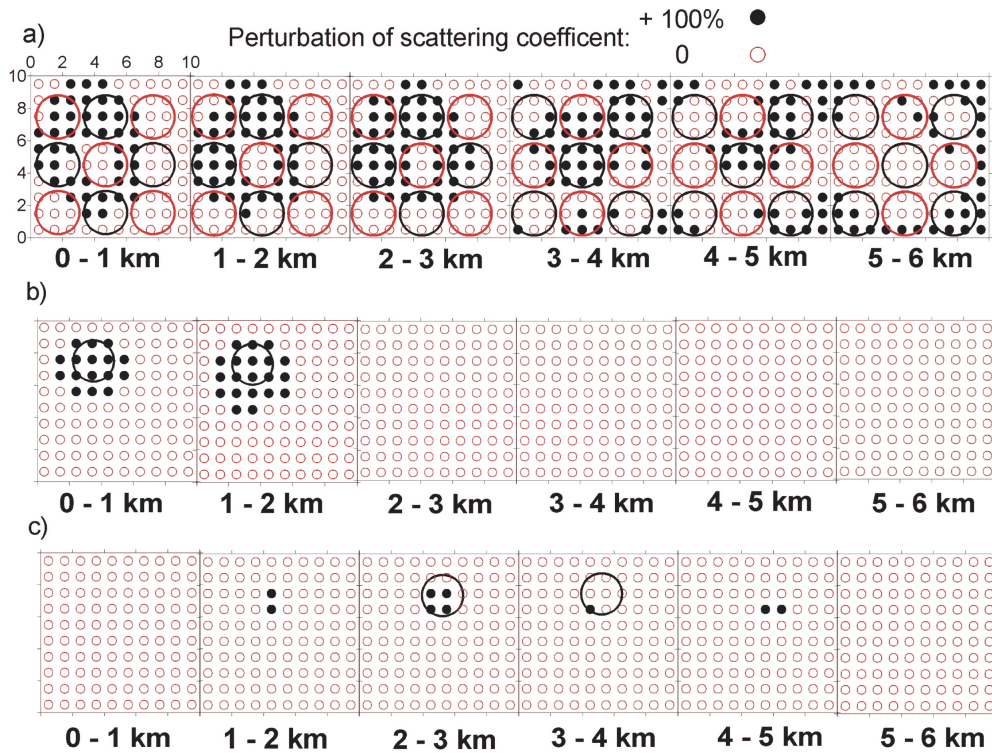
Figure 6.5: The results of the tests made using: a) a "checkerboard" structure with alternating scattering contrast (+100%, big black circle; 0, big red circle) The test input is given by blocks of 3 x 3 x 3 km, represented by the big circles. Output is calculated for blocks of 1 x 1 x 1 km, represented by small circles. Black color indicates +100% scattering contrast. b) single strong scattering body with a positive 100% contrast (big black circle) with dimensions of 3 x 3 x 2 km and upper face at zero level depth; and c) single strong scattering body with a positive 100% contrast (big black circle) with dimensions of 3 x 3 x 2 km and upper face at 2 km of depth .

I have excluded all of the values with a percentage variance that is greater than 0.3. In these cases, no symbols are shown. The deepest layer, S4, is not represented in figure 6.6, as it is fully uniform. In figure 6.7, the results obtained at a frequency of 18 Hz for the data stacked over the ground motion components are represented with the addition of the deepest layer, S4, and the geological features (superimposed on the upper-left panel).

The central portion of the studied zone remains unfocused, notwithstanding that the data coverage is good. This is because the central blocks often correspond to coda segments that do not fulfill the condition that the lapse time is greater than twice the S wave travel time. This is a condition that we impose a priori on the whole data set to avoid the sampling of the seismogram portion following the direct S wave packets, as already discussed, which can be affected by radiation pattern effects. This strongly
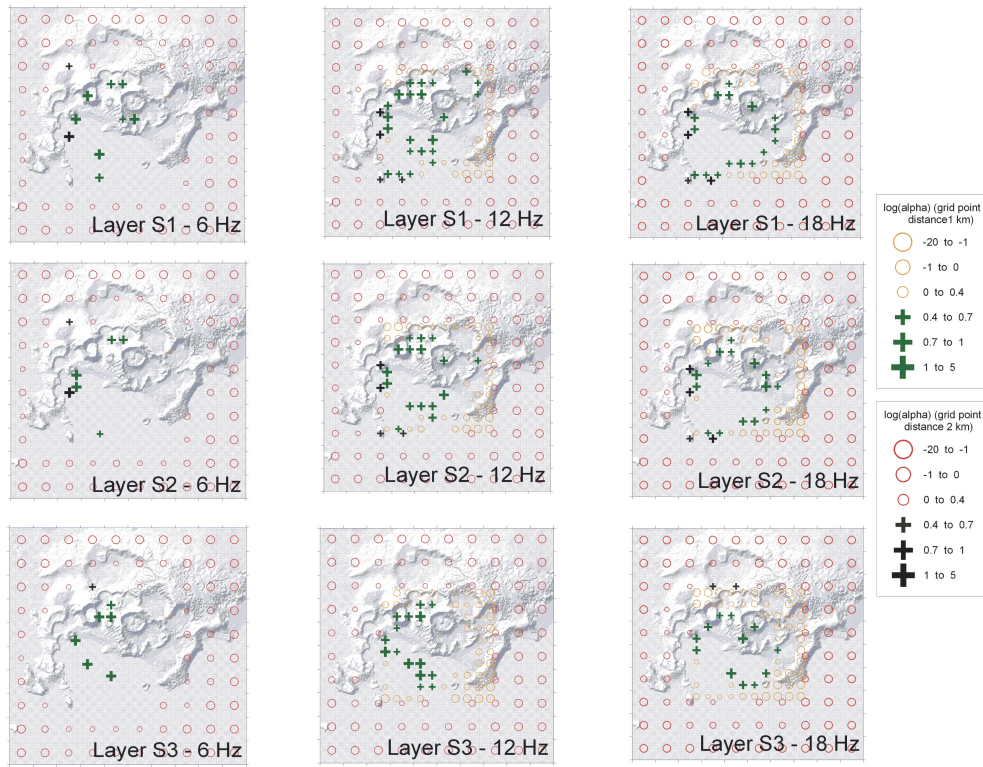
Figure 6.6: The results from the inversions of the stacked (over the components) signals. The crosses and circles represent the zones with high and low scattering strengths, respectively, as indicated in the right-hand key panels.

reduces the data available, and hence increases the variance.

The data at all of the frequency bands show that the main heterogeneity is confined to the central zone of the earth volume under investigation, approximately corresponding to the Gulf of Pozzuoli. The heterogeneous volume spans the first 3-4 km of the crust. At 6 km in depth, the pattern of the relative scattering coefficient is uniform. A high-scattering zone is located in coincidence with Solfatara crater, the site of a fumarole field and of a mud crater, where most of residual volcanic activity of Campi Flegrei is now located. This high-scattering zone is very close to the area of maximum uplift, and coincides with the highest concentration of earthquake foci that occurred during the 1982-84 crisis (figure 6.2).

At the 18 Hz frequency band, positive anomalies of the scattering coefficient coincide with the inner part of the subaerial caldera rim, as revealed by its geology (figure 6.1 and upper-left panel of figure 6.7). The pattern of positive anomalies of the scattering coefficient in the shallowest layer at 18 Hz (upper-right panel of figure 6.7) is almost ring-shaped, and it appears to delineate the gross features of the submerged
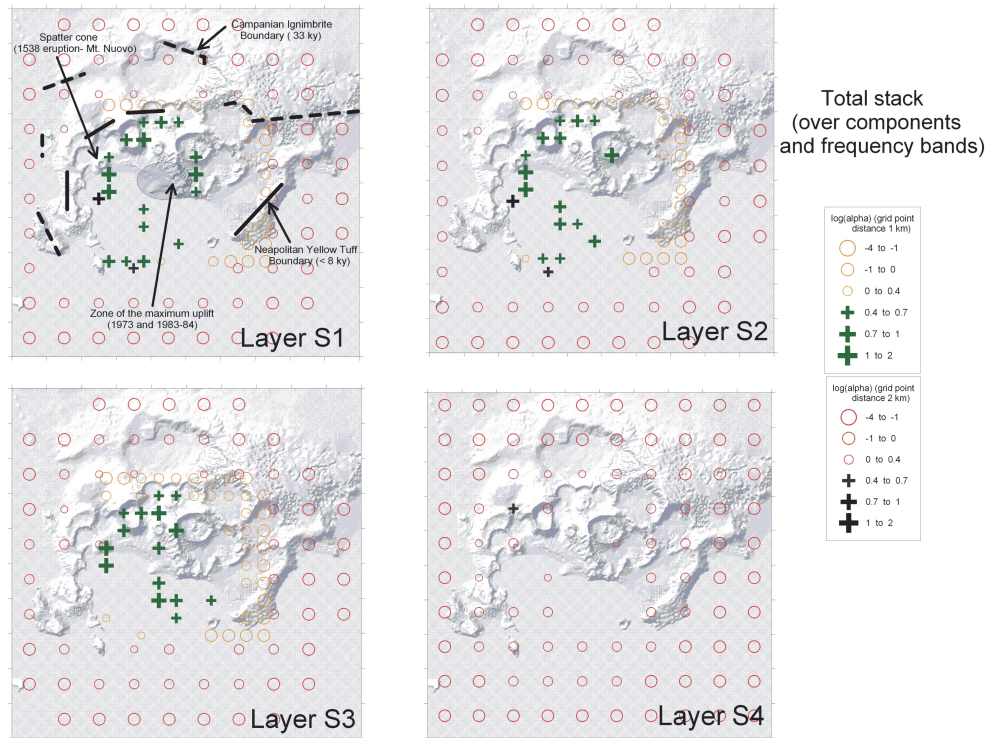
Figure 6.7: As for figure 6.6, for a frequency of 18 Hz, with the addition of layer S4. Some of the geological features, as described in figure 6.1, have been superimposed on the top-left panel, which corresponds to the S1 layer.

caldera rim in the southern part of Pozzuoli Bay. Layers S2 and S3 are almost identical, showing high scattering strength in the North East and South East sectors of the Grid 1 zone.

6.5   Interpretation of the results

6.5.1   Previous studies on the velocity and attenuation structure at Campi Flegrei.

As mentioned before, many studies have been carried out in this area that have been aimed at the imaging of the first 5 km below the surface. In this section, we summarize the main results, reporting the principal features in a sketch map that will be useful for a comparison with the other studies discussed (figure 6.8).

- Passive P and S travel-time tomography has been obtained for the first 3 km of the crust (the maximum depth of the microearthquakes) by Aster and Meyer (1988). This study showed an anomalous zone that is located north-east of Pozzuoli, between 1
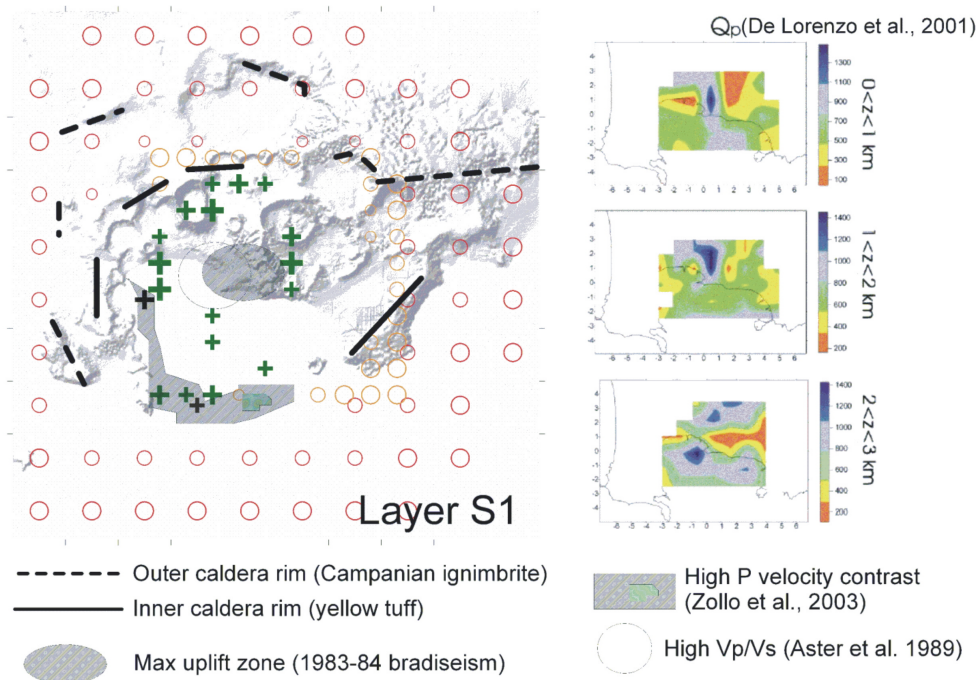
Figure 6.8: The main results from the attenuation, velocity (active and passive) and scattering tomography at 18 Hz (see text). For reference, some of the geological features already shown in figure 6.1 have been included.

and 3 km in depth, with a low Vp and a low Vs, and a high Vp/Vs ratio. This anomaly was interpreted as being due to the presence of porous and vapor-filled materials in the inner section of the caldera (left-shaded area in figure 6.8). Recently, Vanorio et al. (2005) found similar velocity trends using an improved data set with respect to that used by Aster and Meyer (1988(Aster and Meyer, 1988)). Their interpretation was based on information on physical rock properties, which led them to exclude the presence of a molten zone below a depth of 4 km, as instead hypothesized by Ferrucci et al. (1992). The Vp/Vs anomaly found by Vanorio et al. (2005) at 4 km in depth was interpreted as the top of a cracked formation, which is enriched in gas under supercritical conditions.

- An active seismic survey that was carried out during 2001 in the Gulfs of Naples and Pozzuoli allowed the inversion of the P wave travel times (SERAPIS experiment; Zollo et at., 2003). The results showed a clearly delineated, high P wave velocity and density, ring-shaped body located in the southern part of Pozzuoli Bay at a depth between 0.8 and 2 km. This was interpreted as being the buried rim of the Campi Flegrei caldera (cross-gridded zone of figure 6.8). Moreover, a limestone basement was also revealed in the same study, at less than 4 km in depth.

- Q imaging was obtained by De Lorenzo et al. (2001a), which has been improved more recently by De Lorenzo et al. (2007), using as observables the P-pulse duration for a subset of the same data set as used for the above-described velocity tomography. The main feature was a large low-Q_P anomaly located north-east of Pozzuoli. The extension of this zone was largest in the first layer (between 0 and 1 km), decreasing with increasing depth. A high Q_P zone was located between the surface and 2 km in depth in the central part of the caldera, which separated two low-Q_P zones.

6.5.2   Scattering imaging and other informations: a comparison

Comparing the present results with those described previously and with the main geological features revealed in the study by Orsi et al. (1996), I conclude that the high-scattering zone revealed at high frequency in the first two layers (down to a depth of 2 km) is superimposed under the sea on the high velocity zone inferred from the P-velocity tomography. This image reveals a P wave velocity contrast which borders the Bay of Pozzuoli in the sea to the south. The main result of the present study is that on land, the high-scattering zone almost coincides with the inner part of the subaerial caldera rim inferred by geological observations, and it continues in a regular fashion out to the sea. I thus suggest that the scattering image obtained at high frequency in the present study delineates the inner caldera border, which matches the geological border of the yellow tuff formation, with the only exception being on the eastern side. Scattering imaging is thus shown to be a robust method that greatly helps in the delineation of the geological structures of the volcanoes. Unfortunately, the velocity and attenuation tomography images are not entirely comparable with each other, as they do not match the same area; for this reason, the total attenuation in the zone of the high P-velocity and scattering contrast that delineates the southern border of the inner caldera is still unknown.

The scatterers obtained using the data filtered at 6 and 12 Hz are located near to the zone of Solfatara crater. The strongest low-Q_P anomaly is also located at the same site. This is the zone with the highest concentration of earthquake foci, which is characterized by the presence of densely fractured, porous and fluid-filled rocks, and by a strong thermal anomaly.

We have relatively poor information for the central zone, where the scattering imaging is unfocused, as indicated above. A high Vp/Vs anomaly and the zone of maximum uplift are both located in this area.

At depths greater than 5 km, the Nishigami method furnishes an almost homogeneous image, with no strong scatterers. This evidence cannot resolve the apparent discrepancies between the results of De Lorenzo et al. (2001a), who estimated the top of a magma chamber at a depth greater than 4 km (from the Q_P-inferred temperature field), and the more recent results from Vanorio et al. (2005), who, as already

discussed above, gave a different interpretation in terms of a cracked formation, enriched in supercritical gas. In fact, a large magma body underlying the whole area under investigation, or a homogeneously cracked formation of the same extent, would have produced the absence of small-scale contrasts in the relative scattering coefficient. I favor the interpretation of Vanorio et al. (2005) on the basis of a previous study (Del Pezzo et al., 1996) that indicated that the scattering attenuation predominates over the intrinsic dissipation down to a depth of more than 10 km in this area. The presence of a large magma chamber would have indicated the opposite, i.e. a predominant intrinsic dissipation.

Chapter 7

Scattering image of Mt. Vesuvius

Mt. Vesuvius, dormant since the last eruption in 1944, is considered the most potentially dangerous volcano in the world, due to the high population density. Crucial for the Civil Protection is the correct establishment of possible scenarios, possibly based on volcanological models, which, in turn need a structural model of the volcano, with emphasis on the details about the location and the volume of the possible magma patches underneath.

An increase of scientific interest for this volcano dates back in 1981 (Sheridan et al., 1981) when the detailed analysis of pumice flows and other pyroclastic products clearly showed in the last 19,000 years the sequences of 5 plinian eruptions and a larger number of subplinian, lastly occurred in 472 and 1631 A.D. Volcanological models of this last kind of activity require continuous magma filling from a reservoir located in the shallow crust at 3–6 km depth (Civetta and Santacroce, 1992). Realistic simulations of its pyroclastic flows also showed the dramatic scenario deriving from a possible future renewal of this activity due to presence of about 700,000 people living on its flanks, within a 15 km radius from the central crater. A more recent observation is the detection in the last decade of a small increase in magnitude of the largest earthquakes, some of them felt by population (Bianco et al., 1999). As a consequence of this renewed interest, Mt. Vesuvius has been the object, in the last years, of accurate geophysical and volcanological studies (Gasparini, 1998). A discussion of the recent results on the structure of Mt. Vesuvius is contained in the book by Capuano et al., (2003) and the numerous references therein. Recent attempts to improve the resolution of the images are the tomographic inversion of first-P arrival times from microearthquakes (Scarpa et al., 2002) reaching a resolution of about $300 - 500$ m and the tomography attenuation image obtained by Del Pezzo et al. (2006). The velocity

tomography allows for a precise relocation of the local seismicity; in particular two zones of clustered hypocenters separated by a positive P wave velocity contrast were identified. The main structural results were: a) the presence of a high P-velocity body beneath the crater, surrounded laterally by lower P-velocity volcanic rocks; and b) the carbonate basement positioned at 2-2.5 km b.s.l. (consistent with TOMOVES - Tomography of Mt. Vesuvius - active seismic results; Auger et al., 2001), at the top of which, on the crater axis, almost all the energy and stress-drop seismicity is located (Del Pezzo et al., 2004). At the border of the carbonate basement with the overlying volcanic structures the maximum magnitude earthquake ever recorded at Mt. Vesuvius in the last 40 years took place (October 9, 1999 - M=3.6). Zollo et al. (1998) and Scarpa et al. (2002) interpreted the tomographic structures inferred from active and passive seismic data in terms of the absence of any magma chamber in the investigated depth range. A high Vp/Vs ratio region found in the upper layers (1 km below the topography) was related by Scarpa et al. (2002) to the presence of a highly fractured aquifer rocks, permeated by intense circulation of hot fluids. Attenuation image is consistent with velocity structure (Del Pezzo et al., 2006a), with a correspondence between high velocity and high total-Q.

In this chapter I will describe the modification of Nishigami's technique used to determine the 3-D scattering image of Vesuvius. This modification are introduced to take into account the realistic velocity model, the particular configuration of the stations with respect to the hypocenters and the size of the studied area.

This work is described in the article Tramelli el al. (submitted).

7.1 Data set

In this analysis I use 2261 local volcano-tectonic (VT) and low-magnitude (ML up to 3.6) events (figure 7.1) recorded between January 1996 and April 2000 by the seismic monitoring network of Istituto Nazionale di Geofisica e Vulcanologia, Naples.

The recording stations (figure 7.2) were: 9 low dynamic range analogical stations whose data were telemetered to the Data Analysis Center (Centro di Sorveglianza) sampled at 100 sps and 7 high dynamic range digital stations (in figure 7.2 are indicated by the last letter M) with local recording sampled at 125 sps. The coordinate of the stations are reported in the table 7.1. The sensors were 1 Hz Mark Products L4-C vertical component seismometers for the analogically telemetered stations and -3D for the digital ones. Hypocenters are located using a grid search method (see section 7.3.2) that uses the 3-D velocity model proposed by Scarpa et al. (2002) for Mt. Vesuvius. The hypocenters are mainly located below the volcano crater with a maximum depth of 7 km (figure 7.1). Due to the high cultural noise and the low-magnitude of the events many of the seismic recordings show a low signal to noise ratio. I consider only the high-quality events. In particular I discard all the events with a localization error
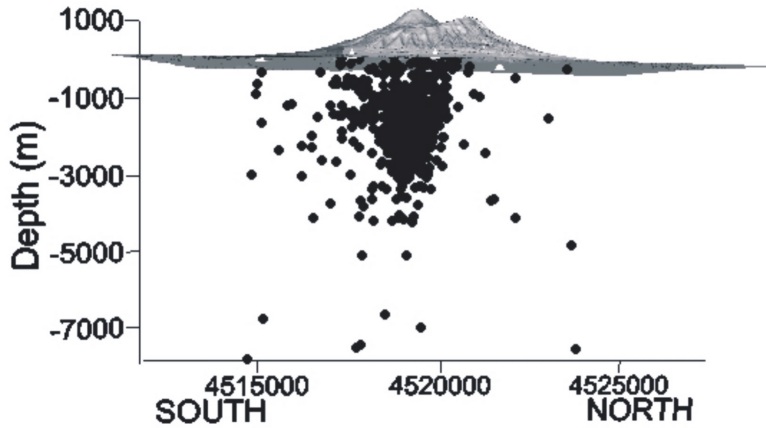
Figure 7.1: Projection on the vertical plane (Longitude-Depth) of the shaded relief map of the Somma-Vesuvius volcano with the earthquakes (black circles) used for the analysis. Axes dimensions are in meters (UTM 33); the depth is referred to the sea level.

larger than 0.3 km and I discard all the events which visually show a bad quality.

7.2 Method

I apply a modification of the Nishigami's approach (section 5.1) to obtain a 3-D scattering image of Mt. Vesuvius. Consistently with Nishigami, I assume isotropic S to S scattering and spherical source radiation, but differently, I do not assume any particular distribution of scatterers. In the standard Nishigami's method an exponential coda decay (single scattering model) is fit to the coda and an average coda Q is obtained. Than, the variation of the experimental coda decay respect to the model curve accounts for the local space variations of η_s-coefficient in the medium. My master envelope is instead calculated as the smoothed stack of the normalized envelopes as I will explain in the next section. In this way I avoid making assumptions on the distribution of background scatterers. With this variation the method maintain its validity even if the seismic waves undergo principally a diffusion process, since Wegler (2004) showed that the diffusion approximation is the one that better describes the attenuation characteristics of Mt. Vesuvius. As we are looking for the scattering anomalies overlapping the background, the method is valid whatever the characteristics of the background are. A second variation of Nishigami's method is the introduction of a 3-D velocity model obtained by Scarpa et al. (2002). Using this model I calculate the travel time with the ray-bending algorithm developed by Block (1991) that is an improvement on the Thurber method (Thurber, 1981). I modify this algorithm to take into account the sharp variations of the Vesuvius velocity field.

Name	Location	UTM Latitude (m)	UTM Longitude (m)	Elevation (m)
BAFM	Baracche forestali	4518054	450394	590
BKE	Bunker Est	4518687	452675	863
BKNM	Bunker Nord	4519986	451957	865
CPV	Cappella Vecchia	4514737	451244	190
FALM	S. Giuseppe Vesuviano	4519608	456237	200
FTCM	Forestale Trecase	4516300	452702	150
HR9	Ercolano	4517315	445075	34
OTV	Ottaviano	4521040	455009	363
OVO	Osservatorio Vesuviano	4519783	449127	584
POLM	Pollena	4522493	447965	181
SGG	S. Gregorio Matese	4470860	447306	880
SGVM	Seggiovia	4518682	450595	734
SMC	S. Maria di Castello	4522482	452348	406
SSB	S. Sebastiano al Vesuvio	4520867	447659	175
SVTM	S. Vito	4519189	446761	200
TDG	Torre del Greco	4517381	448730	300
TRZ	Terzigno	4517465	455746	175

Table 7.1: Name, location and coordinate of the utilized stations

I write the equation (5.3) for the energy density $E(t)$ at a lapse-time t and in a frequency band centered on f (Sato and Fehler, 1998, Nishigami, 1991) in terms of travel times:

$$E(t) = \overline{E(t)} \sum_{i=1}^{N} \delta(t - \frac{r_{a,i} + r_{b,i}}{v}) \frac{\alpha_i}{t_{a,i}^2 t_{b,i}^2} \tag{7.1}$$

where r_{ai} and r_{bi} are the distances between the source and the i-th scatterer and between the i-th scatterer and the receiver, respectively, and v is the mean velocity of the medium. N is the number of scatterers located in a position that satisfy the following condition on the travel time: $t_{ai} + t_{bi} \simeq t$ and δ is the Dirac delta function. α_i is the relative scattering coefficient that satisfies: $\eta_s = \overline{\eta_s} * \alpha_i$. $\overline{E(t)}$ represents the "average" scattering process at the frequency band centered on f occurring in the earth medium spanned by the coda waves. It is expressed by the experimental master coda envelope that I calculate for each station.

Dividing the bandpass filtered envelope calculated for each seismogram for the envelope master curve relative to the station that recorded it I obtain the new relation corresponding to equation (5.5):

$$res(t) = \frac{\sum_{i=1}^{N} \frac{\alpha_i}{t_{ai}^2 t_{bi}^2}}{\sum_{i=1}^{N} \frac{1}{t_{ai}^2 t_{bi}^2}} \tag{7.2}$$

where $res(t)$ is the observable energy residual associated with the time window centered in t, $[t - \delta t, t + \delta t]$; this window is valued as described in section 6.3. The matrix to be
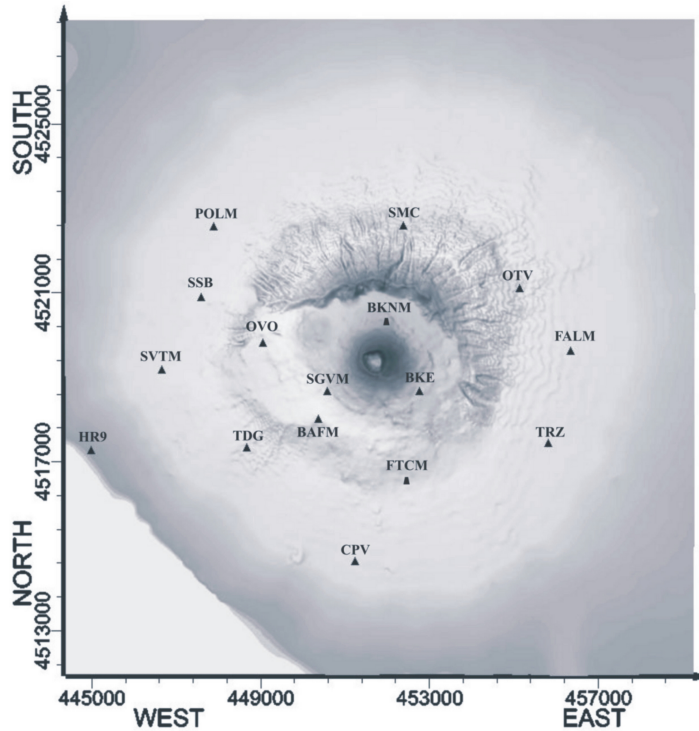
Figure 7.2: Shaded relief map of the Somma-Vesuvius volcano with the 16 stations used in the analysis (black triangles). The stations witch name ends with M are the digital ones. Axes dimensions are in meters (UTM 33).

solved will be composed of a number of rows equal to the hypocenter - station couple (the number of available seismograms) times the number of time windows analyzed. Solving the inverse problem of equation (7.2), I get the image of the distribution of the relative scattering coefficient in the medium.

The advantage that I get using the time space instead of the distance space is the fact that the time space maintains its linearity also in a complex velocity medium. In fact in equation (7.2) I just associate the energy residual to a lapse time, that is the lapse time read in the seismogram. The second step is to associate the lapse time of the residual to the space and in this case I use a detailed velocity model. Coming back to the image of prolate ellipsoid described in the Nishigami's technique paragraph, we can imagine that, in a medium with a complex velocity field, the prolate ellipsoid with hypocenter and station as foci has the standard shape in the time space, while it gets a complex shape in the distance space.

7.3   Data analysis

7.3.1   Answers to the data peculiarity

The data set available for the analysis show a peculiar geometrical configuration as all the hypocenters are located just below the Vesuvian crater in a quite narrow volume (figure 7.1) and the stations are positioned all around it (figure 7.2). Another important characteristic to take into account is the low magnitude of the earthquakes, as over all the 2261 local VT events the highest magnitude is ML=3.6. In addition, the flanks of Vesuvius are highly populated generating a background of high anthropic noise. For these motivations I have many data collected at the stations located close to the crater while the good (high signal to noise ratio) data collected by the farther stations are few. This means that I can use a big number of seismograms sampling waves that span the same little volume below the cone while I have just few seismogram sampling waves that span the wide volume around Vesuvius. Consequently I decide to assign an high weight to the good data collected by the farther stations respect to the others. For this reason, separately for each station, I define the master curve and calculate the fluctuations. In this way I aim to avoid the ellipsoidal ghost images that comes out from the association between energy residuals and space heterogeneity (Taira and Yomogida, 2003). Help in this direction is also provided by the use of the realistic travel times obtained using the 3-D velocity model. As the velocity model obtained by Scarpa et al. (2002) does not cover all the analyzed grid, I gradually extrapolated it to the regional velocity model used at Osservatorio Vesuviano for the hypocentral localizations (Finetti and Morelli, 1974).

7.3.2   Pre-analysis

Firstly I localized the events of the data set. For this scope I piked the P and S phases of the seismograms and I run the NonLinLoc program developed by Lomax to search the localization of each event (Lomax et al., 2000). This program provide a non-linear, global-search earthquake location in 3-D structures. The velocity model used for the localization is the one found by Scarpa et al. (2002).

I develop all the analysis using two frequency bands centered at 12 and 18 Hz: the first spanning the interval between 8 and 16 Hz and the second between 14 and 22 Hz. I tempted to solve also the frequency band centered on 6 Hz but, as the analyzed events have low magnitude, their coda is relatively short (maximum lapse time < 16 s) and I couldn't get a stable shape for the envelope master curve. I apply a fourth order bandpass Butterworth filter to each seismic trace for the two frequency bands and then I calculate the envelope using the Hilbert transform as in equation (6.1).

I best fit the filtered envelopes of all the seismograms with the single scattering equation as in the standard Nishigami's approach. The best fit starts, after two times

the travel time of the S waves, from the maximum of the smoothed envelope and ends at 16 s. The energy residuals are calculated as the ratio between the real envelope and the exponential best fit. Then I solve the equation (5.4) in a constant velocity model obtained averaging the velocity model of Scarpa et al. (2002) ($v = 1800$ m/s). The inversion problem is solved applying the approximated technique described in Nishigami (1991) that utilizes the overlap of the prolate ellipsoids. The solution obtained in this way shows clearly the circular ghost images (Taira and Yomogida, 2003) caused by the use of the prolate ellipsoids, as is clearly evidenced from figure 7.3. This is due to the fact that this approximated technique uses a statistical approach that works well if the events and stations are uniformly distributed in the volume analyzed. Using a large number of hypocenter - station couples many different ellipsoids that overlap in different points are obtained. For each overlapping point I can analyze the probability to have a strong scatterer.

7.3.3 Analysis

Separately for each station, I calculate the envelope master curve as the sum of the envelopes relative to the seismic events recorded by the analyzed station, after synchronizing them on the lapse time. This procedure, for the two analyzed frequency band is represented in figure 7.4. As all the events used have not the same source function, before summing, I had to normalize all the envelopes for the mean value in the window 10-12 s (the same procedure used in Del Pezzo et al., 2006b).

I use a multiscale approach. I discretize the analyzed space using two cubic-box grids, one included into the other. The first analysis is performed using a 1500 m grid space and the obtained result is used as starting solution in the inversion process referred to the second grid with 900 m grid space. The overall grid has a global cubic dimension of 15 km in the first analysis and 9 km for the second one (see figure 7.5). The grid sizes are chosen to contain a minimum of 5 wavelengths for the analyzed frequency.

I solve the problem for the vertical and horizontal component separately. For the solution I consider only nodes with at least 50 energy residuals.

The observables are the ratio between an individual envelope and the master curve for each time interval δt. δt is chosen equal to 1.5 s for the bigger grid and 0.9 s for the smaller one. In this way I get the system of equations (7.2) in the form:

$$A\mathbf{m} = \mathbf{d} \qquad\qquad (7.3)$$

where A is the matrix composed of all the terms of the sum in the right part of equation (7.2), m is the vector of the relative scattering coefficients related to each cubic clock of the grid and d is the vector of the data: the energy residuals. As the system is highly overdetermined, the best technique to solve the inversion, saving computer memory
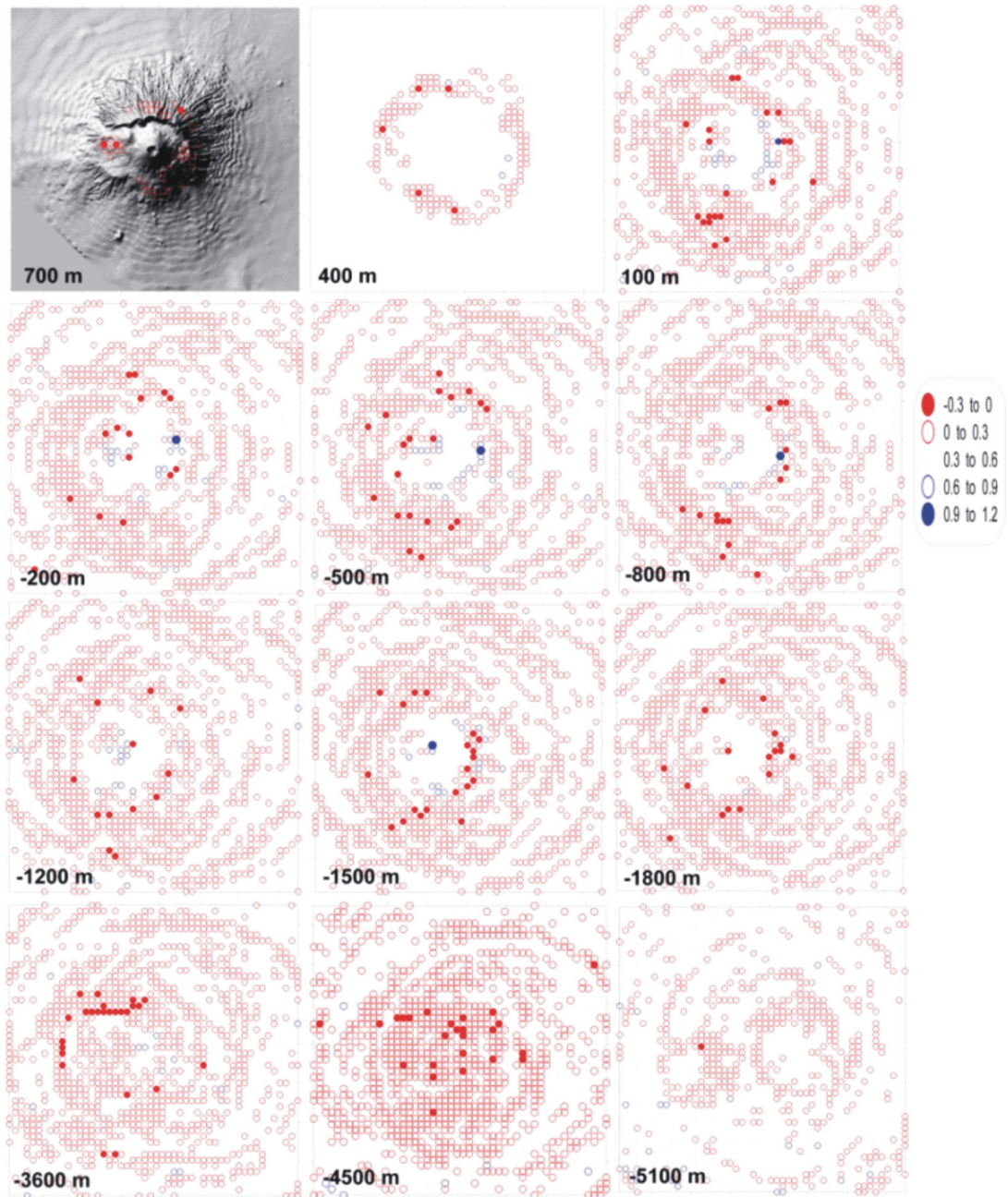
Figure 7.3: Layers representing the scatterers distribution obtained with the standard Nishigami's technique in a constant velocity model. The layers start from 700 m going down till -5100 m. The value represented by the circles is the relative scattering coefficient.
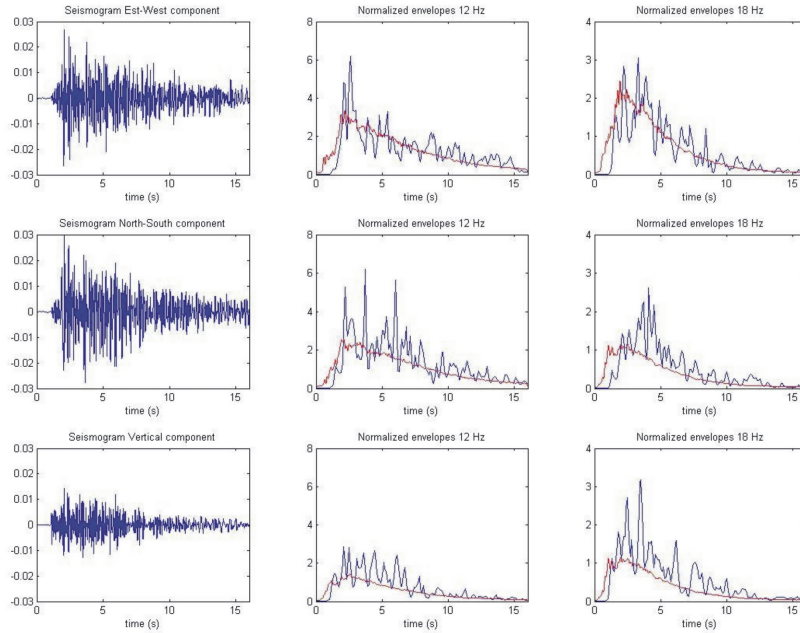
Figure 7.4: On the left: the three components of the seismogram of the event '990507150726' recorded at the station BKEM. In the center and on the right: the normalized master envelope relative to the station BKEM (red) and the normalized envelope relative to the event '990507150726' (blue); for the frequency band centered on 12 Hz (center) and 18 Hz (right).

and time, is the Conjugate Gradient Method (CGM) (Paige and Saunders, 1982). This method allows to find the local minimum of the error function. This method works particularly well in solving largely overdetermined problem with the condition that the initial solution has to be close to the real one.

I start from the solution obtained using the simplified technique. To obtain this solution I study separately each station and I use the realistic velocity model for the calculus of the travel times. Developing this task, I apply a weighting function computing a solution separately for each station. I average the solutions using the inverse of the variance of each node as a weight. Firstly I solved the inversion for the grid with 1500 m step than I rescaled this solution and used it as initial solution for the smaller grid, the 900 m step one.
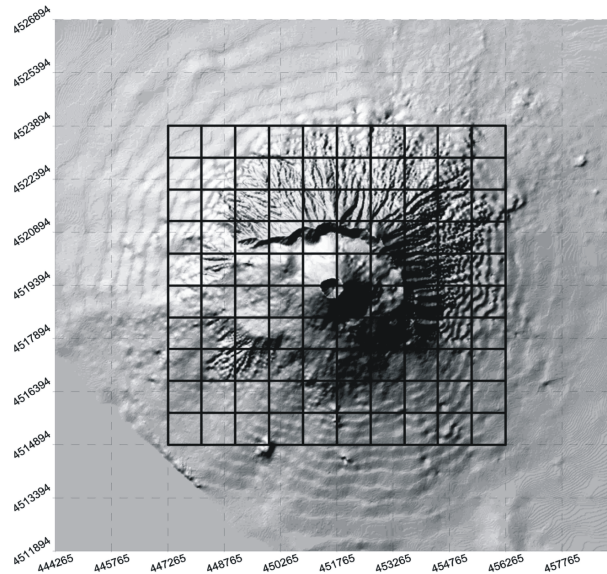
Figure 7.5: The same map as in figure 2 but with the grid representation. Dashed lines show the grid with 15 km size and steps of 1500 m; continuous lines show the grid with 9 km size and steps of 900 m. Axes dimensions are in meters (UTM 33).

7.4   Results

I find evidence of a low scattering zone below the crater, extending from sea level down to -1.5 km (figures 7.6 and 7.7). This volume is surrounded in the upper part by an high scattering zone. This pattern is particularly clear for the frequency band center on 12 Hz (figure 7.6) whereas, for 18 Hz (figure 7.7), the presence of the low scattering zone is still evident but the surrounding areas are smoothed. Another finding is the presence of a low scattering zone below the eastern part of the crater (figures 7.6a, 7.6c, 7.7a, 7.7c); this zone extends from depth of 2 to 7 km. The seismic activity at shallower depth below the Vesuvius crater is associated with local stress due to the increase in fluid pore pressure of the shallow aquifers (Saccorotti et al. 2002). I notice that most of the shallower hypocenters are located in the low scattering zone and are surrounded by an aseismic high scattering volume (figure 7.9).The shape and the position of the scattering anomalies correlates particularly well with the shape and position of the velocity anomalies showed by Scarpa et al. (2002). I would expect high scattering associated with high velocity contrast. This condition is verified especially in the western part of the map (figure 7.8). In the shallow part, east of the crater axis I note a high η_s zone that overlaps an area with high change in velocity.

For the vertical component of 12 Hz (figures 7.6c, 7.6d) I notice the presence of a high scattering zone below the low scattering area at 3 km depth on the crater axis in
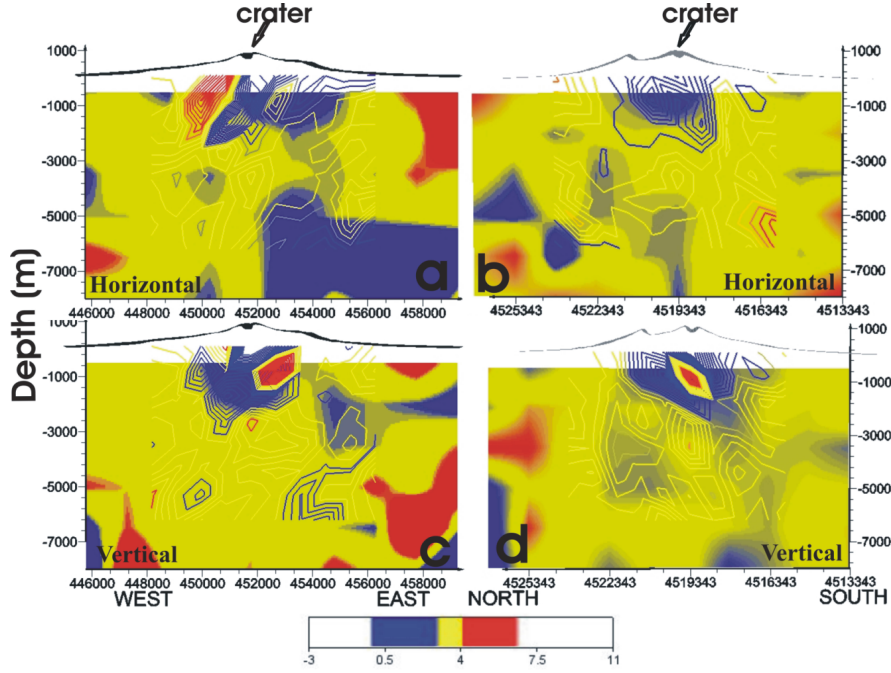
Figure 7.6: Scattering images obtained for the frequency band centered on 12 Hz for the 1500 m grid size (orthoimage) and 900 m grid size (contour plot). The colors represent the relative scattering coefficient. Axes dimensions are in meters (UTM 33).

coincidence with the area where all the more powerful events are located (Lomax et al., 2001; Scarpa et al., 2002).

It is noteworthy that, as the scattering strengths found are proportional to the relative scattering coefficient, as discussed in section 6.2.1, this value should be insensitive to the real scattering regime acting in the earth medium.

I tested the stability of the solution by introducing white noise into the initial solution. The obtained solution is unchanged from that found using the row data except for the border. I decided not to constrain the solution as it already satisfies almost all the physical conditions. In particular I should force the solution to be positive everywhere, as the scattering coefficient, η_s, must be positive and as a consequence also α have to be greater than zero ($\eta_s = \overline{\eta_s} * \alpha$). I verified that there are no negative values except for the nodes that are located immediately below the crater. This is due to the fact that we have a small number of energy residuals referred to these nodes. I would have also constrained the solution obtained for the smaller size grid (900 m) to be compatible with the solution obtained for the larger size grid (1500 m). I found that they are very similar anyway and the fact that I do not force the proximity gives me a bigger confidence in its validity.
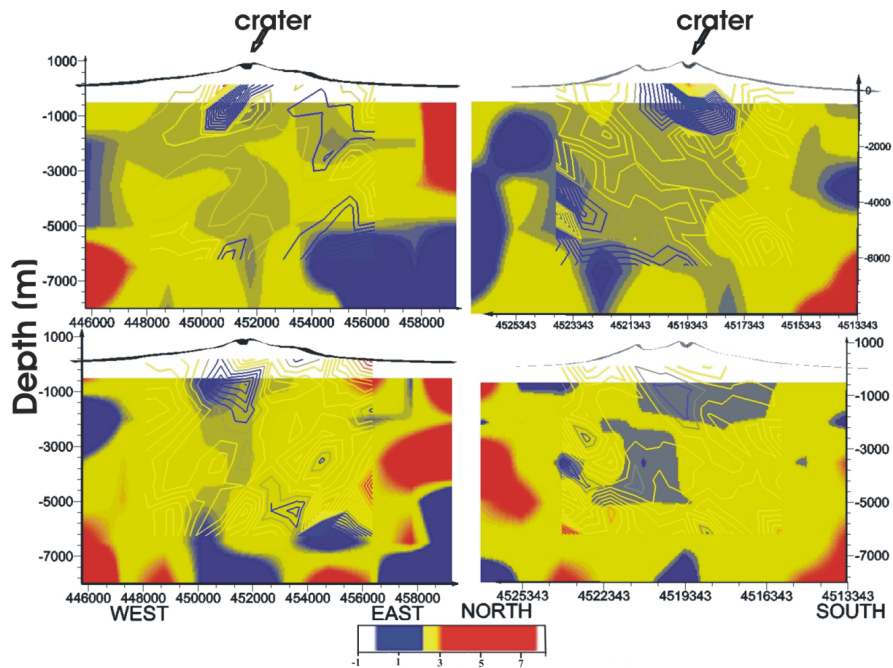
Figure 7.7: The same as in figure 4 but for the frequency band centered on 18 Hz.

7.5　Limits of the technique and interpretation of the results

This work is done with the purpose of adding information on the structure of the Vesuvius volcanic edifice.

Despite the modifications I have introduced in the method I cannot obtain a resolution better than that associated with a 900 m cell side. This limitation is partly due to the particular distribution of the earthquake sources with respect to the seismic stations, and partly by the unfavorable signal to noise ratio of the area, which makes the analysis in the late coda impossible.

In recent years many studies have been focused onto the knowledge of the deep geological structure of this volcano, the majority of them being investigations of the structural properties. Active (Zollo et al., 2002, Auger et al., 2001, Capuano et al. 2003) and passive (Scarpa et al. 2002, De Natale et al., 2004) seismic tomographies show that Mt. Vesuvius is located on the Mesozoic limestone that sinks below the caldera. This depression is filled with an high velocity body that can be associated to a paleo-volcanic or sub-volcanic (solidified dikes) structure (Zollo et al. 2002). Around 8 km depth Auger et al. (2001) found an interface that reflect P and S waves that is interpreted as the top of a fluid-containing layer. Another two phase, solid-fluid, body is located by
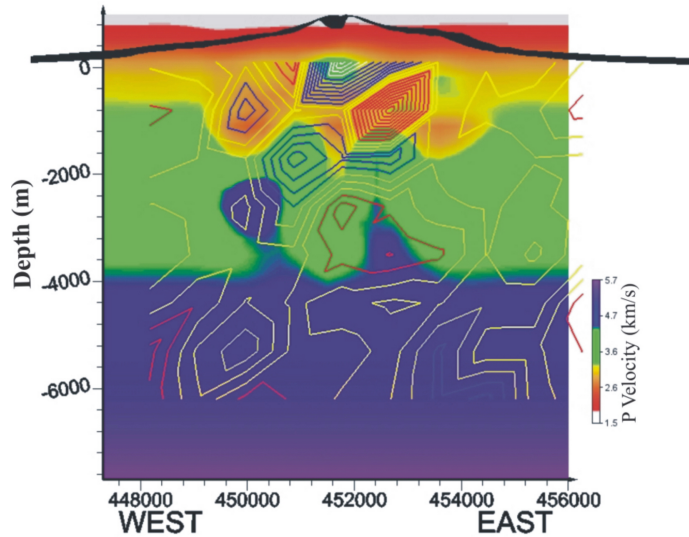
Figure 7.8: Overlapping of the vertical profile obtained by the velocity tomography (Scarpa et al. 2002) (orthoimage) and the image obtained in this work for the frequency band centered on 12 Hz (contour plot). For the scattering images the color palette is the same as in figure 7.6. Axes dimensions are in meters (UTM 33).

Chiodini et al. (2001) between 1 to 4 km b.s.l. below the caldera. The seismograms from shots recorded during the TOMOVES (Gasparini, 1998) experiment with a small aperture array were also analyzed by La Rocca et al. (2001) to locate the source of the coherent phases in the coda, and hence to determine the locations of "strong" scatterers; in this work the authors analyzed a wide area spanning all the Neapolitan gulf and found that the topographical relief plays an important role in the scattering of high frequency waves. They produced an image at a scale that is larger than that used in our analysis. In a review of their previous papers, De Natale et al. (2006) interpreted the high velocity body located around the crater axis as a shallow high rigidity body. It is surrounded by low velocity rocks that are interpreted as compacted pyroclastic and fragmented products deposed during past eruptions. The same high-velocity feature was found by Scarpa et al. (2002) with a better resolution. The most peculiar result of the present work is the identification of a low scattering zone around the crater axis extending from the surface to 2.5-3 km of depth laterally surrounded in the upper part by a high scattering area. The high scattering regions are interpreted as zones of high
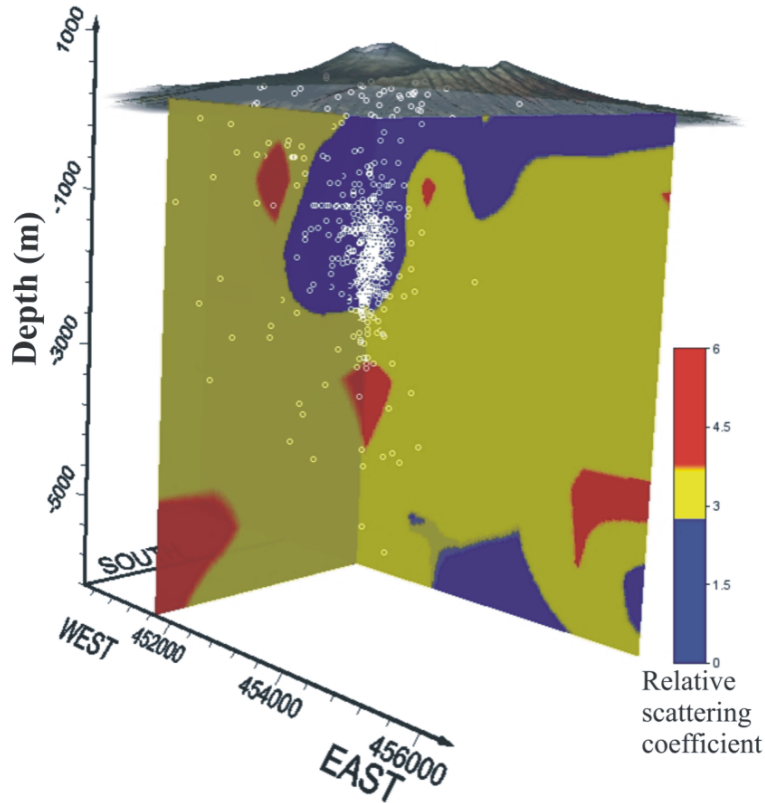
Figure 7.9: Comparison between the localization of the earthquakes happened in the Vesuvian area between 1996 and 2000 (white circles) and the scattering image obtained in this work for the frequency band centered on 12 Hz. Axes dimensions are in meters (UTM 33); the depth is referred to the sea level.

structural contrast. The joint interpretation of the scattering with velocity images lead me to think that the high scattering is due to the contrast between the high rigidity body located beneath the crater and the low rigidity materials located around it. Aki and Ferrazini (2000) found the same pattern (high Vp and low scattering) at Piton de la Fournaise volcano. They explained this result with the presence of a medium characterized by fluid-filled cracks (Berryman, 1988, Berryman, 1988); such a medium can vary velocity and direction of the waves passing through it. The presence of fluid filled cracks below the crater of Mt. Vesuvius is described by Chiodini et al. (2001) who place an hydrothermal reservoirs just below the volcano crater connected with the fumarolic vents visible on Vesuvius. This reservoir is in the same position where I find a low scattering area and where the velocity tomography shows high values of Vp and Vp/Vs ratio (Scarpa et al. 2002).

In the interpretation of the results from scattering imaging, it is necessary to take

into account the frequency bands in which the analysis is carried out, as the wavelength is a crucial parameter in the definition of the scattering regime (Wu and Aki, 1988a). I assume the "large angle" scattering regime (see section 3.4) as in this regime the scattering effects are most significant. In this regime $ka \approx 1$, where k is the wave number and a is the heterogeneities scale. In the frequency band analyzed in the present paper (centered on 12 and 18 Hz), the size of heterogeneities spans from 2 to 500 m approximately. All the heterogeneities with size out of this interval are too small to be seen or to big to generate significant scattering energy.

Interestingly, most of the shallower hypocenters are located in the low scattering zone and are surrounded by an aseismic high scattering volume, while the events with higher magnitude are located at the bottom of this area where I find a high scattering zone (see figure 7.9). This shallow seismic activity has been associated by Del Pezzo et al. (2004) with an increase of local stress due to the increase in fluid pore pressure of the shallow aquifers.

To obtain a better resolution different techniques are necessary: I am planning for this purpose to use the data collected by a small aperture array positioned on the Vesuvian flank and to apply array techniques to localize the scatterers.

Chapter 8

Anomalous character of the coda envelopes on Vesuvius: coda localization?

The Earth medium has various scales of inhomogeneities as already discussed in section 4.2. When the inhomogeneities are strong and highly anisotropic, the wave propagation is confined to a few kilometers from the source or the receiver (Papanicolaou, 1998). In the case that the random inhomogeneities act to spatially limit the propagation of wave energy, the regime of wave localization is reached.

The concept of localization was introduced by Philip Anderson (1958) for electrons in a semiconductor. His theoretical prediction was followed by the observation of a weak form of light localization due to coherent backscattering. In a perfect atomic crystal visible light travels ballistically and, occasionally is scattered off from a lattice atom. As disorder increases the frequency of scattering increases as well, and the passage of light through the crystal becomes diffusive. When the disorder is such that interference occurs between individual scattering events, then light can become spatially localized (Vardeny and Raikh, 2007). Many experiments have shown that when interference phenomena occur, the underlying wave character can no longer be neglected.

In classical elasticity the same phenomena occur. When the elastic wave propagates in a random medium where disorder is very large, interference effects dominate and multiple scattering can no longer be described classically. The elastic wave localization is the total trapping of the wave energy by scattering from the random inhomogeneities. In seismology the coda localization manifests itself in fat codas of seismograms or codas with envelopes characterized by an anomalous slow time decay. Friedrich and Wegler (2005) emphasize that the term 'Anderson localization' (a physical model) should

not be mixed up with the term 'coda localization' (an observation). The regime of Anderson localization is reached if the Ioffe Regel criterion $kl < 1$ is met, where k is the wave number and l is the scattering mean free path. In volcano seismology effects of Anderson localization were discussed by Aki and Ferrazzini (2000) and Wegler and Luhr (2001).

Aki and Ferrazzini (2000) studied volcano tectonics events for tracing the magma movement in the volcano Piton de la Fournaise in La Reunion. They found that the site amplification factor systematically depends on the location of the source: the coda waves are strongly localized in the summit area when the source is under the summit. They justified this phenomenon with the generation of slow waves trapped in the fluid-solid two-phase system of magma body. Such an energy concentration at the center of the volcano has been found also by Friedrich and Wegler (2005) at Merapi volcano, Indonesia. Yoshimoto et al. (2006) analyzed the local earthquakes with high magnitude in the Tohoku region, Japan, and observed a clear lateral variation of coda energy. In particular they found that at high frequencies the coda energy is distributed homogeneously in the forearc, while it decreases monotonically from the volcanic front in the backarc. They underlined as their and previously studies indicate that the assumption of uniformity of the spatial distribution of the coda wave energy should not be adopted without verification. It is expected that a non uniform distribution of coda wave energy will in general be observed near the boundary of different seismic attenuation structures.

8.1 Space changes of coda envelope decay rate at Vesuvius

It has been verified that sometimes Q_c^{-1} takes different values inside a restricted tectonic region, especially in correspondence with volcanic structures (Aki and Ferrazzini, 2000, Friedrich and Wegler, 2005, Yoshimoto et al., 2006). In order to search if "localization" phenomena are present in the scattered waves of the local seismograms recorded at Mt. Vesuvius, I carry on a study of the coda envelope shape for these seismograms. The coda envelope shape can be easily parametrized through the Q_c^{-1} value, discussed in section 4.2.

For this task I analyze the spatial distribution of Q_c^{-1} at Mt. Vesuvius using the data set described in section 7.1 and I calculate its value as the slope of the straight line fitting the measured $\ln(t^2 E_{ss}(\omega|t))$ as a function of the lapse time, t, as described in section 4.2. The starting point for the fit is taken as the maximum value of the envelope found after two times the S waves travel time. The end point is taken at 16 s. I analyzed the two frequency band centered at 12 and 18 Hz described in section 7.3.

Firstly I studied whether Q_c^{-1} shows any variation with increasing hypocentral depth. I studied the values separately for each station and I found no variation with depth.

Successively I analyzed the spatial variation of Q_c^{-1}. For this purpose I calculated the value relative to each station using the envelope master curve estimated for the scattering analysis described in section 7.3. The use of this staked envelope allows to reduce the error associated with the single estimates of Q_c^{-1}. The results obtained are plotted in figures 8.1 and 8.2 for the frequency band centered at 18 and 12 Hz respectively. The relative error associated with the fit is of the order of 10%. As is

Figure 8.1: Plot of the Q_c^{-1} relative to the frequency band centered on 18 Hz associated with the single stations. The values are calculated using the vertical component of the registration.

shown in figures 8.1 and 8.2, the Q_c^{-1} pattern shows a higher value at the volcano summit that radially decreases, except for SVT. This means that the coda envelopes at the stations BAF, SGV and BKN decrease faster than those at the farthest stations. Excluding SVT, BAF shows the highest values of Q_c^{-1}: 0.004 and 0.003 for 18 and 12 Hz respectively. I will not give any interpretation about the vales found for the station SVT as the number of seismograms recorded by this station is too low to ensure a sufficient stability of Q_c^{-1} estimate.
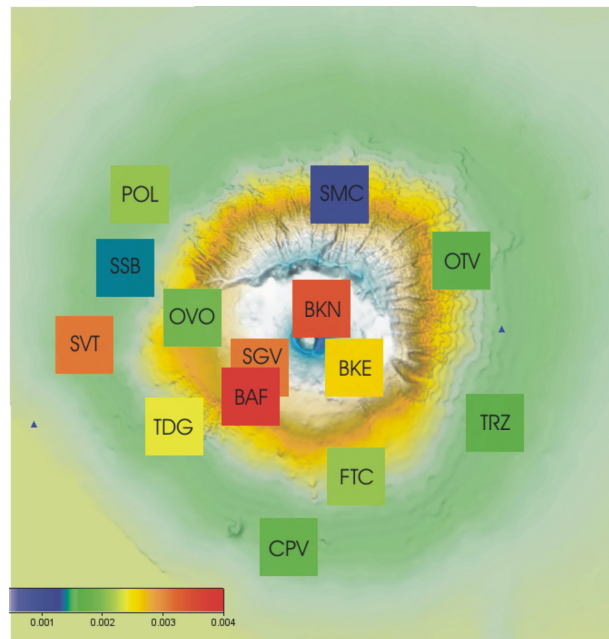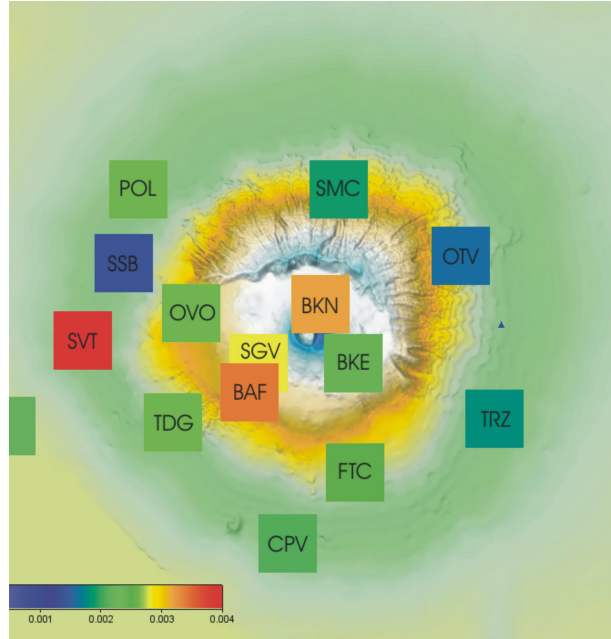
Figure 8.2: Plot of the Q_c^{-1} relative to the frequency band centered on 12 Hz associated with the single stations. The values are calculated using the vertical component of the registration.

8.2 Applicability of the coda normalization method at Vesuvius

The existence of the coda localization effect in the scattered wave field at Mt. Vesuvius implies that most of the analysis, based on the space uniformity of the scattered wave field, can not be applied to the local data. In particular, in the present thesis, I discuss the application of the coda normalization method, widely applied through the world to estimate the average total attenuation coefficient (see section 4.3).

For this analysis I used part of the data set used for the Q_c^{-1} analysis. I apply the coda normalization method to the seismograms. For each seismogram I measured the spectral amplitude of both the direct S wave and of coda waves (in a time window centered at 9 s lapse time).

I filtered the seismograms with a fourth order bandpass Butterworth filter for different frequency bands centered at 3, 6, 12 and 18 Hz; the filtering windows are reported in table 8.2.

The S wave spectral amplitude, described by equation (4.5), is estimated calculating the logarithmic mean of the filtered seismogram in a time window of 2 s staring from the S wave arrival. The time window length of 2 seconds allows to neglect the radiation

Central frequency (Hz)	Frequency window (Hz)
3	1 - 5
6	3 - 9
12	8 - 16
18	14 - 22

pattern effects as experimentally demonstrated by Del Pezzo et al. (2006) for seismic events sharing the same characteristics of those utilized in the present work. The coda wave spectral amplitude, described by equation (4.6), is estimated from the logarithmic mean of the filtered seismogram calculated in the lapse time window between 8 and 10 s; I checked also the window between 10 and 12 s finding no differences in the results. As described by equation (4.7) I calculate the logarithm of the ratio of the S wave multiplied for the hypocenter - station distance and the coda waves amplitude. For clarity I rewrite equation (4.7) here:

$$\left\langle \ln\left(\frac{A_i(\omega)D}{A_i^C(\omega, t_0)}\right)\right\rangle_{D\pm\Delta D} = a - \frac{\pi f Q_S^{-1}}{v}D \tag{8.1}$$

The distance is taken in kilometers as I take the critical distance for the far field condition equal to 1 km (see section 4.3). The analysis is done separately for the horizontal and vertical component. The two horizontal components are composed through the geometrical mean of their envelopes. I show the results in figure 8.3, 8.4 and 8.5. It is evident from the plots that the quantity at the left side of equation 8.1 can be fitted with a straight line with positive angular coefficient for the stations closer to the cone (upper graphs of the plot). The line tends to become parallel to the abscissa for the farthest stations: FAL, POL, SVT. Unfortunately there are too few data collected at the farthest stations, especially at SVT, and the trend can not be studied for these stations. Anyway, for the closest stations the trend is always positive and the angular coefficient of the fit seems to increase with decreasing frequency.

This result contrasts with the theory, as the ratio represented in the plots 8.3, 8.4 and 8.5 should be fitted with the line: $y = a - \frac{\pi f Q_S^{-1}}{v}D$, where Q_S^{-1} is the mean S wave attenuation in the medium. Assuming that this method is applicable for the seismograms registered at Mt. Vesuvius, the "non-physical" conclusion that Q_S^{-1} is less than zero may be deduced. Consequently, the coda normalization method can not be applied on these data.

8.3 Discussions on the results

The positive trend of the plots may be explained hypothesizing that the coda amplitude decreases with increasing source - receiver distance, the contrary to what experimentally observed worldwide for most of the tectonically active areas. This observation
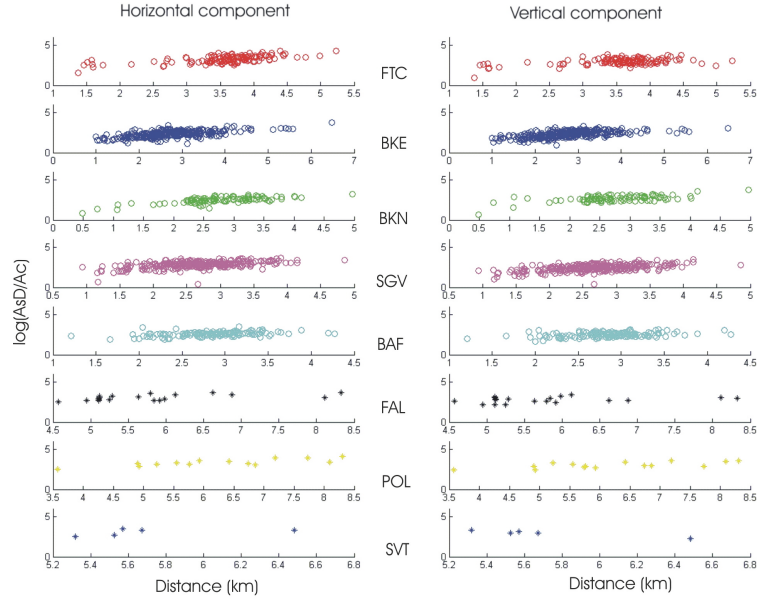
Figure 8.3: Plot of the logarithm of the ratio of the S wave amplitude over the coda wave amplitude corrected for the geometrical spreading for the frequency window centered on 6 Hz. The left panels show the results obtained for the horizontal components whereas the right panels show the vertical one. Each row is relative to an analyzed station.

can be interpreted in terms of coda localization phenomena, as done by Friedrich and Wegler (2005). These authors analyze the seismic data collected at the volcano Merapi finding a systematic decrease of the coda amplitude with the distance from the summit of the volcano. They justify this result with the trapping of the scattered waves inside the volcano area. There, strong multiple scattering phenomena occur, and the coda amplitude can be larger than the amplitude of the direct wave, as demonstrate by Nakamura (1977) analyzing the moonquakes.

An excessive amount of coda energy in the early coda is also found by Hoshiba (1995) in western Japan. He calculates the ratio of the energy in the early coda to the energy of the late coda, $\frac{E_{early}}{E_{late}}$. He shows that, if the scattering is isotropic, this ratio decreases with increasing source - receiver distance, D, whereas if the forward scattering is predominant, the early coda amplitude is bigger than the expected and the ratio $\frac{E_{early}}{E_{late}}$ increases with D. The values of the scattering coefficient used by Hoshiba span from $\eta_s \rightarrow 0$ to $\eta_s = 0.1$ km^{-1}.

This considerations can explain the figures 8.3, 8.4 and 8.5.

The same figures can also be interpreted in a different way as Q_c^{-1} is close to Q_I^{-1} (see section 4.2). The Q_c^{-1} results indicate that at Mt. Vesuvius the part of the volcano
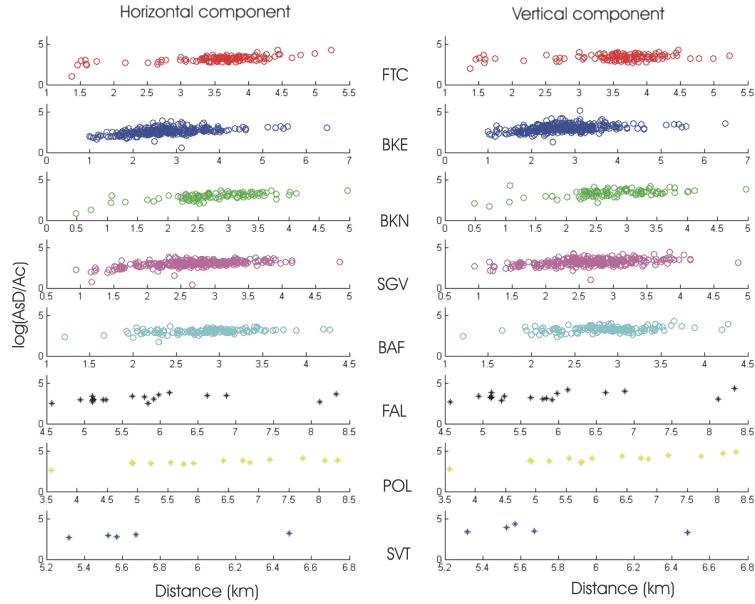
Figure 8.4: The same plot as in figure 8.3 but for the frequency window centered on 12 Hz.

below the crater is more dissipative (high Q_I^{-1}) than that outside the volcano crater.

An opposite behavior was found by Mayeda et al. (1992) at the Kilauea volcano, Hawaii. These authors find that, at low frequencies, the stations close to the crater are characterized by low values of Q_c^{-1} if compared to the values measured at the farthest stations, whereas they find no differences at high frequencies. They associate this variation with the length of the coda waves, i.e. a longer coda is needed to estimate the Q_c^{-1} relative to low frequencies. In fact, they verified that extending the coda amplitude measurements to later lapse time the differences in the values decrease. Unfortunately, the data collected at Vesuvius do not allow to use codas longer than the ones I used, as all the earthquakes have low magnitude. Anyway, because of this limit, I analyzed just high frequencies.

An other phenomenon that should be taken into account is the site effect. The site transfer function should not influence the analysis done on the ratio of S to coda amplitude. Tsujura (1978) showed that the site effect for the S coda waves is the same as that for direct S waves (the same is not demonstrated for P waves). However, it can influence the coda decay rate. I considered the analysis performed by Galluzzo (2007) on the site effects of some of the stations located on Mt. Vesuvius. He calculates the site transfer function with different techniques and compares the results. He finds that, for the stations located close to the cone, the site amplification calculated with the coda waves is higher than the amplification found with other methods. This result
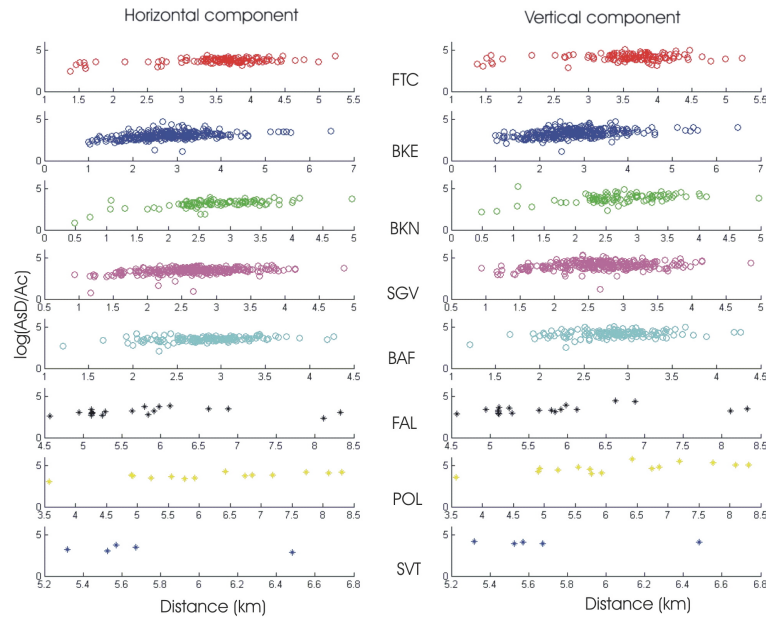
Figure 8.5: The same plot as in figure 8.3 but for the frequency window centered on 18 Hz.

indirectly confirms the interpretation that the phenomenon of coda localization is possibly located in the volume below the cone of Mt. Vesuvius.

In other terms, the behavior of the $\frac{A_S * D}{A_{coda}}$ ratio as a function of the distance may be explained as follows. Due to the presence of a highly heterogeneous low velocity volume, coincident with the volcanic cone, the seismic waves move to the homogeneous and faster zone located below. The seismic events are located principally at the bottom of this heterogeneous volume and the energy emitted, due to the Fermat's principle, travels below the volcanic edifice through the zone characterized by higher velocity reaching the farthest stations. The waves that pass through the volcano edifice are slow and tend to be trapped into the volcanic edifice. This explain the positive trend of the curve $log(\frac{A_S * D}{A_{coda}})$ vs distance and the lack of energy in the codas of the seismograms recorded by the stations located at the summit of the volcano (high Q_c^{-1}). This is an alternative way to justify the same observations that can be interpreted in terms of coda localization phenomena.

Conclusions

In this thesis I describe the results obtained from a study of the scattering properties of the earth medium below two campanian volcanoes: Campi Flegrei and Vesuvius (some of these results are also described in Tramelli et al. (2006) and Tramelli et al. - submitted).

Both volcanoes are extensively studied and monitored being of crucial importance for the Italian Civil Protection due to the high population density present in these two areas. Within the Italian Civil Protection projects, in cooperation with the INGV, I developed a scattering analysis of those areas with the aim to improve the knowledge of the structural model of these volcanoes.

The power of the scattering analysis is related to the frequencies that compose the seismic wave spectrum of the analyzed earthquake. The scattering manifests itself principally when the size of the heterogeneities is similar to the size of the wavelength of the seismic waves. In this case the scattering imaging allows to give additional informations on the seismic and attenuation tomographies. It supply informations about the mean scattering properties of the medium and allows to locate the high heterogeneities. The scattering imaging is particularly useful in detecting contrasts in the elastic properties of the earth medium, as, for example, variation in the velocity field, or fracture systems, or zones with a heterogeneous lithology, or volumes characterized by a density anomaly. The scattering images need to be analyzed in connection with other geophysical properties of the medium. In this sense I analyzed the results found for Campi Flegrei and Vesuvius.

For the Campi Flegeri area the scattering imaging shows an high scattering zone in correspondence with the submerged caldera rim in the southern part of the Pozzuoli bay. The border is well visible in high frequency images, and it corresponds to a probably fractured zone. This high scattering area coincides with an high P waves velocity zone (Judenherc and Zollo, 2005, Vanorio et al., 2005). The results of Orsi et al. (1996), based on field geology, confirmed the presence below the sea of the collapsed caldera related to the eruption of the Neapolitan Yellow Tuff (12 ka). These authors based the location of the structural rim of the caldera mostly on gravimetric and magnetic data, distribution of vents younger than 12 ka and distribution of dated

level surfaces in the submerged portion of Campi Flegrei. The results of the scattering imaging are possibly influenced by the topography, as it is possible that the high scattering values in correspondence with the subaerial caldera are generated by the topography itself. On land, an high scattering zone is found almost coincident with the inner part of the subaerial caldera rim as inferred by geological observations (Orsi et al. 1996).

In lower frequency images (central frequency equals to 6 and 12 Hz) an high scattering zone is found below the Solfatara crater. This is the area with the highest concentration of earthquake hypocenters and in the same position the strongest low-Q_P anomaly is found (De Lorenzo et al., 2001a). The area of the Solfatara crater is also characterized by the presence of densely fractured, fluid-filled rocks and by a strong thermal anomaly (Chiodini et al., 2001a).

For Mt. Vesuvius scattering images show a low scattering area immediately below the cone surrounded by an high scattering area. I interpret the high scattering regions as zones of high structural contrast. The high scattering zone seems to be due to the contrast between the high rigidity body located beneath the crater and the low rigidity materials located around it. Quareni et al. (2007) found a magmatic tip located just below the volcanic cone that is surrounded by heated rocks that create a rigid "carapace" formed as a consequence of the mineral phase precipitation from hot brines. This "carapace" seams to coincide with the high scattering zone found in this thesis work. Chiodini et al. (2001) placed an hydrothermal reservoirs just below the volcano crater that is located in the same position where the scattering imaging shows a low scattering area and where the velocity tomography shows high values of Vp and Vp/Vs ratio (Scarpa et al. 2002). Following Aki and Ferrazini (2000), the presence of the two phase, solid - fluid body below the caldera of Mt. Vesuvius can modify the velocity and direction of S waves passing through it generating a low scattering volume.

The strong heterogeneity present inside the volcanic edifice causes the "coda localization" phenomenon. The analysis done on the coda of the local VT earthquakes recorded on Vesuvius shows how the volcanic edifice tends to trap the seismic waves at the bottom of its structure. The seismic energy seems to be channelled in the high velocity structure below the volcano.

The analysis of the temporal change of the Q_c^{-1} parameter shows that there are no changes during the analyzed time period (1996-2000).

The studies conducted in this thesis on the peculiar shape of the coda envelopes relative to local VT earthquakes can give practical advantage for the future seismological studies that will be conducted on Mt. Vesuvius. The analysis that uses the coda of the seismogram have to take into account the results described in chapter 8.

A better understanding of small scale heterogeneities in the two volcanic areas studied in this thesis, could be obtained interpreting them in terms of geological properties

of the medium. A new project, financed by the Civil Protection Department of Italy, in cooperation with the INGV, aims to understand the connection between the physical properties obtained with different tomographies. This project takes advantage of the previous analysis developed in the volcanic areas of Campi Flegrei and Vesuvius. The images developed in this thesis constitute part of these previous informations.

The scattering imaging developed in Campi Flegrei and Mt. Vesuvius has been developed considering scatterers with time invariant nature and position. The variation of the position or of the properties of the small scale heterogeneities can have important consequences on the dynamics of volcanic system. The coda wave interferometry analysis can determine changes in the velocity of the earth medium. Changes in the position of scatterers can be determined applying the interferometry techniques to data collected by an array. For this motivation it may be interesting to conduct this studies on Mt. Vesuvius and Campi Flegrei. It would be interesting to see if there have been any variation in the scattering properties in correspondence with the different bradyseismic phenomena of Campi Flegrei or if there have been any temporal variation in the attenuation parameter characterizing Mt. Vesuvius despite its relatively low seismicity.

Bibliography

Abubakirov, I. R. and Gusev, A. A., 1990, Estimation of scattering properties of lithosphere of Kamchatka based on Monte-Carlo simulation of record envelope of a near earthquake, *Phys. Earth Planet. Inter.* **64**, 52–67.

Aki, K., 1956, Correlogram analyses of seismograms by means of a simple automatic computer, *J. Phys. Earth* **4**, 71–79.

Aki, K., 1966, Generation and propagation of G waves from the Niigata earthquake of June 16, 1964, *Bull. Earthquake Res. Inst., Tokyo Univ.* **44**, 23–88.

Aki, K., 1969, Analysis of the seismic coda of local earthquakes as scattered waves, *J. Geophys. Res.* **74**, 615–631.

Aki, K., 1980a, Attenuation of shear-waves in the lithosphere for frequencies from 0.05 to 25 Hz, *Phys. Earth Planet. Inter.* **21**, 50–60.

Aki, K., 1980b, Scattering and attenuation of shear waves in the lithosphere, *J. Geophys. Res.* **85**, 6496–6504.

Aki, K., 1982, Scattering and attenuation, *Bull. Seismol. Soc. Am.* **72**, S319–S330.

Aki, K., 1985, Theory of earthquakes prediction with special reference to monitoring of the quality factor of lithosphere by the coda method, *Earthq. Predict. Res.* **3**, 219–230.

Aki, K., 1992, Scattering conversions P to S versus S to P, *Bull. Seismol. Soc. Am.* **82**, 1969–1972.

Aki, K., 1996, Scale dependence in earthquake phenomena and its relevance to earthquake prediction, *Proc. Natl. Acad. Sci. USA* **93**, 3740–3747, Colloquium Paper.

Aki, K. and Chouet, B., 1975, Origin of coda waves: Source, Attenuation, and Scattering Effects, *J. Geophys. Res.* **80**, 3322–3342.

Aki, K. and Ferrazzini, V., 2000, Seismic monitoring and modeling of an active volcano for prediction, *J. Geophys. Res.* **105**, 16617–16640.

Aki, K. and Richards, P., 1980, Quantitative Seismology - Theory and Methods, W. H. Freeman, San Francisco.

Aki, K. and Tsujiura, M., 1959, Correlation study of near earthquake waves, *Bull. Earthquake Res. Inst., Tokyo Univ.* **37**, 203–232.

Aki, K., Tsujiura, M., Hori, M., and Goto, K., 1958, Spectral study of near earthquake wave, *Bull. Earthquake Res. Inst., Tokyo Univ.* **36**, 71–98.

Akinci, A., Taktakj, A. G., and Ergintav, S., 1994, Attenuation of coda waves in Western Anatolia, *Phys. Earth Planet. Int.* **87**, 155–165.

Anderson, P. W., 1958, Absence of diffusion in certain random lattice, *Phys. Rev.* **109**, 1492–1505.

Asano, Y. and Hasegawa, A., 2004, Imaging the fault zones of the 2000 western Tottori earthquake by a new inversion method to estimate three–dimensional distribution of the scattering coefficient, *J. Geophys. Res.* **B06306**(109).

Aster, R. and Meyer, R., 1988, Three dimensional velocity structure and hypocenter distribution in the Campi Flegrei caldera, Italy, *Tectonophysics* **149**, 195–218.

Aster, R., Meyer, R., Natale, G. D., Martini, M., Pezzo, E. D., Iannaccone, G., and Scarpa, R., 1989, Seismic investigation of the Campi Flegrei: a synthesis and summary of results, Editors: K. Aki and P. Gasparini and R. Scarpa. In: Volcanic Seismology, Proc. Volc. series III, Springer-Verlag, San Francisco.

Auger, E., Gasparini, P., Virieux, J., and Zollo, A., 2001, Seismic Evidence of an Extended Magmatic Sill Under Mt. Vesuvius, *Science* **294**, 1510–1512.

Baqer, S. and Mitchell, B. J., 1998, Regional variation of Lg coda Q in the continental United Stataes and its relation to crustal structure and evolution, *Pure Appl. Geophys.* **153**, 613–638.

Berryman, J. G., 1988, Seismic wave attenuation in fluid-saturated porous media, *J. Pure Appl. Geophys.* **128**, 423–432.

Bianco, F., Castellano, M., Milano, G., Vilardo, G., Ferrucci, F., , and Gresta, S., 1999, The seismic crises at Mt. Vesuvius during 1995 and 1996, *Phys. Chem. Earth* **24**, 977Ű–983.

Bisztricsany, E. A., 1958, A new method for the determination of the magnitude of earthquakes, *Geofiz. Kozlemen* **7**(2), 69–76.

Blakeslee, S. N. and Malin, P. E., 1990, A comparison of earthquake coda waves at surface versus subsurface seismometers, *J. Geophys. Res.* **95**, 309–326.

Block, L. V., 1991, Joint hypocenter–velocity inversion of local earthquake arrival time data in two geothermal regions, Ph.d. dissertation, Massachusetts Institute of Technology, Cambridge.

Capuano, P., Gasparini, P., Zollo, A., Virieux, J., Casale, R., and Yeroyanni, M., 2003, The internal structure of Mt. Vesuvius, Liguori, Napoli.

Chandrasekhar, S., 1960, Radiative treansfer, Dover, Mineola, New York.

Chiodini, G., Frondini, F., Cardellini, C., Granieri, D., Marini, L., and Ventura, G., 2001a, CO_2 degassing and energy release at Solfatara volcano, Campi Flegrei, *J. Geophys. Res.* **106**, 16213–16221.

Chiodini, G., Gasparini, P., Zollo, A., Virieux, J., Casale, R., and Yeroyanni, M., 2001b, The internal structure of Mt. Vesuvius, Liguori, Napoli.

Chouet, B., 1979, Temporal variation in the attenuation of earthquake coda near Stone Canyon, California, *Geophys. Res. Lett.* **6**, 143–146.

Civetta, L. and Santacroce, R., 1992, Steady-state magma suppl in the last 3400 years of Vesuvian activity, *Acta Vulcanol.* **2**, 147Ű–159.

Dainty, A. M. and Toksoz, M. N., 1981, Seismic codas on the Earth and the Moon: a comparison, *Phys. Earth Planet. Interiors* **26**, 250–260.

De Lorenzo, S., Gasparini, P., Mongelli, F., and Zollo, A., 2001a, Thermal state of the Campi Flegrei Caldera inferred from seismic attenuation tomography, *J. Geodynamics* **32**, 476–486.

De Lorenzo, S., Zollo, A., and Mongelli, F., 2001b, Source parameters and three-dimensional attenuation structure from the inversion of microearthquake pulse width data: Qp imaging and inferences on the thermal state of the Campi Flegrei caldera (southern Italy), *J.Geophys. Res.* **106**, 16265–16286.

De Lorenzo, S., Zollo, A., Trabace, M., and Vassallo, M.: 2007, QP and QS of Campi Flegrei from the inversion of rayleigh waves recorded during the SERAPIS project. Earth-Prints.
URL: *http://hdl.handle.net/2122/3044*

De Natale, G., Troise, C., Pingue, F., Mastrolorenzo, G., and Pappalardo, L., 2006, The Somma–Vesuvius volcano (Southern Italy): Structure, dynamics and hazard evaluation, *Earth Sci. Rev.* **74**, 73–111.

De Natale, G., Troise, C., Triglia, R., Dolfi, D., and Chiarabba, C., 2004, Seismicity and 3–D substructure at Somma–Vesuvius volcano: evidence for magma quenching, *Social Science Computing Review* **221**, 181–196.

Del Pezzo, E., Allotta, R., and Patane, D., 1990, Dependence of Qc (coda Q) on coda duration time interval:model or depth effect?, *Bull. seism. Soc. Am.* **80**, 1028–1033.

Del Pezzo, E., Bianco, F., De Siena, L., and Zollo, A., 2006a, Small scale shallow attenuation structure at Mt. Vesuvius, *Phys. Earth Planet. Interiors* **157**, 257–268.

Del Pezzo, E., Bianco, F., Patanè, G., and q. Ferrari: 2007, Observation of coda signals from regional and local earthquakes recorded from a downhole-uphole couple of broad-band seismometers. IUGG XXIV, Perugia, Italy.

Del Pezzo, E., Bianco, F., and Saccorotti, G., 2004, Seismic source dynamics at Vesuvius volcano, Italy, *J. Volcanol. Geotherm. Res.* **133**, 23–39.

Del Pezzo, E., Bianco, F., and Zaccarelli, L., 2006b, Separation of Qi and Qs from passive data at Mt. Vesuvius: A reappraisal of the seismic attenuation estimates, *Phys. Earth Planet. Interiors* **159**, 202–212.

Del Pezzo, E., Natale, G., Martini, M., and Zollo, A., 1987, Source parameters of microearthquakes at Phlegraean fields (Southern Italy) volcanic area, *Phys. Earth Planet. Interiors* **47**, 25–42.

Del Pezzo, E., Rocca, M. L., and Ibanez, J., 1997, Observations of High-Frequency scattered waves using dense arrays at Teide volcano, *Bull. Seism. Soc. Am.* **87**, 1637–1647.

Del Pezzo, E., Simini, M., and Ibanez, J., 1996, Separation of intrinsic and scattering Q for volcanic areas: a comparison between Etna and Campi Flegrei, *J. Volcanol. Geoth. Res.* **70**, 213–219.

Dziewonski, A. M., 1979, Elastic and anelastic structure of the earth, *Geophys. Space Phys.* **17**, 303–312.

Fehler, M. C., Roberts, P., and Fairbanks, T., 1988, A temporal change in coda wave attenuation observed during an eruption of Mount St. Helens, *J. Geophys. Res.* **93**, 4367–4373.

Ferrucci, F., Hirn, A., Virieux, J., Natale, G. D., and Mirabile, L., 1992, P-Sv conversions at a shallow boundary beneath campi Flegrei caldera (Naples, Italy): evidence for the magma chamber, *J. Geophys. Res.* **97**, 351–359.

Finetti, I. and Morelli, C., 1974, Esplorazione sismica a riflessione dei Golfi di Napoli e Pozzuoli (Italian), *Boll. Geof. Teor. Appl.* **16**, 175–222.

Frankel, A. and Clayton, R. W., 1986, Finite difference simulations of seismic scattering Implications for the propagation of short-period seismic waves in the crust and models of crustal heterogeneity, *J. Geophys. Res.* **91**, 6465–6489.

Frankel, A. and Wennerberg, L., 1987, Energy-flux model of seismic coda: separation of scattering and intrinsic attenuation, *Bull. Seismol. Soc. Am.* **77**, 1223–1251.

Friedrich, C. and Wegler, U., 2005, Localization of seismic coda at Merapi volcano (Indonesia), *Geoph. Res. Lett.* **32**(14), L14312.

Galluzzo, D., 2007, Metodologie di analisi dei segnali sismici per lo studio degli effetti di sito, Ph.d. dissertation, Università degli stud Federico II, Napoli.

Gao, L. S., Lee, L. C., Biswas, N. N., and Aki, K., 1983, Comparison of the effects between single and multiple sacttering on coda waves for local earthquakes, *Bull. Seismol. Soc. Am.* **73**, 377–389.

Gasparini, P., 1998, Looking inside Mt. Vesuvius, *EOS Trans., AGU* **79**, 229–232.

Gupta, I. N., S., L. C., and A., W. R., 1990, Broadband f-k analysis of array data to identify sources of local scattering, *Geoph. Res. Lett.* **17**(2), 183–186.

Hemmer, P. C., 1961, On a generalization of Smoluchowski's diffusion equation, *Physica* **27**, 79–82.

Herraiz, M. and Espiosa, A. F., 1987, Coda waves: a review, *PAGEOPH* **125**, 499–577.

Hoshiba, M., 1991, Simulation of multiple–scattered coda wave excitation based on the energy conservation law, *Phys. Earth Planet. Inter.* **67**, 123–136.

Hoshiba, M., 1992, Comment on 'Compact solution for multiple scattered wave energy in time domain' by Yuehua Zeng, *Bull. Seismol. Soc. Am.* **82**(3), 1552–1553.

Hoshiba, M., 1993, Separation of scattering attenuation and intrinsic absorption in Japan using the multiple lapse time window analysis of full seismogram envelope, *J. Geophys. Res.* **98**, 15809–15824.

Hoshiba, M., 1995, Estimation of nonisotropic scattering in western Japan using coda wave envelopes: Application of a multiple nonisotropic scattering model, *J. Geophys. Res.* **100**, 645–657.

Huang, L.-J. and Mora, P., 1996, Numerical simulation of wave propagation in strongly heterogeneus media using a lattice solid approach, *Soc. Photo-Optical Inst. Eng.* **2822**, 170–179.

Jackson, D. D. and Anderson, D. L., 1970, Physical mechanisms of seismic wave attenuation, *Rev. Geophys. Space Phys.* **8**, 1–63.

Jin, A. and Aki, K., 1986, Temporal change in coda Q before the Tangshan earthquake of 1976 and the Haicheng earthquake of 1975, *J. Geophys. Res.* **96**, 18215–18231.

Jin, A. and Aki, K., 1988, Spatial and temporal correlation between coda Q and seismicity in China, *Bull. Seismol. Soc. Am.* **91**, 665–673.

Jin, A. and Aki, K., 1989, Spatial and temporal correlation between coda Q and seismicity and its physical mechanism, *J. Geophys. Res.* **94**, 14041–14059.

Jin, A. and Aki, K., 1993, Temporal correlation between coda Q and seismicity: Evidence for a structuralunit in a brittle-ductile transition zone, *J. Geodyn.* **17**, 95–119.

Jin, A. and Aki, K., 2005, High-resolution maps of coda Q in Japan and their interpretation by the brittle-ductile interaction hypotesis, *Earth Planets Space* **57**, 403–409.

Jin, A., Mayeda, K., Adams, D., and Aki, K., 1994, Separation of intrinsic and scattering attenuation in southern California using TERRAscope data, *J. Geophys. Res.* **99**, 17835–17848.

Judenherc, S. and Zollo, A., 2005, The bay of Naples (southern Italy): Constraints on the volcanic structures inferred from a dense seismic survey, *J. Geophys. Res.* **109**, doi:10.129/2003JB002876.

Kopnichev, Y. F., 1977, The role of multiple scattering in the formation of seismogram's tail (English trans.), *Izv. Akad. Nauk. SSSR, Fiz.Zemli* **13**, 394–398.

Kosuga, M., 1992, Dependence of coda Q on frequency and lapse time in the western Nagano region, central Japan, *J. Phys. Earth.* **40**, 421–445.

La Rocca, M., Del Pezzo, E., Simini, M., Scarpa, R., and De Luca, G., 2001, Array analysis of seismograms for explosive sources: evidence for surface waves scattered at the main topographical features, *Bull. Seismol. Soc. Am.* **91**, 219–231.

Lerche, I. and Menke, W., 1986, An inversion method for separating apparent and intrinsic attenuation in layered media, *Geophys. J. R. Astron. Soc.* **87**, 333–347.

Lomax, A., Virieux, J., Volant, P., and Berge, C., 2000, Probabilistic earthquake location in 3D and layered models: Introduction of a Metropolis-Gibbs method and comparison with linear locations in Advances in Seismic Event Location, Thurber, C.H., and N. Rabinowitz (eds.), Springer, Kluwer, Amsterdam.

Lomax, A., Zollo, A., Capuano, P., and Virieux, J., 2001, Precise, absolute earthquake location under Somma Vesuvius volcano using a new three dimensional velocity model, *Geophys. J. Int.* **146**, 313–331.

Margerin, L., Campillo, M., Shapiro, N. M., and Tiggelen, B. V., 1998a, Residence time of diffuse waves in the crust as a physical interpretation of coda Q: application to seismograms recorded in Mexico, *Geophys. J. Int.* **138**, 343–352.

Margerin, L., Campillo, M., and Tiggelen, B. V., 1998b, Radiative transfer and diffusion of waves in a layered medium: New insight into coda Q, *Geophys. J. Int.* **134**, 596–612.

Matsumoto, S., 1995, Characteristics of Coda Waves and Inhomogeneity of the Earth, *Geophys. J. Int.* **67**, 101–108.

Matsumoto, S. and Hasegawa, A., 1989, Two dimensional coda Q structure beneath Tohoku, NE Japan, *Phys. Earth Planet. Inter.* **99**(1), 101–108.

Matsumoto, S., Obaraand, K., and Hasegawa, A., 1998, Imaging P-wave scatterer distribution in the focal area of the 1995 M7.3 Hyogo-ken Nanbu (Kobe) Earthquake, *Geophys. Res. Lett.* **25**(9), 1439–1442.

Matsunami, K., 1991, Laboratory tests of excitation and attenuation of coda waves using 2-D models of scattering media, *Phys. Earth Planet. Inter.* **67**, 36–47.

Mayeda, K., Koyanagi, S., Hoshiba, M., Aki, K., and Zeng, Y., 1992, A comparative study of scattering, intrinsic and coda Q for Hawaii, Long Valley, and Central California between 1.5 and 15.0 Hz, *J. Geophys. Res.* **97**, 6643–6659.

Mayeda, K. and Walter, W. R., 1996, Moment, energy,stress drop and source spectra of western United States earthquakes from regional coda envelopes, *J. Geophys. Res.* **101**, 11195–11208.

Nakamura, Y., 1970, Seismic energy transmission in an intensively scattering medium, *J. Geophys.* **43**, 389–399.

Nakamura, Y., Latham, G. V., Ewing, M., and Dorman, J., 1970, Lunar seismic energy transmission, *EOS Trans., AGU* **51**, 776.

Nikolaev, A. and Troitskiy, P., 1987, Lithospheric studies based on array analysis of Pcoda and microseism, *Tectonophysics.* **143**, 103–113.

Nishigami, K., 1991, A new invertion method of coda waveforms to determine spatial distribution of coda scatterers in the crust and uppermost mantle, *Geophys. Res. Lett.* **12**(18), 2225–2228.

Nishigami, K., 1997, Spatial distribution of coda scatterers in the crust around two active volcanoes and one active fault system in central Japan: Inversion analysis of coda envelope, *Phys. Earth Planet. Inter.* **104**, 75–89.

Nishigami, K., 2000, Deep crustal heterogenity along and around the San Andreas fault system in central California and its relation to the segmentation, *J. Geophys. Res.* **105**, 7983–7998.

Nishigami, K., 2006, Crustal Heterogeneity in the Source Region of the 2004 Mid Niigata Prefecture Earthquake: Inversion Analysis of Coda Envelopes, *Pure Appl. Geophys.* **163**, 601–616.

Nishimura, T., Fehler, M., Baldridge, W. S., Roberts, P., and Steck, L., 1997, Heterogeneous structure around the Jemez volcanic field, New Mexico, USA, as inferred from the envelope inversion of active-experiment seismic data, *Geophys. J. Int.* **131**, 667–681.

Orsi, G., Vita, S. D., and Vito, M. D., 1996, The restless resurgent Campi Flegrei caldera (Italy): constraints on its evolution and conFiguration, *J. Volcanol. Geoth. Res.* **74**, 179–214.

Orsi, G., Vito, M. D., and Isaia, R., 2004, Volcanic hazard assessment at the restless Campi Flegrei caldera, *Bull. Volcanol.* **66**, 514–530.

Paasschens, J. C. L., 1997, Solution of the time-dependent Boltzmann equation, *Phys. Rew.* **56**(1), 1135–1141.

Paige, C. and Saunders, M., 1982, Algorithm 583; LSQR: Sparse linear equations and least–squares problems, *TOMS* **2**(8), 195–209.

Papanicolaou, G., 1998, Mathematical Problems in Geophysical Wave Propagation, *Doc.Math.J.DMV Extra Volume ICM I* pp. 403–427.

Phillips, W. S. and Aki, K., 1986, Site amplification of coda waves from local earthquakes in central California, *Bull. Seismol. Soc. Am.* **76**, 627–648.

Quareni, F., Moretti, R., Piochi, M., and Chiodini, G., 2007, Modeling of the thermal state of Mount Vesuvius from 1631 A.D. to present and the role of CO_2 degassing and the volcanic conduitclosure after 1944 A.D. eruption, *J. Geophys. Res.* **112**, B03202.

Rautian, T. G. and Khalturin, V. I., 1978, The use of the coda for determination of the earthquake source spectrum, *Bull. Seismol. Soc. Am.* **68**, 923–948.

Rytov, S. M., Kravtsov, Y. A., and Tatarskii, V. I., 1987, Principles of Statistical Radiophysics, vol. 4, Wave Propagation Through Random Media, Springer-Verlag, New York.

Saccorotti, G., Ventura, G., and Vilardo, G., 2002, Seismic swarmsrelated to diffusive processes: The case of Somma Vesuvius volcano, Italy, *J. Volcanol. Geotherm. Res.* **67**, 199–203.

Sarker, G. and Abers, G. A., 1998, Comparison of seismic body wave and coda wave measure of Q, *Pure Appl. Geophys.* **153**, 665–684.

Sato, H., 1977, Energy propagation including scattering effects single isotropic scattering approximation, *J. Phys. Earth* **25**, 27–41.

Sato, H., 1982, Amplitude attenuation of impulsive waves in random media based on travel time corrected mean wave formalism, *J. Acoust. Soc. Am.* **71**, 559Ű–564.

Sato, H., 1987, A precursor-like change in coda excitation before the western Nagano earthquake (Ms=6.8) of 1984 in central Japan, *J. Geophys. Res.* **92**, 1356–1360.

Sato, H., 1989, Broadening of seismogram envelopes in the randomly inhomogeneous lithosphere based on the parabolic approximation: southeastern Honshu, Japan, *J. Geophys. Res.* **94**, 17735–17747.

Sato, H. and Fehler, M., 1998, Seismic Wave Propagation and scattering in the heterogeneous earth, Springer and Verlag, New York.

Sato, H., Shomahmadov, A. M., Khalturin, V. I., and Rautian, T. G., 1988, Temporal change in spectral coda attenuation Q-1 associated with the K=13.3 earthquake of 1983 near Garm, Tadjikistan region in Soviet central Asia (in Japanese), *J. Geophys. Res.* **41**, 39–46.

Scarpa, R., Tronca, F., Bianco, F., and Pezzo, E. D., 2002, High resolution velocity structure beneth Mount Vesuvius from seismic array data, *Geophys. Res. Lett.* **21**(29), 2040.

Scherbaum, F., Gillard, D., and Deichmann, N., 1991, Slowness power spectrum analysis of the coda composition of two microearthquake clusters in northern Switzerland, *Phys. Earth Planet. Inter.* **67**, 137–161.

Shang, T. and Gao, L., 1988, Transportation theory of multiple scattering and its application to seismic coda waves of impulsive source, *Scientia Sinica (series B, China)* **31**, 1503–1514.

Shearer, P. M., 1999, Introduction to Seismology, Cambridge University press, Cambridge.

Sheridan, M. F., Barberi, F., Rosi, M., and Santacroce, R., 1981, A model for Plinian eruptions of Vesuvius, *Nature* **289**, 282Ű–285.

Singh, S. and Herrmann, R. B., 1983, Regionalization of crustal coda Q in the continental United States, *J. Geophys. Res.* **88**, 527–538.

Snieder, R., 2006, The theory of coda wave interferometry, *Pure Appl. Geophys.* **163**, 455–473.

Solov'ev, S. L., 1965, Seismicity of Sakhalin, *Bull. Earthquake Res. Inst., Tokyo Univ.* **43**, 95–102.

Spudich, P. and Bostwick, T., 1987, Studies of the seismic coda using an earthquake cluster as a deeply buried seismograph array, *J. Geophys. Res.* **92**, 10526–10546.

Su, F. and Aki, K., 1995, Site amplification factors in central and Southern California determined from coda waves, *Bull. Seismol. Soc. Am.* **85**, 452–466.

Su, F., Aki, K., and Biswas, N., 1991, Discriminating quarry blast from earthquakes using coda waves, *Bull. Seismol. Soc. Am.* **81**, 162–178.

Taira, T., 2004, Quantitative imaging of Small-Scale Heterogenities around Active Fault System as Seismic Wave Scattyerers, Ph.d. thesis, Graduate school of Science, Hokkaido University.

Taira, T. and Yomogida, K., 2003, Characteristic of Small-Scale Heterogenities in the Hidaka, Japan, Region Estimated by Coda Envelope Level, *Bull. Seismol. Soc. Am.* **93**(4), 1531–1541.

Thurber, C., 1981, Earth Structure and Earthquake Locations in the Cojote Lake Area, Central California, Ph.D. Dissertation, Massachusetts Institute of Technology, Cambridge.

Tramelli, A., Pezzo, E. D., and Fehler, M., submitted, 3D scattering image of Mt. Vesuvius, *Bull. Seismol. Soc. Am.* .

Tsujiura, M., 1978, Spectral analysis of the coda waves from local earthquakes, *Bull. Earthquake Res. Inst., Tokyo Univ.* **53**, 1–48.

Vanorio, T., Virieux, J., Capuanoand, P., and Russo, G., 2005, Three-dimensional seismic tomography from P wave and S wave microearthquake travel time and rock physics characterization of Campi Flegrei Caldera, *J. Geophys. Res.* **111**, doi:10.1029/2004JB003102.

Vardeny, Z. V. and Raikh, M., 2007, Light localized on the lattice, *Nature* **446**, 37–38.

Walsh, J. B., 1965, The effects of cracks on the compressibility of rocks, *J. Geophys. Res.* **70**, 381–Ű389.

Weaver, R. L., 1990, Diffusivity of ultrasound in polycrystals, *J. Mech. Phys. Solids* **1**(38), 55–Ű86.

Wegler, U., 2004, Diffusion of seismic waves in a thick layer: Theory and application to Vesuvius volcano, *J. Geophys. Res.* **109**, B07303.

Wegler, U. and Luhr, B. G., 2001, Scattering behaviour at Merapi Volcano (Java) revealed from an active seismic experiment, *Geophys. J. Int.* **145**, 579–592.

Wennerberg, L., 1993, Multiple-scattering interpretation of coda-Q mesurements, *Bull. seism. Soc. Am.* **83**, 279–290.

Wu, J., Jiao, W., Ming, Y., and Su, W., 1988, Attenuation of coda waves at the Changbaishan Tianchi volcanic area in Northeast China, *Pure Appl. Geophys.* **163**, 1351–1368.

Wu, R. S., 1982, Attenuation of short period seismic waves due to scattering, *Geophys. Res. Lett.* **9**, 9Ű–12.

Wu, R. S., 1985, Multiple scattering and energy transfer of seismic waves - Separation of sacttering effect for intrinsic attenuation, I, *Geophys. J. R. Astron. Soc.* **82**, 57–80.

Wu, R. S. and Aki, K., 1988a, Introduction: Seismic wave scattering in three-dimensionally heterogeneous Earth, *PAGEOPH* **128**, 1–6.

Wu, R. S. and Aki, K., 1988b, Multiple scattering and energy transfer of seismic waves - Separation of sacttering effect for intrinsic attenuation, II, *Pure Appl. Geophys.* **128**, 49–80.

Yan, F. and Mo, H., 1984, Coda of the 1982 Jianchuan earthquake (in Chinese), *J. Seismol. Res.* **7**, 505–510.

Yoshimoto, K., Sato, H., and Ohtake, M., 1993, Frequency-dependent attenuation of P and S waves in the Kanto area, Japan, based on the codanormalization method, *Geophys. J. Int.* **114**, 165–Ű174.

Yoshimoto, K., Wegler, U., and Korn, M., 2006, A volcanic front as a boundary of seismic-attenuation structures in northeastern Honshu, Japan, *Bull. Seismol. Soc. Am.* **96**(2), 637–646.

Zeng, Y., 1991, Compact solution for multiple scattered wave energy in time domain, *Bull. Seismol. Soc. Am.* **81**, 1022–1029.

Zeng, Y., 1993, Theory of scattered P– and S–wave energy in a random isotropic scattering medium, *Bull. Seismol. Soc. Am.* **83**, 1264–1276.

Zeng, Y., 1996, Scattered surface wave energy in the seismic coda, *Pure Appl. Geophys.* **163**, 533–548.

Zeng, Y., Su, F., and Aki, K., 1991, Scattering wave energy propagation in a random isotropic scattering medium I. Theory, *J. Geophys. Res.* **96**, 607–619.

Zollo, A., D'Auria, L., Matteis, R. D., andJ. Virieux, A. H., and Gasparini, P., 2002, Bayesian estimation of 2-D P-velocity models from active seismic arrival time data: imaging of the shallow structure of Mt Vesuvius (Southern Italy), *Geophys. J. Int.* **151**, 566–582.

Zollo, A., Gasparini, P., Virieux, J., Biella, G., Boschi, E., Capuano, P., de Franco, R., dell'Aversana, P., de Matteis, R., De Natale, G., Iannaccone, G., Guerra, I., Le Meur, H., and Mirabile, L., 1998, An image of Mt. Vesuvius obtained by 2D seismic tomography, *J. Volcanol. Geotherm. Res.* **82**, 161–173.

Zollo, A., Judenherc, S., Auger, E., D'Auria, L., Virieux, J., Capuano, P., Chiarabba, C., de Franco, R., Makris, J., Michelini, A., and Musacchio, G., 2003, Evidence for the buried rim of Campi Flegrei caldera from 3-d active seismic imaging, *Geophys. Res. Lett.* **30**(19), doi:10.1029/2003GL018173.

Acknowledgements

From experience I can tell that this is going to be the most read page of my PhD thesis, as everybody likes to find out whether his or her name appears here.

I would like to underline the fact that my mind, after this thesis effort, has gone on strike and if you will not find your name here it does not mean that I think that you did not helped me somehow.

First of all, I have to thank the DPC projects that allowed me to go to meetings during these years and all the people that keep the seismic network of Osservatorio Vesuviano working.

I would like to thank Mike Fehler that welcomed me at the Los Alamos National Laboratory for six months and showed me the enthusiasm in the research. Thank to Scott Phillips that gave me useful suggestions and programs.

I also would like to thank Massimo for cooking every evening and cleaning my house while I was writing, Gaia, my little niece, for waking me up each morning with her songs and Francy, my sister, (and Ricky, my brother-in-law) for Gaia. Thank also to my parents for their psychological (and financial) nourishment for my studies.

Then, I want to thank Luca D'Auria as he always answers to my scientific and non-scientific questions and Rosario "Vax" Peluso for the "fancy" style of this thesis.

A particular thank goes to Sara Abbate and Eric Loomis, everywhere they are in the world, as they made my stay in Los Alamos a great experience.

Thank to Francesca Bianco that always finds a solution to every problem I had, Danilo Galluzzo that tries to infect me with his calmness and Maurizio Ciampi that always finds a way to resurrect my PC.